FOLIO
TA 7
C6
CER 72/73-21

Project THEMIS
Technical Report No. 21

PERIODICITY OF COMBINED HEAT TRANSFER FROM HORIZONTAL CYLINDERS

by

Shrinivas K Nayak
and
Virgil A. Sandborn

FLUID MECHANICS PROGRAM
ENGINEERING RESEARCH CENTER
COLLEGE OF ENGINEERING
COLORADO STATE UNIVERSITY
FORT COLLINS, COLORADO

COLORADO STATE UNIVERSITY

Project THEMIS
Technical Report No. 21

PERIODICITY OF COMBINED HEAT TRANSFER FROM HORIZONTAL CYLINDERS

by

Shrinivas K Nayak
and
Virgil A. Sandborn

Prepared under
Office of Naval Research
Contract No. N00014-68-A-0493-0001
Project No. NR 062-414/6-6-68(Code 438)
U.S. Department of Defense
Washington, D.C.

"This document has been approved for public release and sale; its distribution is unlimited."

Fluid Dynamics and Diffusion Laboratory
College of Engineering
Colorado State University
Fort Collins, Colorado

March 1973

CER72-73SKN-VAS23

187 168CSU XL 213
05/01 38-000-00 GBC

ABSTRACT

PERIODICITY OF COMBINED HEAT TRANSFER

Based on experimental and flow visualization studies, a model for directly opposed free and forced convection flow around a heated cylinder (0.01 mm diameter) was developed. Three modes of flow were identified. For velocities less than 15 cm/sec (cylinder Reynolds number, Re_{dw}=0.08) a free convection or a buoyant force dominated flow was observed. The interacting free convection plume and the ambient flow form a stagnation region well upstream of the heated cylinder. Heat was convected from the cylinder through the plume to the stagnation region. In the stagnation region random vortex pockets of heated mass were formed.

For velocities greater than 15 cm/sec but less than 21.4 cm/sec the magnitudes of the forced and free convection flows were nearly equal. A periodic oscillation of the stagnation region was observed. The flow regime where the periodic oscillations occur was found to be defined by a specific relation between the Grashof and Reynolds numbers. The periodic oscillations, which were in the range from 3 to 15 cycles per minute, were correlated in terms of Strouhal number and Reynolds number.

For velocities greater than 21.4 cm/sec the forced convection was found to dominate over the free convection. The stagnation region was fixed for each flow velocity at one position above the cylinder. A potential like flow (laminar sheet) was formed shrouding the thermal layer of the cylinder.

The mean heat transfer from the cylinder decreases with increasing Reynolds number for both the case of dominant free convection and the case of equal free and forced convection. The mean heat transfer

abruptly and rapidly increases with increasing Reynolds number in the forced convection dominated region. For all these cases the thermal layer surrounding the hot cylinder was approximately 600 times larger than the diameter of the cylinder.

ACKNOWLEDGMENT

This work was supported by the Office of Naval Research, U.S. Department of Defense under contract No. N00014-68-A-0493-0001, project No. NR062-414/6-6-68 (Code 438). The author gratefully acknowledges this support.

TABLE OF CONTENTS

TABLE OF CONTENTS - Continued

LIST OF FIGURES

LIST OF FIGURES - Continued

LIST OF FIGURES - Continued

LIST OF FIGURES - Continued

LIST OF SYMBOLS

Symbols	Definition
C_p	Specific heat at constant pressure
d	Diameter
E	Voltage
E_n	Eckert number – Temperature parameter
$f_1 f_2$	Functions
f	Frequency
f_i	Acceleration in the i direction
g	Gravitational acceleration
G_r	Grashof number
h	Asymptotic distance
h^*	Stand off distance
I	Electrical current
K	Coefficient of thermal conductivity
K_n	A dimensionless parameter
L	Characteristic length
m	Strength of source per unit length & angle
n	Exponent
P	Pressure difference ($P - P_\infty$)
p	Pressure dimensionless
Pr	Prandtl number
Q	External heat source
R	Resistance of the cylinder
Re	Reynolds number

Symbols	Definition
γ	Ratio of hot to cold resistance of the cylinders R_h/R_c
S	Strength of the line source length
Sn	Strouhal number
T	Temperature
ΔT	Temperature difference $(T - T_\infty)$
t	Time
$\bar{t}$	Time, $\frac{t}{T}$
U	Velocity in the direction of x-axis
u	Dimensionless velocity, u/U_c
V	Velocity in the direction of y-axis
v	Dimensionless velocity, v/U_c
x	Coordinate axis, vertically upwards
X	Dimensionless coordinate, X/L
Y	Coordinate axis perpendicular to x-axis
y	Dimensionless coordinate, y/L
ρ	Mass density of the fluid
$\Delta\rho$	Difference in mass density
γ	Weight density of the fluid = ρg
$\Delta\gamma$	Difference in weight density
τ	Shear stress
β	Coefficient of thermal expansion of fluid
θ	Temperature difference $(T-T_{ref.})$
θ^*	Dimensionless temperature difference
ϕ	Velocity potential

Symbols	Definition
ψ	Stream function
α	Coefficient of thermal resistance
μ	Coefficient of viscosity of the fluid
υ	Kinematic viscosity of the fluid
α_1	A constant defining variations of viscosity
α_2	A constant defining variations of thermal conductivity

Subscripts

W	Wire
c	Core, cold , characteristic
h	Hot
u=o	No flow condition
V	Virtual condition
∞	Condition at infinity
r	Condition at radial distance r

LIST OF TABLES

CHAPTER I

INTRODUCTION

A difficult problem in fluid mechanics and heat transfer is that of directly opposed combined free and forced convection. In general, this type of problem is avoided, but it can be encountered in special cases. One example is the use of a hot wire anemometer for the measurements of flow velocities in gravitational fields. In a vortex type of flow, it is possible to have the velocity directed down on the hot wire, so that the flow velocity directly opposes the free convection from the hot wire. Some manufacturing processes may also encounter similar flow conditions.

Experimental study of heat transfer from horizontal cylinders has been mainly limited to either forced or free convection alone. A limited number of studies have been reported for the case of combined free and forced convection heat transfer (6, 11, 12, 25, 26, 27,43). The case where forced convection directly opposes free convection was reported by Oostuizen and Madan (26, 27) for cylinders, and by Pei (32) for spheres. For the above studies, only the long time average heat transfer was observed. When the free and forced convection flows oppose each other, it was found that the heat transfer was less than that for free convection alone, for a limited range of convective velocities. No details on combined free and forced convection flow fields were reported.

No exact analytical solution is available for the case where the forced convection directly opposes the free convection from horizontal cylinders. Acrivos (1) made an inspectional analysis of the problem and found that the parameter, Grashof number (Gr) divided by the square of the Reynolds number (Re) is of fundamental importance. The parameter

is the ratio of buoyant force to inertial force. Reynolds number is the ratio of inertial force to viscous force. The heat transfer measurements of Oostuizen and Madan (26, 27) and Pei (32) were found to be well correlated by the parameter Gr/Re^2 . Hieber and Gebhart (14,15), using the method of matched asymptotic expansions, have obtained solutions for the velocity, temperature, and pressure field around a heated sphere when the forced convection is in the same direction as the free convection. A study of combined free and forced convection heat transfer from vertical thin needles in a uniform stream was reported by Narain and Uberoi (25). Their analysis does not indicate periodicity in the rate of heat transfer. Wood (43) reported a study of free and forced convection from fine hot wires for the aiding flow case.

A definite periodic behavior in the heat transfer process was noted by Townsend (40) while making measurements of temperature fluctuations over a heated horizontal surface. Howard (17) attributed the phenomenon to a Rayleigh type instability of the conduction layer, which he postulated as periodic. Sparrow, Husar and Goldstein (38) confirmed the generation of thermals at regular intervals from a hot horizontal plate by using flow visualization technique. However, the conditions under which thermals were generated and the mechanism of their generation were not established.

A detailed study of the basic aspects of directly opposed free and forced convection heat transfer from horizontal cylinders is reported in the present investigation. A physical model for the combined flow is proposed. The model explains the observed reduction of heat transfer by convective velocity within a limited range. It is observed that a periodic heat transfer exists over a limited range of flow conditions.

CHAPTER II

MECHANISM OF DIRECTLY OPPOSED FREE AND FORCED CONVECTION HEAT TRANSFER FROM HORIZONTAL CYLINDERS

The phenomenon of either free or forced convection heat transfer from horizontal cylinders is generally well understood. However, the case where the two convections are directly opposed to each other has received little attention. The two opposed flows will be shown to form a stagnation type flow at some distance upstream from the heated cylinder. The basic model for this type of flow was developed mainly from direct flow visualization studies. In addition, heat transfer and direct flow temperature measurement were employed to develop the model.

2.1 General Free Convection Flow

The development of a thermal plume for the case of free convection from a horizontal cylinder is well known (see for example the interference photograph, Figure 11.9 of Eckert and Drake, Ref. 8). The free convection plume is a laminar flow for many diameters above the cylinder. At some distance above the cylinder the plume may become unstable and develop into a turbulent flow.

The thermal layer developed around the horizontal cylinder is mainly a function of the surrounding fluid. Figure 1a shows a typical set of temperature measurements made across the thermal layer of a 0.01 mm (0.0004 inch) diameter hot cylinder. Temperature surveys were made at a position 0.25 mm above the cylinder. From figure 1b, it was found that the thermal layer thickness was approximately six hundred times larger than the cylinder diameter. The thickness of the thermal layer is independent of the cylinder temperature and must depend mainly on the fluid properties. In the development of the

model for the opposed free and forced convection flow it will be important to consider the thermal layer thickness as the major length parameter.

The shape of the plume for small diameter cylinders may differ somewhat from the classical picture given by Eckert and Drake (Ref. 8, Fig. 11.9). The general picture is that the plume reduces down to a width less than the cylinder diameter. However, for a very small cylinder the plume was observed to spread outward slightly. Figure 2a shows typical measurements of the temperature distribution at several locations in the space plume above the cylinder. The lateral spread of the plume was found to be approximately 2 mm in a height of 50 mm. The plume width for the small cylinder is approximately the same size as that for large cylinders. (i.e. the cylinders shown by Eckert and Drake.) The center line temperature and average plume temperature variations for the measurements of figure 2a are shown in figure 2b. Both the center line and the average plume temperatures decrease rapidly with height. The buoyant force within the plume also decreases with height.

The present measurements and discussions have dealt mainly with the thermal aspects of free convection. There is also a velocity field set up by the free convection. Brodowicz and Kierkus (3, 4) have investigated the velocity field for free convection above a horizontal wire. A technique of visualization of streamlines by means of small dust particles was used for the velocity measurements. Brodowicz and Kierkus' velocity measurements show the same growth of the plume structure as that implied by the temperature measurements of figure 2a.

2.2 Opposed Free and Forced Convection Flow

When a mean flow velocity field opposes the gravitational flow field, it is obvious that the free convection plume will be altered. In the present study, three distinct regimes of flow were identified: a) Dominant free convection; b) Equal free and forced convection; c) Dominant forced convection. For the 0.01 mm diameter cylinder, operating at 2020° F, employed in the studies, where the time varying heat transfer is shown in figure 3a to 3j, the dominant free convection regime was limited to flow velocities less than approximately 15 cm/sec (0.5 ft/sec). The regime of equal free and forced convection (figure 3K to 3z) was found to be in the range from 15 to 21.4 cm/sec (0.5 to 0.7 ft/sec). The dominant forced convection (figure 3zz) was for flow velocities greater than 21.4 cm/sec. The actual range of the flow velocities was found to be a function of the temperature difference between the cylinder and the ambient fluid.

The directly opposed interaction of two flows will form a stagnation line or region at some location where their forces are in balance. The general model for heat transfer from the cylinder will depend on the development and position of the stagnation region. For the dominant free convection regime, the stagnation region was far above the cylinder, and in general not well organized. For the equal free and forced convection regime, the stagnation position was found to be a periodic function of time. For the dominant forced convection regime, the stagnation line was well established at a position near the cylinder.

The three regimes of directly opposed free and forced convection flow could be identified from the nature of the heat transfer variations at the heated cylinder. For the case of dominant free convection, the rate of heat transfer at the cylinder fluctuates with time in a random

manner. The mean rate of heat transfer for the dominant free convection regime was found to be less than that for free convection alone. For the case of equal free and forced convection flow, the variation of the heat transfer was found to be periodic. For the case of dominant forced convection, the rate of heat transfer at the cylinder remained steady and became a function of the convective velocity. The regions of dominant free convection, equal free and forced convection, and the dominant forced convection are indicated as R_1 , R_2 and R_3 respectively in figure 4 , which is a plot of the mean rate of heat transfer as a function of Reynolds number. Figures 4a through 4i show the heat transfer measurements for a series of different Grashof numbers (wire temperatures).

a). Dominant free convection

Figures 3a through 3j show the rate of heat transfer from the cylinder as a function of time. It was observed that the mean rate of heat transfer was much reduced compared to that by free convection alone. Flow visualization indicated that the mean position of the stagnation zone moved closer to the cylinder as the convective velocity was increased. In the stagnation zone, "vortex pockets" of heated mass were formed and subsequently carried away by the ambient flow. The formation of vortex pockets occurred in a disorganized manner. The fluctuating flow in the stagnation zone resulted in the random fluctuations of heat transfer at the cylinder. Movement of the mean position of the stagnation zone towards the cylinder was found to reduce the mean rate of heat transfer at the cylinder. It was obvious that the local disturbances in the ambient flow could greatly influence the location of the stagnation zone and, hence, the rate of heat transfer

at the cylinder. The high sensitivity of the flow process of dominant free convection heat transfer to local conditions made accurate heat transfer measurements difficult.

b). Equal free and forced convection

Figures 3j through 3z represent the variation of heat transfer at the cylinder with time for the case of equal free and forced convection. The mean rate of heat transfer for this regime was also found to be less than that for free convection alone. The variation of the heat transfer developed a definite periodicity for a specific range of convective velocities for a given constant temperature of the cylinder. Figure 5, which is a series of smoke visualization photographs, shows that the stagnation zone moves above the heated cylinder in a periodic manner. The heat transfer decreased when the stagnation zone moved near the cylinder and increased as the zone moved away from the cylinder. Figure 5, taken from a motion picture study, indicated that the movement of the stagnation flow vertically upwards continued until the flow formed a vortex filament of heated mass. The vortex filament separated from the rising plume and stretched laterally. Continuous loss of heat to the ambient fluid reduced the buoyant force, whereas, the lateral spread increased the viscous drag. Ultimately the vortex ring of heated mass was carried downstream by the ambient flow. The annular space of the vortex ring permitted a direct action between the rising plume and the ambient flow. The ambient flow forced the rising plume down and moved the stagnation zone very close to the cylinder. The stagnation flow developed with time near the cylinder until it started to move upward again. This process continued in a periodic manner. A summary set of drawings of the process is detailed

at approximately 1:1 scale in the sketches shown in figures 6a through 6L.

Figure 5 indicates that the movement of the heated mass was restricted into a narrow region shrouding the heated cylinder. Smoke visualization studies indicated also that the flow was laminar. Thus, the region could be viewed as a laminar sheet of moving heated mass, as represented in figure 6. Measurements of the temperature variations, as the stagnation zone moved upward, as shown in figure 7, indicated that the temperature was uniformly varying and further supported the concept of the laminar movement of heated mass in a sheet.

The frequency and amplitude of variation of heat transfer at the cylinder are determined by the movement of the stagnation zone. Maximum height to which the stagnation zone can rise determined the amplitude of variation, whereas, the time taken for the movement determined the period of variation. Time-space history of the laminar sheet, as shown in figure 8 , indicated that the velocity was constant for a major part of its movement. In general, for a given constant temperature of the cylinder, the time period and the amplitude of the variation increased with the increase of ambient velocity.

The periodic variations in heat transfer at the heated cylinder were due to the fact that the two modes of heat transfer were approximately equal. Change from the dominant free convection heat transfer to the periodic form was gradual. The minimum ambient velocity at which the periodicity occurred will be referred to as the lower critical velocity, (U_{Lcrit}). The maximum ambient velocity at which the periodicity occurred was quite distinct in each case. The maximum velocity is referred to as the upper critical velocity (U_{Ucrit}).

In general, it was found that the magnitudes of the upper critical velocity, the lower critical velocity, and the range of ambient velocities within the periodic variations occur (R_2) increase with the increase of the cylinder temperature (Figure 4).

c). Dominant Forced Convection

In the dominant forced convection regime, the position of the stagnation zone was well established near the cylinder; hence, the rate of heat transfer remained steady with time. Figure 9 indicates that the laminar sheet shrouding the cylinder becomes unstable at a certain distance downstream and forms vortex rings of heated mass. The vortex rings develop fully as they move downstream, but they separate from the laminar sheet at definite intervals. The vortices are carried away by the ambient flow. The flow visualization studies clearly show that the increase of ambient velocity delays the formation of vortex rings and, hence, maintains a longer length of laminar sheet shrouding the cylinder. Figures 4a to 4i show the variation of heat transfer with ambient velocity for this region (R_3). Within the dominant forced convection regime (R_3), the rate of increase of heat transfer with convective velocity was significantly greater for velocities close to the critical velocity than for much higher velocities. The increase of average rate of heat transfer at the critical velocity appeared to be abrupt and was quite significant. The magnitude of the step like decrease of heat transfer at the critical value was determined by the magnitude of the periodic variations for the ambient velocity just smaller than the critical velocity.

For the present discussion free convection effects are still important. The larger thermal layer still exists so that the

characteristic length is still many times greater than the cylinder diameter. No doubt the reduced rate of change of heat transfer with Reynolds number at the higher Reynolds number is due to free convection becoming unimportant.

2.3 Characteristics of Periodic Heat Transfer

During the periodic heat transfer process, a quantity of heat is periodically stored and convected from the region near the cylinder. The periodic heat transfer process takes place when the rate at which heat is put into a system is greater than the rate at which it is convected away. The excess heat put into the system is stored and builds up with time. When sufficient heat is stored, the mechanism of heat transport changes to one with a higher capacity. Such a situation occurs at regular intervals and constitutes a periodic heat transfer. In the case of the heated cylinder subjected to directly opposed convective velocity, less than the upper critical velocity, free convection heat transfer dominates during half of the time of each cycle of variations, and forced convection dominated during the second half of the cycle. When the forced convection dominates the stagnation zone is held close to the cylinder. The heated mass is forced by the ambient flow to convect along the laminar sheet. However, the rate at which the heated mass is convected away must be less than that supplied. With time this process builds up the buoyant force in the region. A time is reached when the buoyant force exceeds the inertial force and moves the entire laminar sheet vertically upwards, until a vortex filament of stored heated mass is formed. The vortex filament separates from the heat source and looses heat to the ambient flow. When the

buoyant force is sufficiently reduced, the ambient flow is able to carry the vortex filament downstream.

a). Equilibrium of the Stagnation Flow

Equilibrium of the stagnation flow is determined by the three primary forces acting on the laminar sheet: Inertial force due to the ambient flow; buoyant force due to the heated mass in the laminar sheet; and the viscous shear force acting on the laminar sheet due to the velocity gradient across the sheet. The inertial force acting on the laminar sheet is determined by the magnitude of the ambient fluid velocity and the shape of the laminar sheet. The buoyant force is determined by the average temperature and volume of fluid in the heated region. The volume in the region was found to increase with time. When sufficient volume of heated fluid was collected in the region, the static equilibrium changes and the sheet moves upwards. The viscous shear force is directly dependent on the velocity gradient in the shear layer and also on the viscosity. For a given ambient velocity, the viscous forces will remain approximately constant.

Figure 10 is a nondimensional plot of Grashof number versus Reynolds number which defines the region where periodicity was observed. The relations for critical Reynolds numbers in terms of Grashof number were found to be

$$Re_{Lcrit} = 30 \log Gr - 44.12 \quad \text{for} \quad Gr > 4000$$

$$Re_{Ucrit} = 36.18 \log Gr - 91.68 \quad \text{for} \quad Gr > 4000$$

Figure 11 is a plot of the Stouhal number versus the ratio of local Reynolds number to the upper critical Reynolds number. The relation

between Strouhal number and the ratio of Reynolds number is approximately

$$S_n = 0.0428 \left(1.072 - \frac{Re}{Re_{Ucrit}}\right) \quad \text{for} \quad Re > 38.7$$

b). Effect of Temperature of the Cylinder

Experiments were conducted for several different values of cylinder temperature. The heat flux and, hence, the buoyant force in the rising plume will increase with the increase of the cylinder temperature. Increase of cylinder temperature is equivalent to an increase in the virtual pressure gradient (as will be considered in Chapter III) of the rising plume. The lower critical velocity occurs at a value where the ambient flow is able to push the stagnation zone close to the cylinder, which initiates the periodic variations. Thus, the increase of cylinder temperature increases the lower critical velocity. During the periodic variation of heat transfer, the rate at which the heated mass is supplied to the region becomes a function of the cylinder temperature. The upper critical velocity is reached when the inflow of heated mass equals that convected away. Thus, the magnitude of the upper critical velocity increases with the increase of cylinder temperature. As noted in the previous section, figure 10 shows how the upper and lower critical Reynolds numbers vary for the present measurements. The Grashof number reflects mainly the temperature difference (for the present study) of the cylinder and the flow. Reynolds number variation is due to the change in flow velocity. It was found that the range of ambient velocities for periodic variations of heat transfer increases with the increase of cylinder temperature. No periodic variations of heat transfer were

noticed for temperatures corresponding to Grashof number, referred to the diameter of the thermal layer, less than 4000.

c). Effect of Length and Diameter of the Cylinder

The flow visualization and figure 6 show a two-dimensional type of behavior of the phenomenon as a whole. Introduction of an extended thin solid vertical plane along the cylinder (downstream) as shown in figure 12, did not influence the phenomenon, confirming the overall two-dimensional behavior. Experiments were conducted for cylinder lengths from 2 mm to 75 mm and diameters 0.01 mm to 0.4 mm (0.4 mm cylinder - used for AC heating). It was found, as shown in figure 13, that the influence of length and diameter on the periodic behavior was negligible. The heat transfer process was primarily governed by the thermal layer thickness which in the present study varies from 150 to 600 times the diameter of the cylinder. Thus, the influence of the diameter of the cylinder was negligible. Dimensional analysis of the governing equations which is presented in Chapter III, equations (26) and (27), also indicates that the thermal layer thickness is the characteristic length. While the dominant flow appears to be two-dimensional in nature, the measured heat transfer may be in error due to the end effects. The value of the ratio of length to diameter of the cylinder was large, but the value of the ratio of length to thermal layer thickness was of the order of 2.

d). Effect of the Type of Heat Source

The influence of the type of source employed in heating the cylinder was examined by using three distinctly different types of heating: Constant temperature heating; constant current heating; and

A.C. heating. No major difference in heat transfer characteristics was observed in the three modes of heating.

Constant temperature heating was achieved by using a battery operated constant temperature anemometer. Suitable materials for the cylinders were selected in order to accommodate the limitations of the power output of the anemometer. The periodic variations observed are shown in figures 3a through 3z. The heat supplied in these cases was proportional to the square of the output voltage of the anemometer. Constant current heating was achieved by employing a suitable constant current source. For constant current case the temperature of the cylinder does not remain constant. The periodic variations in hot wire output for constant current heating is shown in figures 14a through 14k. The mean hot wire output voltage as a function of Reynolds number for constant current operation is shown in figures 15a and 15b. The regions of different heat transfer are found to be the same as those for constant temperature operation.

The case of A.C. heating was studied by applying an A.C. voltage (60 c/s) to heat the cylinder. The power supply was set by monitoring the applied voltage, and measured by noting the voltage across and current flowing through the cylinder. Periodic variations of heat transfer were detected by sensing the vertically upward movement of the laminar sheet of heated mass, using a resistance thermometer as shown in figure 16. The temperature variation shown in figure 16 is quite similar to the constant temperature results shown in figure 7.

e). Influence of Direction of the Ambient Velocity

The periodic variation of heat transfer was quite sensitive to the direction of ambient velocity. It is clear from the previous

discussion that the process of periodic heat transfer is quite sensitive to local disturbances. Any anularity of the ambient flow with the vertical introduces a lateral component of the velocity. The influence of the inclination of the ambient flow is primarily due to the lateral component. Experiments showed that periodic variations of heat transfer were exhibited when the ambient velocity made a small angle with the vertical, as shown in figure 17. Figure 18 shows the variation of mean heat transfer as a function of Reynolds number, when the forced convection was at an angle of 15° from the vertical.

f). Effect of Inclination of the Cylinder

Inclination of the cylinder was found to have a great influence on the variation of heat transfer. Due to the added complexity of the mechanism of inclined case, a systematic investigation was not undertaken. When the cylinder was yawed at an angle of 15° from the vertical (cylinder axis made an angle of 15° with the mean downward flow), very large periodic fluctuations in heat transfer were observed. These large fluctuations exceeded the usable limits of the electronic operating circuits. Apparently heat along the cylinder acts to reinforce the periodic effect observed for the horizontal cylinder. The inclined cylinder case may be an interesting area for further research.

2.4 Characteristics of Thermal Layer

The measurements of temperature distribution within the thermal layer (Figure 1) indicated that the thickness of the layer was nearly insensitive to the temperature of the cylinder. Such a phenomenon can be attributed to the thermal diffusion process by molecular action (conduction). Increase of cylinder temperature can increase the

intensity of thermal diffusion and, hence, redistribute the temperature variations within the layer thickness. Under such circumstances the zone of molecular diffusion of heat becomes a function of the properties of the fluid. The temperature gradient in such a zone is found to be quite high. Beyond the diffusion zone the convective heat transfer process greatly reduces the temperature gradient. The measurements made in air for the present study, figure 1, indicate that high temperature gradients are maintained in the region of a fixed diameter surrounding the cylinder for a wide range of temperatures. Flow visualization indicates that the size of the zone of high temperature gradient remains nearly undisturbed during the periodic variations of heat transfer at the cylinder. Thus, the region of high temperature gradient is termed as the hot core (figure 19).

The temperature measurements made for points within the hot core (Figures 20, 21, 22, 23) during periodic variation of heat transfer at the cylinder indicate a good correlation between the temperature within the hot core and the rate of heat transfer. Reduction of heat transfer at the cylinder was accompanied by the increase of temperature within the hot core. The increases of heat transfer were found to generate severe fluctuations of temperature in the hot core. Minimum temperature was found to prevail in the core at the time when the rate of heat transfer at the cylinder reached the maximum value.

During the dominant free convection heat transfer (Figure 22a), the temperature within the hot core was found to fluctuate in a random manner at a frequency much higher than that of the heat transfer variations at the cylinder. The mean temperature, however, was found to be higher than that observed in the free convection case alone.

Figure 23e shows the variation of temperature during the time of dominant forced convection heat transfer. The variation of fluid properties within the hot core can be quite significant. The heat transfer from the cylinder wall starts with thermal diffusion by molecular action and is followed by the process of convective heat transfer. Thus, the size of the region of thermal diffusion is of fundamental importance in determining the heat transfer process. The diameter of the hot core is considered the characteristic length in the present study (see also the discussion at the end of Chapter III).

2.5 Characteristics of the Flow

The flow region consists of the hot core, the rising plume of heated fluid, the stagnation region, a laminar sheet, the wake, and the ambient flow. The general characteristics of the hot core were discussed in section 2.4. General features of the rising plume of free convection are well known. However, it is very interesting to note that the rising plume becomes quite sensitive to local disturbances during the periodic behavior. The location of the stagnation region is primarily determined by the balance between the momentum carried by the rising plume and that by the convective flow. Any local disturbance can heavily influence the momentum of the rising plume and, hence, the location and formation of the stagnation flow. Sensitivity to disturbance, thus, makes it impossible to measure the temperature using the resistance thermometer within the plume during the periodic behavior. The effect of sensitivity of the rising plume to local disturbances was recorded while making temperature measurements along the vertical axis of the flow system, figures 20h, 21g, 21h; and also along ahorizontal section above the heated cylinder, figure 24.

Figure 12 shows that the shroud of heated fluid extends beyond the ends of the cylinder. The temperature measurements represented in figure 25 also indicate the spread of the laminar sheet beyond the ends of the cylinder. The transfer of heated mass is partly along the ends of the shroud and partly along the center portion. The net rate of heat transfer, thus, becomes a function of the ratio of length to the diameter of the hot core (see also Ref. 12).

Figures 26a and 26b indicate the temperature distribution in the wake of the cylinder under the influence of dominant forced convection. It can be noted that approximately constant temperature is maintained in the center region far downstream of the wake. Strong temperature gradients are found to exist in the shear region that separates the ambient flow from the wake flow. However, the temperature distribution along the horizontal section close to the cylinder (X = -5 mm) shows that high temperature gradients exist at points close to the vertical axis. It is important to note that the distribution is quite different during the periodic variations of heat transfer. Temperature measurements made during the upward movement of the stagnation flow, figure 7, indicate that the laminar sheet is narrow and possesses continuous temperature variations across its thickness.

2.6 Instability of the Laminar Sheet

Stability of the laminar sheet is determined by the nature of the fluid flow within the sheet. Primary forces controlling the stability of the fluid element are due to buoyancy, viscous shear, curvature of the sheet, and inertia.

The laminar sheet is a free shear layer. On one side of the sheet the velocity is that of the ambient flow, while inside, the velocity is nearly zero. There is a large temperature variation across the sheet. One may view this flow as a classical instability problem similar to the Kelvin-Helmholtz (9), or Taylor (39) type instabilities.

The flow visualization indicates that the higher ambient velocities delay the instability and maintain a longer laminar sheet. Thus, the increase of amplitude and period of heat transfer variations within the region, R_2 , may be related to the increase of the length of the laminar sheet.

CHAPTER III

GOVERNING EQUATIONS

An analytical analysis of the case of directly opposed free and forced convection heat transfer was not obtained. It is possible to make an inspectional analysis of the governing equations to determine the important parameters. The present section outlines the inspectional analysis for the basic flow fields considered.

In general, the differential equations governing the laminar flow of a viscous, compressible, heat conducting fluid which is subject to body force are in rectangular Cartesian tensor notation (24),

$$\frac{\partial \rho}{\partial t} + \frac{\partial}{\partial x_j}(\rho U_j) = 0 \tag{1}$$

$$\rho \frac{\partial U_i}{\partial t} + \rho U_j \frac{\partial U_i}{\partial x_j} = \rho f_i + \frac{\partial}{\partial x_j}\left[\mu\left(\frac{\partial U_i}{\partial x_j} + \frac{\partial U_j}{\partial x_i}\right)\right] - \frac{2}{3}\frac{\partial}{\partial x_i}\left(\mu \frac{\partial U_j}{\partial x_j}\right) - \frac{\partial P}{\partial x_i} \tag{2}$$

$$\rho C_p\left(\frac{\partial T}{\partial t}\right) + \rho C_p U_j\left(\frac{\partial T}{\partial x_j}\right) = Q - U_j \frac{\partial P}{\partial x_j} + \frac{\partial}{\partial x_j}\left(K \frac{\partial T}{\partial x_j}\right) + \mu\left[\frac{\partial U_i}{\partial x_j}\left(\frac{\partial U_i}{\partial x_j} + \frac{\partial U_j}{\partial x_i}\right) - \frac{2}{3}\left(\frac{\partial U_j}{\partial x_j}\right)^2\right] \tag{3}$$

$$\rho = \rho(P,T) \tag{4}$$

$$\mu = \mu(T) \tag{5}$$

$$K = K(T) \tag{6}$$

Equations (1), (2) and (3) express respectively, the conservation of mass, momentum, and energy; equation (4) represents

a thermodynamic equation of state; equations (5) and (6) represent the viscosity-temperature and thermal conductivity-temperature variations. For small temperature differences (far away from the hot core), μ and K can be assumed to be constant. By introducing the coefficient of volumetric expansion, β, to express the body force, equations (2) and (3) become:

$$\rho \frac{\partial U_i}{\partial t} + \rho U_j \frac{\partial U_i}{\partial x_j} = -\rho f_i \beta\theta + \mu\left[\frac{\partial}{\partial x_j}\left(\frac{\partial U_i}{\partial x_j} + \frac{\partial U_j}{\partial x_i}\right) - \frac{2}{3}\frac{\partial}{\partial x_i}\left(\frac{\partial U_j}{\partial x_j}\right)\right] - \frac{\partial P_D}{\partial x_i} \tag{7}$$

$$\rho C_p\left(\frac{\partial\theta}{\partial t}\right) + \rho C_p U_j \left(\frac{\partial\theta}{\partial x_j}\right) = Q - U_j \frac{\partial p}{\partial x_j} + K \frac{\partial^2\theta}{\partial x_j \partial x_j} +$$

$$\mu\left[\frac{\partial U_i}{\partial x_j}\left(\frac{\partial U_i}{\partial x_j} - \frac{\partial U_j}{\partial x_i}\right) - \frac{2}{3}\left(\frac{\partial U_j}{\partial x_j}\right)^2\right] \tag{8}$$

where $\beta = \dfrac{\rho_\infty - \rho}{\rho(T - T_\infty)}$, $P_D = P - P_\infty$, $\theta = T - T_\infty$.

Referring each of the variables in the equations to their respective reference values, $(\tau\ ,\ L\ ,\ U_c\ ,\ \theta)$, and expressing the equations (7) and (8) in dimensionless variables, we get:

$$\left(\frac{U_c}{\tau}\right)\left[\frac{\partial u_i}{\partial t}\right] + \left(\frac{U_c^2}{L}\right)\left[u_j \frac{\partial u_i}{\partial x_j}\right] = (\rho f_i \beta\theta)\ [\theta^*] +$$

$$\left(\frac{\mu U_c}{L^2\rho}\right)\left[\frac{\partial}{\partial x_j}\left(\frac{\partial u_i}{\partial x_j} + \frac{\partial u_j}{\partial x_i}\right) - \frac{2}{3}\frac{\partial}{\partial x_i}\left(\frac{\partial u_j}{\partial x_j}\right)\right] - \left(\frac{U_c^2}{L}\right)\left[\frac{\partial P_D}{\partial x_i}\right] \tag{9}$$

$$\frac{\rho C_p \theta}{\tau}\left[\frac{\partial \theta^*}{\partial t}\right] + \left(\frac{\rho C_p U_c \theta}{L}\right)\left[u_j \frac{\partial \theta^*}{\partial x_j}\right] = (Q)\,[Q^*] + \left(\frac{K\theta}{L^2}\right)\left[\frac{\partial^2 \theta^*}{\partial x_j \partial x_j}\right] +$$

$$\left(\frac{\rho U_c^2}{L}\right)\left[u_j \frac{\partial P}{\partial x_j}\right] + \left(\frac{U_c^2 \mu}{L^2}\right)\left[\frac{\partial u_i}{\partial x_j}\left(\frac{\partial u_i}{\partial x_j} + \frac{\partial u_j}{\partial x_i}\right) - \frac{2}{3}\left(\frac{\partial u_j}{\partial x_j}\right)^2\right] . \quad (10)$$

Taking the inertial terms in equation (2) and the convective terms in equation (3) as a reference, the equations can be expressed in terms of dimensionless variables (the square brackets) and parameters (round brackets):

$$(Sn)\left[\frac{\partial u_i}{\partial t}\right] + \left[u_j \frac{\partial u_i}{\partial x}\right] = \left(\frac{Gr}{Re^2}\right)[\theta^*] +$$

$$\left(\frac{1}{Re}\right)\left[\frac{\partial}{\partial x_j}\left(\frac{\partial u_i}{\partial x_j} + \frac{\partial u_j}{\partial x_i}\right) - \frac{2}{3}\frac{\partial}{\partial x_i}\left(\frac{\partial u_j}{\partial x_j}\right)\right] - \frac{\partial P_D}{\partial x_i} \quad (11)$$

$$(Sn)\left[\frac{\partial \theta^*}{\partial t}\right] + \left[u_j \frac{\partial \theta^*}{\partial x_i}\right] = \left(\frac{QL}{\rho C_p U_c \theta}\right)[Q^*] + \left(\frac{1}{RePr}\right)\left[\frac{\partial^2 \theta^*}{\partial x_j \partial x_j}\right] +$$

$$\left(\frac{U_c^2}{C_p \theta}\right)\left[u_j \frac{\partial P}{\partial x_j}\right] + \left(\frac{U_c^2}{C_p \theta}\right)\left[\frac{\partial u_i}{\partial x_j}\left(\frac{\partial u_i}{\partial x_j} + \frac{\partial u_j}{\partial x_i}\right) - \frac{2}{3}\left(\frac{\partial u_j}{\partial x_j}\right)^2\right] \quad (12)$$

where, $Sn = \frac{L}{\tau U_c} = \frac{fL}{U_c}$ = Strouhal Number

$Gr = \frac{f_i \beta \theta L^3}{2\upsilon}$ = Grashof Number

$Re = \frac{U_c L}{\upsilon}$ = Reynolds Number .

$$\frac{QL}{\rho C_p U_c \theta} = \text{Source Parameter}$$

$$Pr = \frac{\upsilon \rho C_p}{K} = \text{Prandtl Number}$$

and $$E_n = \frac{U_c^2}{C_p \theta} = \text{Eckert Number, temperature parameter}$$

Specific cases can be studied depending upon the relative magnitudes of the forces involved. Three distinctly different but important cases occur when:

1. inertial and buoyant forces dominate over the remaining forces;
2. inertial and viscous forces are approximately equal;
3. buoyant and viscous forces control the flow field.

Case 1 occurs in developing flow fields with strong influences of temperature fields. The case of directly opposed free and forced convection from heated cylinders in its periodic range (R_2) represents the case 1 of equal buoyant and inertial forces. In this case

$$\frac{Gr}{Re^2} \simeq 1 \quad ,$$

$$\therefore \; V_c = \sqrt{\theta \beta f_i L} \quad \text{or} \quad L = \left(\frac{U_c^2}{\theta \beta f_i}\right)$$

V_c and L can be referred to as the characteristic velocity and length respectively for the case (29). Equations (2) and (3) can be expressed as follows:

$$(Sn)\left[\frac{\partial u_i}{\partial t}\right] + \left[u_j \frac{\partial u_i}{\partial x_j}\right] =$$

$$\theta^* + \left(\frac{1}{\sqrt{Gr}}\right)\left[\frac{\partial}{\partial x_i}\left(\frac{\partial u_i}{\partial x_j} + \frac{\partial u_j}{\partial x_i}\right) - \frac{2}{3}\frac{\partial}{\partial x_i}\left(\frac{\partial u_j}{\partial x_i}\right)\right] - \frac{\partial P_D}{\partial x_i} \qquad (13)$$

$$(Sn)\left[\frac{\partial \theta^*}{\partial t}\right] + \left[u_j \frac{\partial \theta^*}{\partial x_j}\right] = \left(\frac{QL^2}{\rho C_p \gamma \theta}\right)\left[Q^*\right] + \frac{1}{Pr\sqrt{Gr}}\left[\frac{\partial^2 \theta^*}{\partial x_j \partial x_j}\right] +$$

$$\left(\frac{\beta f_i L}{C_p}\right)\left[u_j \frac{\partial P}{\partial x_j}\right] + \left(\frac{\beta f_i L}{C_p}\right)\frac{1}{\sqrt{Gr}}\left[\frac{\partial u_i}{\partial x_j}\left(\frac{\partial u_i}{\partial x_j} + \frac{\partial u_j}{\partial x_i}\right) - \frac{2}{3}\left(\frac{\partial u_j}{\partial x_j}\right)^2\right] \qquad (14)$$

$K_n = \left(\frac{\beta f_i L}{C_p}\right)$ a new parameter indicated first by Ostrach (28).

Case 2 occurs only in the absence of dominant temperature fields. An oscillating flat plate in still ambient fluid represents an example of equal viscous and inertial forces. The characteristic length and velocity for case 2 can be derived from the condition $Re \simeq 1$, i.e. $U_c = \frac{\upsilon}{L}$, $L = \frac{\upsilon}{U_c}$. The use of a characteristic length and velocity defined in this way for the analysis of the flow field driven by the temperature field (43), may be unrealistic. Equations (2) and (3) for case 2 can be represented as follows:

$$(Sn)\left[\frac{\partial u_i}{\partial t}\right] + \left[u_j \frac{\partial u_i}{\partial x_j}\right] = \left(\frac{Gr}{Re^3}\right)\left[\theta^*\right] +$$

$$\left[\frac{\partial}{\partial x_j}\left(\frac{\partial u_i}{\partial x_j} + \frac{\partial u_j}{\partial x_i}\right) - \frac{2}{3}\frac{\partial}{\partial x_i}\left(\frac{\partial u_j}{\partial x_j}\right)\right] - \frac{\partial P_D}{\partial x_i} \qquad (15)$$

$$(Sn)\left[\frac{\partial\theta^*}{\partial t}\right] + \left[u_j\frac{\partial\theta^*}{\partial x_j}\right] = \left(\frac{Q\upsilon}{\rho C_p U^2\theta}\right)\left[Q^*\right] + \left(\frac{1}{Pr}\right)\left[\frac{\partial^2\theta^*}{\partial x_j\partial x_j}\right] +$$

$$(E_n)\left[u_j\frac{\partial P}{\partial x_j}\right] + E_n\left[\frac{\partial u_i}{\partial x_j}\left(\frac{\partial u_i}{\partial x_j} + \frac{\partial u_j}{\partial x_i}\right) - \frac{2}{3}\left(\frac{\partial u_j}{\partial x_j}\right)^2\right] \qquad (16)$$

Case 3 represents a fully developed flow driven by the temperature field. The case of fully developed flow in a heated vertical duct is represented by the balance between viscous and buoyant forces. The characteristic length and velocity for such a flow system can be derived from the condition $\frac{Gr}{Re} \simeq 1$ or $V_c = \frac{0\beta f_i L^2}{\upsilon}$ or $L = \sqrt{\frac{\upsilon U_c}{\theta\beta f_i}}$

Incorporating the characteristic length and velocity, equations (2) and (3) can be expressed as follows:

$$(Sn)\left[\frac{\partial u_i}{\partial t}\right] + \left[u_j\frac{\partial u_i}{\partial x_j}\right] = \frac{1}{Gr}\left[\theta^*\right] +$$

$$\left(\frac{1}{Gr}\right)\left[\frac{\partial}{\partial x_i}\left(\frac{\partial u_i}{\partial x_j} + \frac{\partial u_j}{\partial x_i}\right) - \frac{2}{3}\frac{\partial}{\partial x_i}\left(\frac{\partial u_j}{\partial x_j}\right)\right] - \left[\frac{\partial P_D}{\partial x_i}\right] \qquad (17)$$

$$(Sn)\left[\frac{\partial\theta^*}{\partial t}\right] + \left[u_j\frac{\partial\theta^*}{\partial x_j}\right] = \left(\frac{Q\upsilon}{\rho C_p f_i\beta\theta^2}\right)\left[Q^*\right] + \left(\frac{1}{GrPr}\right)\left[\frac{\partial^2\theta^*}{\partial x_j\partial x_j}\right] +$$

$$Gr\left(\frac{\beta f_i L}{C_p}\right)\left[u_j\frac{\partial P}{\partial x_j}\right] + \frac{\beta f_i L}{C_p}\left[\frac{\partial u_i}{\partial x_j}\left(\frac{\partial u_i}{\partial x_j} + \frac{\partial u_j}{\partial x_i}\right) - \frac{2}{3}\left(\frac{\partial u_j}{\partial x_j}\right)^2\right] \qquad (18)$$

The mechanism of each flow process decides the characteristic length and velocity. In the heat transfer process, the thickness of the thermal layer appears to be a fundamental length paramenter. In

the present study, the radius of the zone of high temperature gradient was considered as the fundamental length.

In the case of directly opposed free and forced convection heat transfer from small diameter cylinders, pressure gradient and external heat sources do not exist. The paramenter $K = \frac{\beta f_i L}{C_p}$ remains insignificantly small, suggesting that the pressure work and dissipation are small, compared to heat transfer by convection and molecular diffusion. Equations (2) and (3) then reduce to:

$$(Sn)\left[\frac{\partial u_i}{\partial t}\right] + \left[u_j \frac{\partial u_i}{\partial x_j}\right] = \left[\theta^*\right] + \left(\frac{1}{\sqrt{Gr}}\right)\left[\frac{\partial}{\partial x_j}\left(\frac{\partial u_i}{\partial x_j} + \frac{\partial u_j}{\partial x_i}\right) - \frac{2}{3}\frac{\partial}{\partial x_i}\left(\frac{\partial u_j}{\partial x_i}\right)\right] \quad (19)$$

$$Sn\left[\frac{\partial \theta^*}{\partial t}\right] + \left[u_j \frac{\partial \theta^*}{\partial x_j}\right] = \frac{1}{Pr\sqrt{Gr}}\left(\frac{\partial^2 \theta^*}{\partial x_j \partial x_j}\right) \quad (20)$$

For the two dimensional case the equations can be simplified as follows:

$$Sn\frac{\partial u}{\partial t} + u\frac{\partial u}{\partial x} + v\frac{\partial u}{\partial y} = \theta^* + \frac{1}{\sqrt{Gr}}\left(\frac{\partial^2 u}{\partial x^2} + \frac{\partial^2 u}{\partial y^2}\right)$$

$$Sn\frac{\partial v}{\partial t} + u\frac{\partial v}{\partial x} + v\frac{\partial v}{\partial y} = \frac{1}{\sqrt{Gr}}\left(\frac{\partial^2 v}{\partial x^2} + \frac{\partial^2 v}{\partial y^2}\right) \quad (21)$$

$$Sn\frac{\partial \theta^*}{\partial t} + u\frac{\partial \theta^*}{\partial x} + v\frac{\partial \theta^*}{\partial y} = \frac{1}{Pr\sqrt{Gr}}\left(\frac{\partial^2 \theta^*}{\partial x^2} + \frac{\partial^2 \theta^*}{\partial y^2}\right) \quad (22)$$

Boundary conditions are:

$$\left.\begin{array}{llll} x = r\,, & u = 0\,, & v = 0\,, & T = T_\omega = \text{constant} \\ x = \infty\,, & u = U_\infty & v = 0\,, & T = T_\infty = \text{constant} \end{array}\right\} \quad (23)$$

Effect of fluid properties can be accounted for in the momentum equation

by suitably redefining the variables as follows:

$$x'_j = x_j\sqrt{RePr} \qquad U'_j = \sqrt{RePr}$$

The two equations then reduce to:

$$Sn\,\frac{\partial U'_i}{\partial t} + U_j\frac{\partial U'_j}{\partial x'_j} = Pr\,\frac{\partial^2 U'_i}{\partial x'_j \partial x'_j} + \frac{Gr}{Re^2}\,\theta^* \tag{24}$$

$$Sn\,\frac{\partial U'_i}{\partial t} + U'_j\frac{\partial \theta^*}{\partial x'_j} = \frac{\partial^2 \theta^*}{\partial x_j \partial x_j} \tag{25}$$

For the analysis of the flow field very close to the hot core, where high temperature differences prevail, the assumption of constant coefficients of viscosity and thermal conductivity of a fluid becomes unrealistic. However, as shown in figure 28 , the variation of C_p is insignificant for a temperature range 0^o to 2000^o F. The variable properties of the fluid introduce serious complications in the governing equations of motion. Equations (2) and (3) can be expanded as follows:

$$\rho\frac{\partial U_i}{\partial t} + U_j\frac{\partial U_i}{\partial x_j} = \rho f_i + \left[\frac{\partial \mu}{\partial x_j}\left(\frac{\partial U_i}{\partial x_j} + \frac{\partial U_j}{\partial x_i}\right) - \frac{2}{3}\,\frac{\partial \mu}{\partial x_i}\,\frac{\partial U_j}{\partial x_j}\right] +$$

$$\mu\left\{\frac{\partial}{\partial x_j}\left(\frac{\partial U_i}{\partial x_j} + \frac{\partial U_j}{\partial x_i}\right) - \frac{2}{3}\,\frac{\partial}{\partial x_i}\left(\frac{\partial U_j}{\partial x_j}\right)\right\} - \frac{\partial p}{\partial x_i} \tag{26}$$

$$\rho C_p\frac{\partial T}{\partial t} + \rho C_p U_j\frac{\partial T}{\partial x_j} = U_j\frac{\partial P}{\partial x_j} + \left[\frac{\partial K}{\partial x_j}\cdot\frac{\partial T}{\partial x_j}\right] + K\frac{\partial^2 T}{\partial x_j \partial x_j} +$$

$$\mu\left\{\frac{\partial}{\partial x_j}\left(\frac{\partial U_i}{\partial x_j} + \frac{\partial U_j}{\partial x_i}\right) - \frac{2}{3}\left(\frac{\partial U_j}{\partial x_j}\right)^2\right\} \tag{27}$$

The terms in the square bracket represents the influence of the variable properties of the fluid. The term $\frac{\partial \mu}{\partial x_j}$ can be equivalent to $(\frac{\partial \mu}{\partial T} \cdot \frac{\partial T}{\partial x_j})$. The variation of coefficient of viscosity for air within the temperature range of 0° to 2000° F is shown in figure 28. In special cases the coefficient of viscosity can be approximated by a linear function so that $\frac{\partial \mu}{\partial T} = \alpha_1 = \text{constant}$, similarly $\frac{\partial K}{\partial x_j} = \frac{\partial K}{\partial T} \cdot \frac{\partial T}{\partial x_j}$ and $\frac{\partial K}{\partial T} = \alpha_2 = \text{constant}$, figure 28. The equations for the two dimensional case reduce to the following:

$$\left.\begin{aligned} &(Sn)\ \frac{\partial U}{\partial t} + U\frac{\partial U}{\partial x} + V\frac{\partial U}{\partial y} = \\ &\frac{Gr}{Re^2}\ \theta^* + \left(\frac{\alpha_1\theta}{Re}\right)\left[\frac{\partial \theta^*}{\partial x} \cdot \frac{\partial U}{\partial x} + \frac{\partial \theta^*}{\partial y} \cdot \frac{\partial U}{\partial y}\right] + \frac{1}{Re}\left(\frac{\partial^2 U}{\partial x^2} + \frac{\partial^2 U}{\partial y^2}\right) \\ &Sn\ \frac{\partial V}{\partial t} + U\ \frac{\partial V}{\partial x} + V\ \frac{\partial V}{\partial y} = \left(\frac{\alpha_1\theta}{Re}\right)\left[\frac{\partial \theta^*}{\partial x} \cdot \frac{\partial V}{\partial x} + \frac{\partial \theta^*}{\partial y} \cdot \frac{\partial V}{\partial y}\right] + \frac{1}{Re}\left(\frac{\partial^2 V}{\partial x^2} + \frac{\partial^2 V}{\partial y^2}\right) \end{aligned}\right\} \quad (28)$$

$$Sn\ \frac{\partial \theta^*}{\partial t} + U\ \frac{\partial \theta^*}{\partial x} + V\ \frac{\partial \theta^*}{\partial y} = \left(\frac{\alpha_2\theta}{RePr}\right)\left[\left(\frac{\partial \theta^*}{\partial x}\right) + \left(\frac{\partial \theta^*}{\partial y}\right)^2\right] + \frac{1}{RePr}\left(\frac{\partial^2 \theta^*}{\partial x^2} + \frac{\partial^2 \theta^*}{\partial y^2}\right) \quad (29)$$

$(\alpha_1\theta)$ and $(\alpha_2\theta)$ are new dimensionless parameters describing the variable properties of the fluid. The terms in the square bracket (due to variable fluid properties) are quite comparable with the rest of the terms for the flow field close to the hot cylinder. Thus, any attempt to mathematically solve the problem by considering equations (21), (22), and (23) may be highly unrealistic. The complex nature of the equations (28), (29), and (23) indicates the mathematical solution of the problem is extremely difficult.

General guidelines for the study can be derived from dimensional considerations. According to the Π theorems (for constant Prandtl number say $P_r = 0.72$)

$$Sn = f_1 \left(\frac{Gr}{Re^2}, \frac{\alpha_1 \theta}{Re}, \frac{1}{Re}\right) \tag{30}$$

For the dominant forced convection, S_n does not bear any significance. Thus, the upper critical Reynolds number can be expressed as

$$Re_{Ucrit} = f_2 \left(\frac{Gr}{Re^2}, \frac{\alpha_1 \theta}{Re}\right) \tag{31}$$

for the case of a constant temperature cylinder in air, the parameter $(\alpha_1 \theta)$ remains fixed. Thus

$$Re_{Ucrit} = f_3 (Gr) \tag{32}$$

Similarly

$$Sn = f_4 (Re, Gr) \quad , \quad \text{or} \quad S_n = f_5 \left(\frac{Re}{Re_{Ucrit}}\right) \tag{33}$$

The functional relation f_3 and f_5 were established by the experimental investigation and are shown in figures 10 and 11.

To understand better, each part of the flow field, it is found quite helpful to examine the governing equations. The characteristics of the rising plume can be studied by integrating, with respect to y, the two dimensional equations of conservation of mass, momentum and energy as follows.

Conservation of mass

$$\frac{\partial}{\partial x}\int_0^\infty U\,dy + v(x,\infty) = 0 \tag{34}$$

Equation (34) states that the increase of ascending mass in the rising plume is due to the entrainment of the ambient fluid.

Conservation of momentum

$$\frac{\partial}{\partial x}\int_0^\infty U^2\,dy = \int_0^\infty \frac{\Delta\gamma}{\rho}\,dy \tag{35}$$

Equation (35) states that the increase of vertical momentum in the rising plume is due to the effect of buoyancy.

Conservation of energy

$$\frac{\partial}{\partial x}\int_0^\infty U\Delta\gamma\,dy = 0 \tag{36}$$

Equation (36) indicates that the buoyancy flux of the ascending mass in the plume remains constant as it rises. The equivalent effect of the increase of momentum of the rising mass can be realized better by writing equation (35) as follows:

$$\frac{\partial}{\partial x}\int_0^\infty U^2\,dy = \int_0^\infty \frac{\Delta\gamma}{\rho}\,dy = \frac{\partial}{\partial x}(P_v) \tag{37}$$

where P_v is a virtual pressure equivalent to the increase of momentum such that

$$P_v = \int_0^\infty U^2\,dy \tag{38}$$

Thus, the rising plume of heated mass can be viewed as equivalent to a pressure gradient $\frac{\partial P_v}{\partial x}$. Directly opposed free and forced convection heat transfer can be considered equivalent to a uniform flow field directed downwards which encounters adverse pressure gradient. Development and location of the stagnation flow can be realized better by such a concept.

Examination of the governing equations (11) and (12), taking diameter of the heated cylinder as the characteristic length, leads to unrealistic conclusions. The dimensionless parameter $\frac{Gr}{Re^2}$, which represents the ratio of buoyant force to inertial force, becomes the order of 0.01, whereas, Re^{-1} which is the ratio of viscous force to the inertial force becomes the order of 10. The apparent conclusion is that the buoyant forces are insignificantly small. The real fact is that the phenomenon is governed by the balance between inertial and buoyant forces. If we consider the radius of the hot core as the characteristic length, the dimensionless parameters $\frac{Gr}{Re^2}$ and Re^{-1} assume reasonable value i.e. $(\frac{Gr}{Re^2})$ and Re^{-1} approximately equal to 6 and 0.02 respectively.

CHAPTER IV

EXPERIMENTAL MEASUREMENTS OF HEAT TRANSFER AND TEMPERATURE DISTRIBUTIONS

The experimental measurements of heat transfer and temperature distributions have already been introduced to develop the physical model of the flow. This section is a short description of the techniques employed to obtain the measurements.

4.1 Flow Facility

The flow facility consists of an open circuit type micro velocity tunnel (20) as shown in figure 29. The tunnel permitted the angle between the velocity in the test section and the horizontal direction to be varied. A constant speed blower was employed to force the ambient air into a narrow controlled section of the tunnel. A throttle control at the inlet of the blower was used to vary the flow velocity. The flow from the control section was allowed to pass through an enlarged test section. Honeycombs and wire meshes of suitable sizes were employed to maintain a uniform distribution of velocity across the test section (figure 30a and b). A relation between the dynamic head in the control section and the velocity in the test section was established. The flow facility was calibrated, as reported in reference 20, by employing hot spot anemometer, drag anemometer, hot wire anemometer, and soap bubble technique. The calibration is shown in figure 31. Figures 30a and b show the measured velocity distributions in the control section and the test section respectively. The maximum velocity obtained in the test section was 0.45 m/sec.

4.2 Test Cylinders

Standard hot wire anemometer material was employed for the test cylinders. The major part of the study employed a 0.01 mm (0.0004 inch) diameter, 80% platinum and 20% irridium wire for the test cylinders. Nichrome 0.4 mm (0.0015 inch) diameter wire and 94% platinum - 6% tungsten, 0.02 mm, (0.0008 inch) diameter strain gauge wire were also employed mainly to study the effect of wire diameter. The wires were mounted on typical hot wire anemometer probes. Typical wire lengths were of the order of 8 mm, although longer wires were also used to demonstrate that the end effects were not of major importance. The wire supports were made of 79 gauge steel sewing needles.

For constant temperature operation a commercial battery powered constant temperature hot wire anemometer circuit was employed. A special constant current power supply was employed for constant current operation. For A.C. heating 60 cycles line power was employed together with a variac. Mean voltages were determined with a digital voltmeter. The time varying signals were recorded by standard one and two channel X - Y plotters.

4.3 Resistance Thermometer

A resistance thermometer was used to survey the temperature field. The principle underlying the operation of the resistance thermometer is that the resistance of a metal varies with temperature. Wollaston wire (Rh 10%, Pt 90%) of 0.000025 inch diameter was selected for use as the temperature sensor. The sensor supports were made of sewing needles (79 gauge). Enamel coated copper conductors (68 gauge) were soldered to the sensor supports and passed through a narrow brass tube (3 mm outside diameter). The probe arrangement was held firmly

by epoxy joints. The sensor supports were tinned in order to permit easy soldering of the sensor wire. Mounting of the sensor wire on the supports was a delicate process. The silver coating of the sensor wire was etched away, before soldering, by employing nitric acid (50%). The process of etching was aided by passing direct current through the solution (10 micro amps.), where the Wollaston wire was the anode. The sensor supports were moved near the etched sensor wire. Soldering flux helped in holding the sensor wire attached to the supports during the process of soldering. The sensor supports were heated until the solder melted and held the sensor wire. The process of heating the supports was achieved by bringing the tip of the heated soldering iron close to the supports. The soldering joints were tested by passing a current (10 milliamps.) through the sensor wire. The probe was cleaned by holding it in the vertical position in heated air (300° F). The probe was calibrated against a standard thermometer. Variation of the resistance of the wire with temperature is expressed by

$$R_h = R_c \ (1 + \alpha \Delta T) \ .$$

The coefficient of thermal resistance was found constant and was determined in the calibration procedure. The resistance-temperature curve for the wires used in the present study is shown in figure 32.

A detection current, I , was passed through the probe in order to determine the change in the resistance. The current was small enough to prevent the heating of the sensor wire. The variation of voltage across the sensor wire becomes a measure of the resistance variation (Ref. 5).

$$IR_h = IR_c + IR_c \alpha \Delta T$$

$$E_h - E_c = IR_c \alpha \Delta T$$

$$\left(\frac{\Delta E}{\Delta T}\right) = IR_c \alpha$$

For a given probe, $IR_c \alpha$, remains constant if the detection current is maintained constant. Increase of current through the sensor, increases its sensitivity to temperature measurements. Higher currents through the probe will also heat the sensor wire and make it sensitive to convective velocity. It was experimentally found that for a detection current of 700 microamperes, the wire was not sensitive to velocities less than 15 m/sec. A sensor current of 500 microamperes was used in the present study. The details of characteristics of the resistance thermometer were studied by Chow and Sandborn (5). They determined that the frequency response of the wire was over 3000 cycles per second.

4.4 Flow Visualization

The hot wire was simulated by coupling a line source of heat and smoke. A nichrome wire (1 ohm/mm) was held between two conductor supports and heated by A.C. power. A thin narrow asbestos sheet soaked in paraffin was held close to the nichrome wire in such a way that its obstruction to the flow was minimum. The probe arrangement was mounted in the flow facility for observations. The heat from the nichrome wire melted the paraffin and formed dense smoke. The smoke was carried along with the heated fluid. Thus, it traced the path of the heated fluid flow. The asbestos sheet was charged with

paraffin wax at regular intervals. The intensity of the heat source could be increased by increasing the applied A.C. voltage across the nichrome wire.

Incense sticks were initially used to simulate the conditions. A single incense stick with its burning tip served as a good point source of heat and smoke. A series of incense sticks placed in a line, with the tips burning, could well simulate the line source of the heat and smoke. Flexibility of the heat source was achieved by introducing an electrically heated wire near the burning tips of the incense sticks. A simple schlerien system was also employed in the early studies to comfirm that the heated wire followed closely the effect seen from the smoke studies.

CHAPTER V

DISCUSSION

The present experimental study of directly opposed free and forced convection leads to a definite model for this type of flow. The observation of the formation of a stagnation region and of the potential like source flow around the heated cylinder gives a new insight into the problem. The existance of the large, stable hot core (thermal layer) with large temperature gradients, surrounding the cylinder, is an important aspect of the mechanism of mixed free and forced convection.

The heat transfer model may be summarized as follows:

I. Free Convection.

   a) A large thermal layer is formed around small heated cylinders.

   b) A thermal convection plume of near constant width is formed above the thermal layer.

II. Opposed Free and Forced Convection.

   a) The interaction between the two flows form a stagnation region.

   b) Dominant free convection: The stagnation region is formed well upstream of the cylinder or thermal layer. The stagnation region is unstable and fluctuates in a random manner. Vortex pockets of hot fluid are formed and carried along with the ambient flow. The mean heat transfer from the cylinder is reasonably steady and decreases with the increase of flow velocity.

   c) Equal free and forced convection: The stagnation

region oscillates in a periodic manner. The buoyant force builds up with time and forces the stagnation region upstream. A vortex filament is formed when the stagnation region is forced upstream. The vortex filament is carried away by the mean flow, and a new stagnation region appears near the thermal boundary layer. The cylinder heat transfer varies in a periodic manner and decreases with flow velocity.

d) Dominant forced convection: The stagnation region is stably held at a fixed distance ahead of the thermal layer. A laminar sheet of flowing fluid forms a shroud around the cylinder. The heat transfer from the cylinder is steady and increases with flow velocity.

The experimental study of the time-space history of the laminar sheet, figure 8, indicates that the velocity remains constant during the major part of the upward movement. Any acceleration of the laminar sheet will stop once the increase of viscous force neutralizes the imbalance. Measurements show that the acceleration of the laminar sheet lasts only for a short time.

It is interesting to note the direct correlation between the rate of heat transfer at the cylinder and the relative position of the laminar sheet (with respect to the cylinder). Proximity of the laminar sheet was found to reduce the rate of heat transfer at the cylinder. Experimental measurements of heat transfer made by replacing the laminar sheet by a thin metal shield are shown on the insert of figure 27. These measurements made with a physical shroud agree well with those observed during the periodic behavior.

The mechanism of periodic heat transfer is detailed in figure 6. Formation of the vortex filament is seen from the flow visualization studies, figure 5. The temperature measurements also confirm the detailed mechanism. Temperature measurements close to the rising plume, figure 27, show a single pulse of temperature during each cycle indicating the anular region of the vortex filament. The temperature measurements made at locations away from the rising plume show two pulses. The pulse of continuous temperature variations represents the upward movement of the laminar sheet, whereas the pulse of fluctuating temperature indicates the disorganized motion of the heated mass in the vortex filament during its downward movement. The temperature measurements, figure 7, made at locations far away from the rising plume indicate the extent of the lateral spread of the vortex filament during its downward movement.

The present study indicates that the diameter of the cylinder may not be the representative length characterizing the heat transfer process. The dimensional considerations, examined in equation (11), show that the ratio of buoyant force to inertial force becomes much smaller than the ratio of viscous to inertial forces when the diameter of the cylinder is taken as the characteristic length. This apparently indicates that the buoyant force is much smaller than the inertial and viscous forces. The real fact is that flow system is driven by inertial and buoyant forces. Such an unrealistic indication is due to the diameter of the cylinder being considered as the characteristic length. When the radius of hot core is considered to be the characteristic length, equation (26) is found to represent more realistic values for the dimensionless parameters like $\frac{Gr}{Re^2}$ and Re^{-1} .

Existance of the large, near constant diameter, hot core around a heated cylinder (when held in air) has not previously been reported. The hot core around small heated wires may limit their use for making velocity measurements. If the hot wires are used to measure low fluid velocities very close to the boundary, the hot core will come in contact with the boundary and lead to direct heat transfer by conduction. The heat conducted will be determined by the different factors like thermal conductivity of the wall material, temperature distribution and area of the hot core in contact with the boundary. Effect of the proximity of solid walls on the rate of heat transfer is reported by Wills (29).

Measurements of small scale turbulence and high frequency variations at low velocities by using hot wires need special consideration in the light of the existing hot core around the cylinder. The measurements of fluctuating quantities at high frequency are limited by the inertial effect of the sensor. In the case of the hot wire, the hot core may be acting as a sensor. As such, the measurements of fluctuating velocities at high frequency will be limited by the heat capacity of the hot core, rather than that of the hot wire. Heat capacity of the hot core will be determined by the fluid medium. Thus, the limit on the hot wire for high frequency measurements will also depend on the fluid properties. If the size of the eddies that constitute a turbulent flow is smaller than the diameter of the hot core, the anemometer output will not truly represent the eddy. Thus, the size of the eddy that can be recorded by the hot wire will be limited by the diameter of the hot core and not the cylinder. Use of hot wires for measurements of correlation needs also special consideration.

The wires must be mounted in such a way that the two hot cores do not interfere with each other.

The present study brings out the details of the limitations on the use of hot wire anemometers in mixed flow. Careful examination of the limits of periodic variation of heat transfer, figure 10, shows that uncertainty of heat transfer measurements will increase with the increase of temperature of the cylinder. Experimental measurements, figures 3 and 10, show that the uncertainty of heat transfer measurements becomes insignificant when the temperature of the cylinder is maintained less than 300° F. Thus, it may be necessary to use wires at low temperatures for low velocity measurements. Effects of buoyancy on the heat transfer is most severe when the ambient flow directly opposes the free convection. Thus, the case studied represents the maximum effect of buoyancy.

The effect of the ratio of length to diameter of the cylinder is reported by Gebhart and Pera (12) . The mechanism involved in the end effect on the heat transfer process is realized by the present visualization study. The temperature measurements in the wake of the cylinder beyond its length, figure 25, also demonstrate the end effect.

The action of the hot cylinder in the development of a laminar sheet shrouding the thermal layer appears similar to the development of separation stream surfaces by potential line source in a uniform flow field. The temperature of the hot core corresponds to the strength of the source. Thus, an idealized mechanism to explain the formation of the laminar sheet might be obtained from potential flow analogy. The shape of the separation surface can be derived from the potential

flow analysis for a given strength of source, a, and uniform velocity, U. A derivation of the potential source flow is given in the appendix.

Figure 19 represents the limits of the variations of temperature as a function of distance from the cylinder during the periodic behavior. It is obvious that the maximum, mean and minimum temperature profiles possess high temperature gradients in the thermal layer region covered by a radius of 3 mm. It is important to remember that there cannot be a thermal boundary layer thickness in the present case. At any horizontal distance greater than 3 mm from the cylinder only one temperature pulse due to the vortex filament being carried downstream was recorded during each cycle of variations. The correlation between the temperature variations, inside and outside the hot core, with the heat transfer variations at the cylinder are distinctly different, and are similar to those recorded in figures 20 and 7 respectively. The figure 19 indicates that the size of the hot core remains practically constant during the periodic behavior.

CHAPTER VI

CONCLUSIONS

An experimental and flow visualization study of directly opposed free and forced convection reveals the following physical picture for the flow.

The interaction of the two opposing flows produces a stagnation region or line at some distance above the heat source. The present study employed small diameter heated cylinders (0.01 mm diameter) as the free convection source. For velocities below 15 cm/sec (cylinder Reynolds number, $Re_{dw} \leq 0.08$), the free convection dominates the heat transfer from the cylinder. A stagnation region is formed well upstream of the cylinder and its large thermal layer. Heat is mainly convected through the free convection plume. In the stagnation region random vortex pockets of heated mass were formed.

When the magnitude of the inertial forces, due to the forced convection, was of the same order as the buoyant forces, due to free convection, a periodic oscillation of the stagnation zone was observed. This periodic oscillation occurred for flow velocities, U, in the range of approximately $15 < U < 21.4$ cm/sec ($0.08 < Re_{dw} < 0.115$). The actual range depends on the Grashof number. For Grashof number less than 4000 (based on thermal layer thickness of 3 mm) the buoyant force was not sufficient to produce oscillations. The frequency, f , of the oscillations varied from $3 < f < 15$ cycles per minute.

A lower "critical" Reynolds number, Re_{Lcrit} , where oscillations were first encountered was found to be related to the Grashof number by the relation:

$$Re_{Lcrit} = 30 \log Gr - 44.12 \quad \text{for} \quad (Gr > 4000).$$

The upper "critical" Reynolds number, Re_{Ucrit}, where oscillations abruptly cease to occur is given by the relation:

$$Re_{Ucrit} = 36.18 \log Fr - 91.68 \quad \text{for} \quad (Gr > 4000) .$$

The Strouhal number, S_n, of the periodic oscillations was found to be related to the Reynolds number by the relation:

$$Sn = 0.0428\left(1.072 - \frac{Re}{Re_{Ucrit}}\right) \quad \text{for} \quad (Re > 38.7) .$$

The heat transfer from the cylinder can be directly correlated with the distance of the stagnation region above the cylinder. The magnitude of the heat transfer oscillations can be as great as 10% of the mean. For both the free convection dominated flow and the region of equal free and forced convection flow, the mean heat loss from the cylinder decreased with increasing Reynolds number.

For the case where the forced convection is greater than the free convection (inertial force greater than buoyant force, velocity greater than 21.4 cm/sec), the stagnation region was fixed for each flow velocity at one location. A potential like flow (laminar sheet) is formed shrouding the thermal boundary layer region of the cylinder. The heat transfer from the cylinder in this flow regime increases rapidly with increasing Reynolds number.

The thermal layer was of the order of 600 times the cylinder diameter. Thus, the thermal layer thickness was taken as the characteristic length of the flow field. The present observations should apply to all cylinders that are small compared with the thermal layer thickness. The major factor in determining the thickness of the thermal

layer will be the conduction properties of the fluid. Detailed measurement of the temperature distributions in the thermal layer and the surrounding shroud are given.

It was discovered that the periodic oscillations of the heat transfer for the case of equal inertial and buoyant forces can be prevented by inserting a probe in the thermal plume above the cylinder.

BIBLIOGRAPHY

1. Acrivos, A., 1958. Combined free and forced convection heat transfer in external flows: A.I.Ch.E. Journal, Vol. 4, No. 3, pp. 285-289.

2. Biggs, R. C., 1970. Combined free and forced convective heat transfer of gases: Fourth International Heat Transfer Conference, Paper N.C. 3.1.

3. Brodowicz, K. and Kierkus, W. T., 1966. Experimental investigation of laminar free convection flow in air above horizontal wire with constant heat flux: J. Heat mass transfer, Vol. 9, pp. 81-94.

4. Brodowicz, K. and Kierkus, W. T., 1965. Determination of stream lines and velocity components in free convection: Archwm Budowy Masz. 4.

5. Chao, J. L. and Sandborn, V. A., 1964. A resistance thermometer for transient temperature measurement: Fluid Mech. Paper No. 1, Colorado State University.

6. Collis, D. C. and Williams, M. J., 1959. Two dimensional convection from heated wires at low Reynolds number: J. Fluid Mech., pp. 357-384.

7. Dring, R. P. and Gebhart, B., 1969. Hot wire anemometer calibration for measurements at very low velocity: J. Heat Transfer, Trans. ASME, pp. 241-244.

8. Eckert, E. R. G., and Drake, R. M., 1959. Heat and mass transfer: McGraw-Hill Book Company, Inc., 2nd edition, p. 321.

9. Helmholtz, H., 1968. Uber discontinuirliche flussigkeitbwegungen: Translation by Guthrie in Phil. Mag., Ser. 4, Vol. 36, pp. 337-346.

10. Hermann, R., 1936. Heat transfer by free convection from horizontal cylinders in diatomic gases: NACA, TM 1266.

11. Gebhart, B., Audunson, T., and Pera, L., 1970. Mixed forced and natural convection from long horizontal wires, Experiments at various Prandtl numbers: Fourth International Heat Transfer Conference, Paper NC 3.2.

12. Gebhart, B. and Pera, L., 1970. Mixed convection from long horizontal cylinders: J. Fluid Mech., Vol. 45, Part 1, pp. 49-64.

13. Hatton, A. P., James, D. D., and Swire, H. W., 1970. Combined forced and natural convection with low speed air flow over horizontal cylinders: J. Fluid Mech., Vol. 42, Part 1, pp. 17-31.

14. Hieber, C.A. and Gebhart, B., 1969. Mixed convection from a sphere at small Reynolds and Grashof numbers: J. Fluid Mech., Vol. 38, Part 1, pp. 137-159.

BIBLIOGRAPHY - (continued)

15. Hieber, C. A. and Gebhart, B., 1968. Low Reynolds number heat transfer from a circular cylinder: J. Fluid Mech., Vol. 32, Part 1, pp. 21-28.

16 Hollasch, K. and Gebhart, B., 1972. Calibration of constant temperature hot wire anemometers at low velocities in water with variable fluid temperature: J. Heat Transfer, Trans. ASME, pp. 17-22.

17. Howard, L. N., 1964. Convection at high Rayleigh numbers: Eleventh International Congress, Applied Mech., pp. 1109-1115.

18. King, L. V., 1914. On convection of heat from small cylinders in a stream of fluid. Determination of convection constants of small platinum wires with application to hot wire anemometry: Phil. Trans., A1, 214, pp. 373-432.

19. Kreith, F., 1958. Principles of heat transfer: International Textbook Company.

20. Kung, R. J. and Binder, G. J., 1967. Ultra low speed anemometry: Colorado State University, Civil Engineering Dept., Report.

21. Lee, S. L. and Emmons, H. W., 1961. A study of natural convection above a line fire: J. Fluid Mech., Vol. 11, pp. 353-368.

22. Maslen, S. H., 1958. On fully developed channel flows: Some solutions and limitations, and effects of compressibility, variable properties and body force: NACA Technical Note 4319.

23. Milne-Thomson, L. M., 1955. Theoretical hydrodynamics: The Macmillan Company, Inc., 2nd edition, pp. 199.

24. Moore, F. K., 1964. Theory of laminar flows: Princeton University Press, Vol. 4, pp. 528 - .

25. Narain, J. P. and Uberoi, M. S., 1972. Combined forced and free convection heat transfer from vertical thin needles in a uniform stream: The physics of fluids, Vol. 15, No. 11, pp. 1879-1882.

26. Oosthuizen, P. H. and Madan, S., 1970. Combined convective heat transfer from horizontal cylinders in air: J. Heat Transfer, Trans., ASME, pp. 194-196.

27. Oosthuizen, P. H. and Madan, S., 1971. The effect of flow direction on combined convective heat transfer from cylinders to air: J. Heat Transfer, Trans., ASME, pp. 240-242.

28. Ostrach, S., 1950. A boundary layer problem in the theory of free convection: Doctoral Thesis, Brown University.

BIBLIOGRAPHY - (continued)

29. Ostrach, S., 1952. Laminar natural-convection flow and heat transfer of fluids with and without heat sources in channels with constant wall temperatures: NACA Technical Note 2863.

30. Ostrach, S., 1953. Combined natural - and forced - convection laminar flow and heat transfer of fluids with and without heat sources in channels with linearly varying wall temperatures: NACA Technical Note 3141.

31. Ostrach, S., 1955. Unstable convection in vertical channels with heating from below, including effects of heat sources and frictional heating: NACA Technical Note 3458.

32. Pei, D. C. T., 1959. Heat transfer from spheres under combined forced and natural convection: Chem. Eng. Progress Symp. Series, Heat Transfer, Vol. 61, pp. 57-63.

33. Rayleigh, L., 1916a. On convection currents in horizontal layer of fluid when the higher temperature is on the under side: Scientific Papers, 6, pp. 432-446.

34. Rosenhead, L., 1963. Laminar boundary layers: Oxford Clarendon Press, Chapter 9, on Hydrodynamic Stability by Stuart, J. T., pp. 492-578.

35. Schlichting, H., 1968. Boundary layer theory: McGraw Hill Book Company.

36. Sharma, G. K., and Sukhatme, S. P., 1969. Combined free and forced convection heat transfer from a heated tube to a transverse air stream: J. Heat Transfer, Trans., ASME, pp. 457-459.

37. Sitaramarao, T. L. and Barrow, H., 1971. Combined free and forced laminar convection in the entrance region of ducts of constant cross-section: I. Mech. E. Symposium, C 116/71.

38. Sparrow, E. M., Husar, R. B., Goldstein, R. J., 1970. Observation and other characteristics of thermals: J. Fluid Mech., Vol. 41, Part 4, pp. 793-800.

39. Taylor, G. I., 1931. Effect of variation of density on the stability of superposed streams of fluid: Proc. Roy. Soc. London (A), Vol. 132, pp. 499-523.

40. Townsend, A. A., 1959. Temperature fluctuations over a heated horizontal surface: J. Fluid Mech., Vol. 5, pp. 209-241.

41. Wills, J. A. B., 1961. Correction of hot wire readings for proximity to a solid boundary: J. Fluid Mech., pp. 388-396.

42. Wood, W. W., 1972. Free and forced convection heat transfer from fine hot wires: J. Fluid Mech., Vol. 55, pp. 419-438.

APPENDIX

Analysis of the Source Flow

For the coordinate system shown in figure 6 , let ϕ_1 , and ϕ_2 be the flow potentials representing a uniform flow of velocity $-U$ and source flow of strength S per unit length respectively.

Then

$$\phi_1 = -Ux; \quad U_1 = \frac{\partial \phi_1}{\partial x} = -U \quad V_1 = \frac{\partial \phi_1}{\partial y} = 0$$

$$\phi_2 = \frac{S}{4\pi} \log (x^2 + y^2), \quad U_2 = \frac{Sx}{2\pi(x^2 + y^2)}, \quad V_2 = \frac{Sy}{2\pi(x^2 + y^2)}$$

Net flow potential is $\phi = \phi_1 + \phi_2$

$$\phi = -Ux + \frac{S}{4\pi} \log (x^2 + y^2), \quad \text{and stream function}$$

$$\Psi = -Uy + \frac{S}{2\pi} \tan^{-1} \frac{y}{x} = -Uy + m\theta$$

$$\text{where} \quad m = \frac{S}{2\pi}, \quad \theta = \tan^{-1} \frac{y}{x}$$

Let θ be measured in the counter clockwise direction from negative X-axis. Then the dividing stream line will be given by

$$-m\Pi = Uy + m\theta \quad (\text{for} \quad y > 0)$$

When θ tends to zero, y tends to $h = \frac{m\Pi}{U}$.

The separation stream line thus is held between $y = \pm h$.

The equation of the separation stream line can be written as

$$\frac{1}{x} = \frac{1}{y} \tan \left(\frac{\pi y}{x}\right)$$

Correspondingly the stand of distance is given by

$$h^* = \frac{h}{\pi} = \frac{m}{U}$$

Figure 6 compares the shape of laminar sheet and the separation surface obtained by the above analysis.

Though the formation of the laminar sheet appears similar to that of the development of potential separation surface around a source under similar conditions, the mechanism may differ. The source possesses a center of symmetry in its action, whereas, the heat source at the cylinder is directed by the buoyancy effect, and acts in a direction opposing the gravity. Variation of the strength of the source alone can vary the position of the separation surface with respect to the source when the uniform velocity is maintained constant. But the equilibrium of the stagnation flow is primarily governed by the balance between the buoyant and inertial forces for a given uniform velocity.

TABLES

TABLE I

Variation of the Range of Periodic Heat Transfer from Horizontal Cylinders

$T_\infty = 70^oF$ P = 24.3"Hg $\alpha = 0.000445/^oF$ d= 0.01 mm ℓ = 8 mm Rc = 32.52 ohms

γ	ΔT_{o_F}	Gr_{dc}	Re_{Lcrit}	$\frac{Gr}{Re_{Lcrit}^2}$	Nu	Re_{Ucrit}	$\frac{Gr}{Re_{Ucrit}^2}$	Nu
1.1	225	2704	-	-	-	-	-	-
1.2	450	5406	42	3.067	0.423	44.5	2.736	0.4103
1.3	675	8110	48.4	3.465	0.417	49.9	3.335	0.4100
1.4	900	10813	48.7	4.560	0.412	53.0	3.846	0.405
1.5	1125	13516	50.8	5.230	0.390	55.8	4.329	0.383
1.6	1350	16220	50.8	6.278	0.381	59.6	4.560	0.357
1.7	1575	18923	50.6	6.500	0.368	63.1	4.753	0.344
1.8	1800	21626	57.0	6.640	0.347	65.9	4.975	0.341
1.9	2025	24330	56.5	7.62	0.373	69.1	5.098	0.350

FIGURES

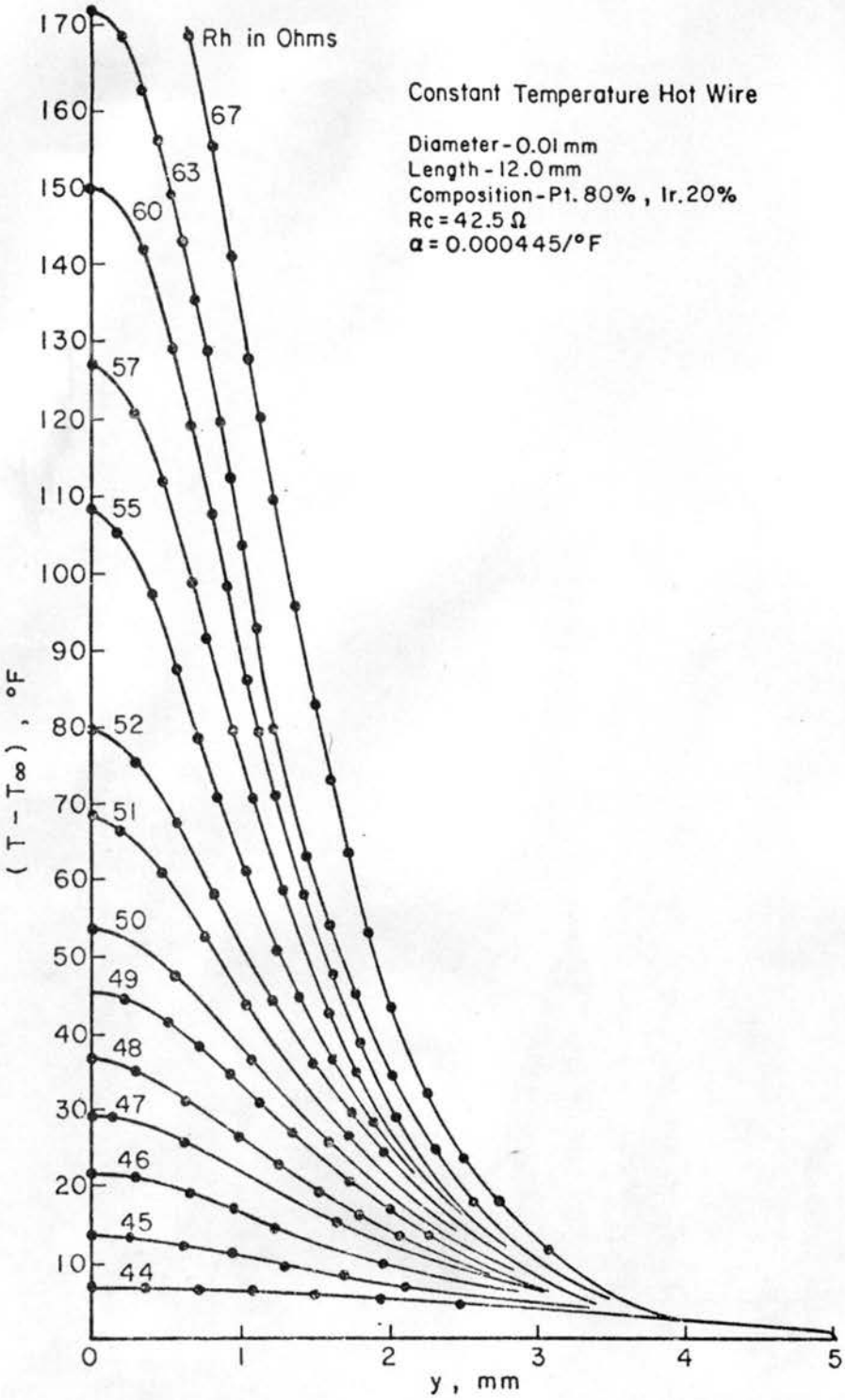

a) different cylinder resistances

Fig. 1. Temperature distribution within the hot core of the constant temperature cylinder; x = 0.25 mm.

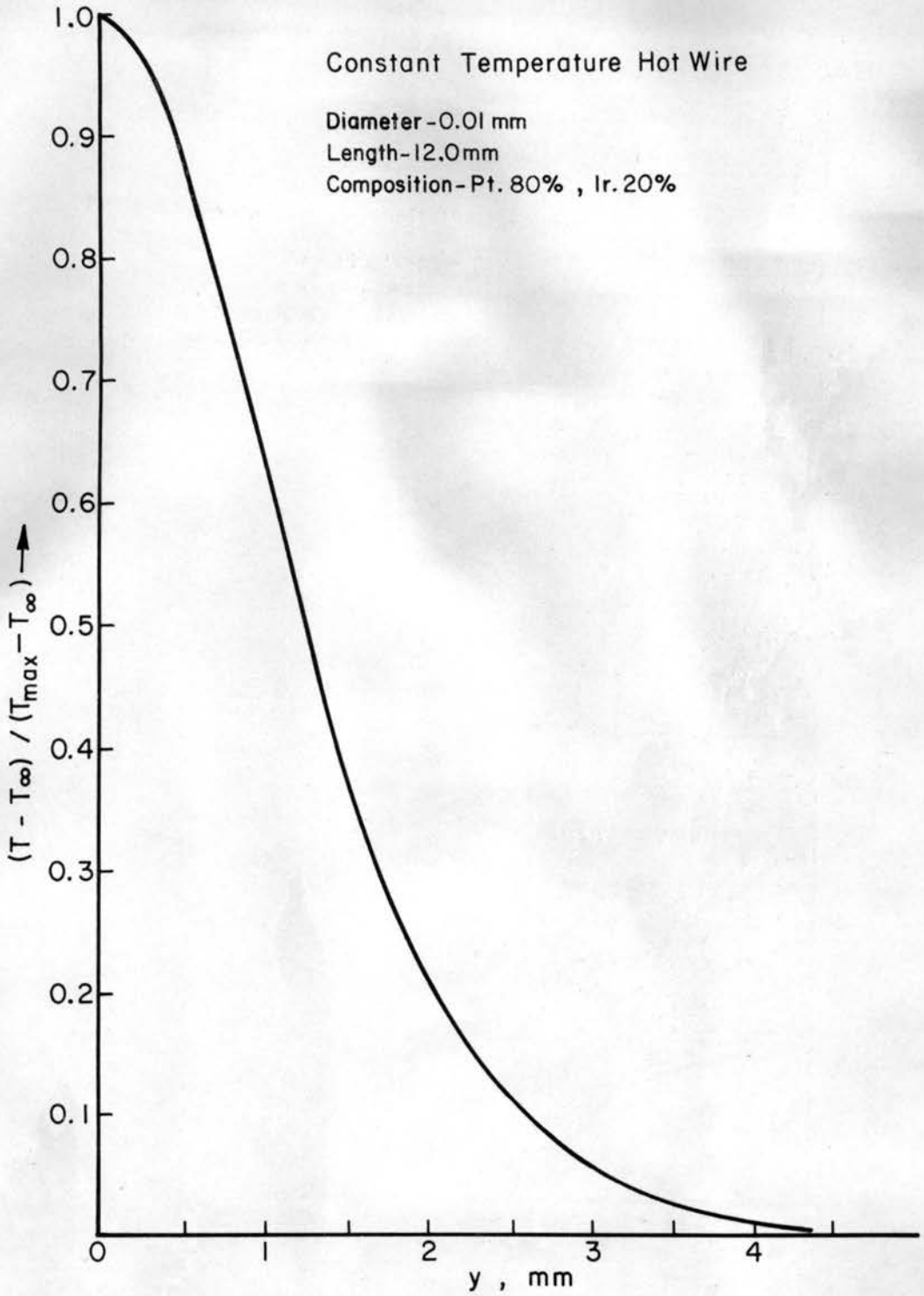

b) mean dimensionless temperature distribution

Fig. 1. (Concluded) Temperature distribution within the hot core of the constant temperature cylinder; x = 0.25 mm.

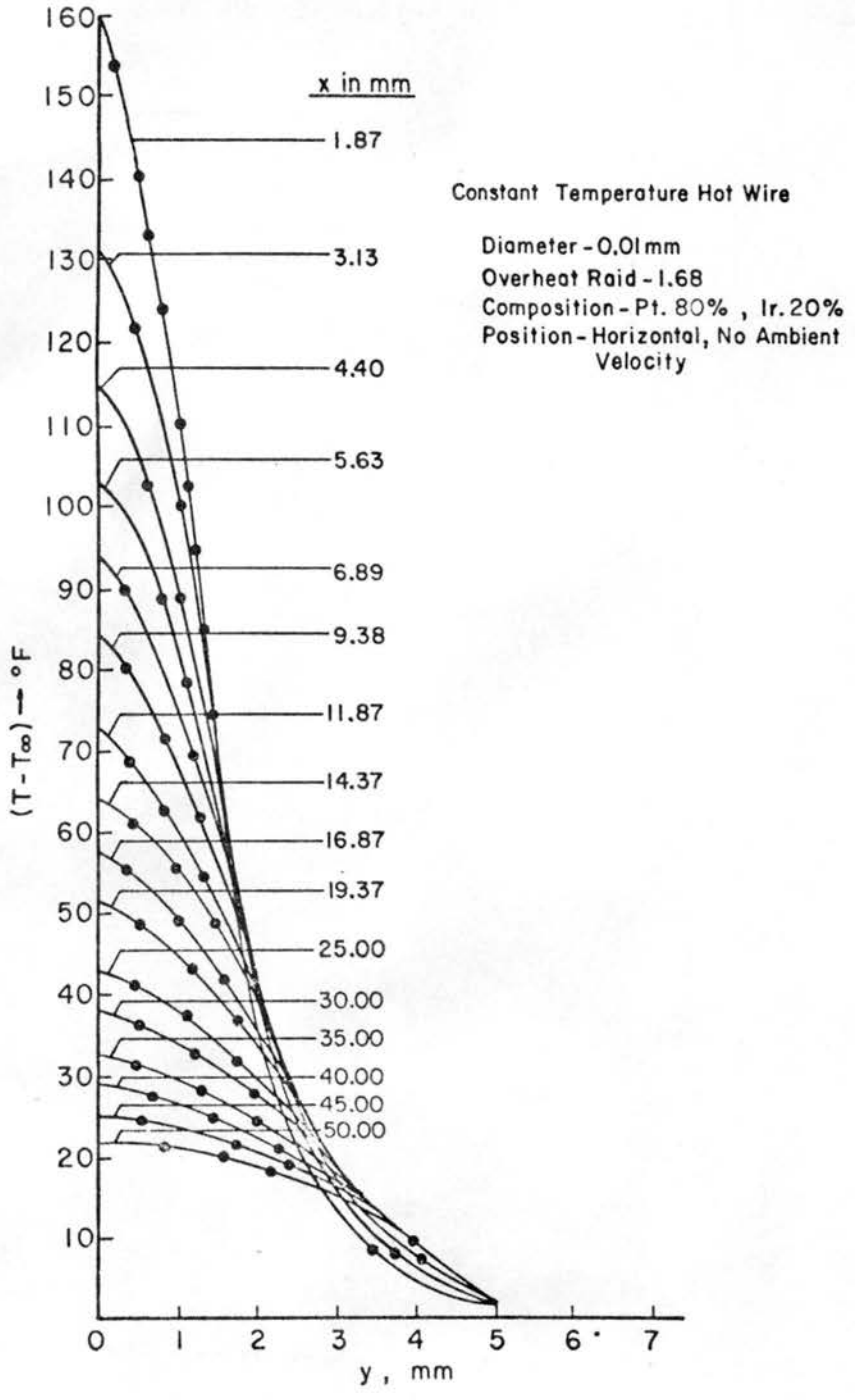

a) temperature distribution across the horizontal sections

Fig. 2. Survey of temperature in the rising plume of free convection from horizontal constant temperature cylinder; d = 0.01 mm, γ = 1.68.

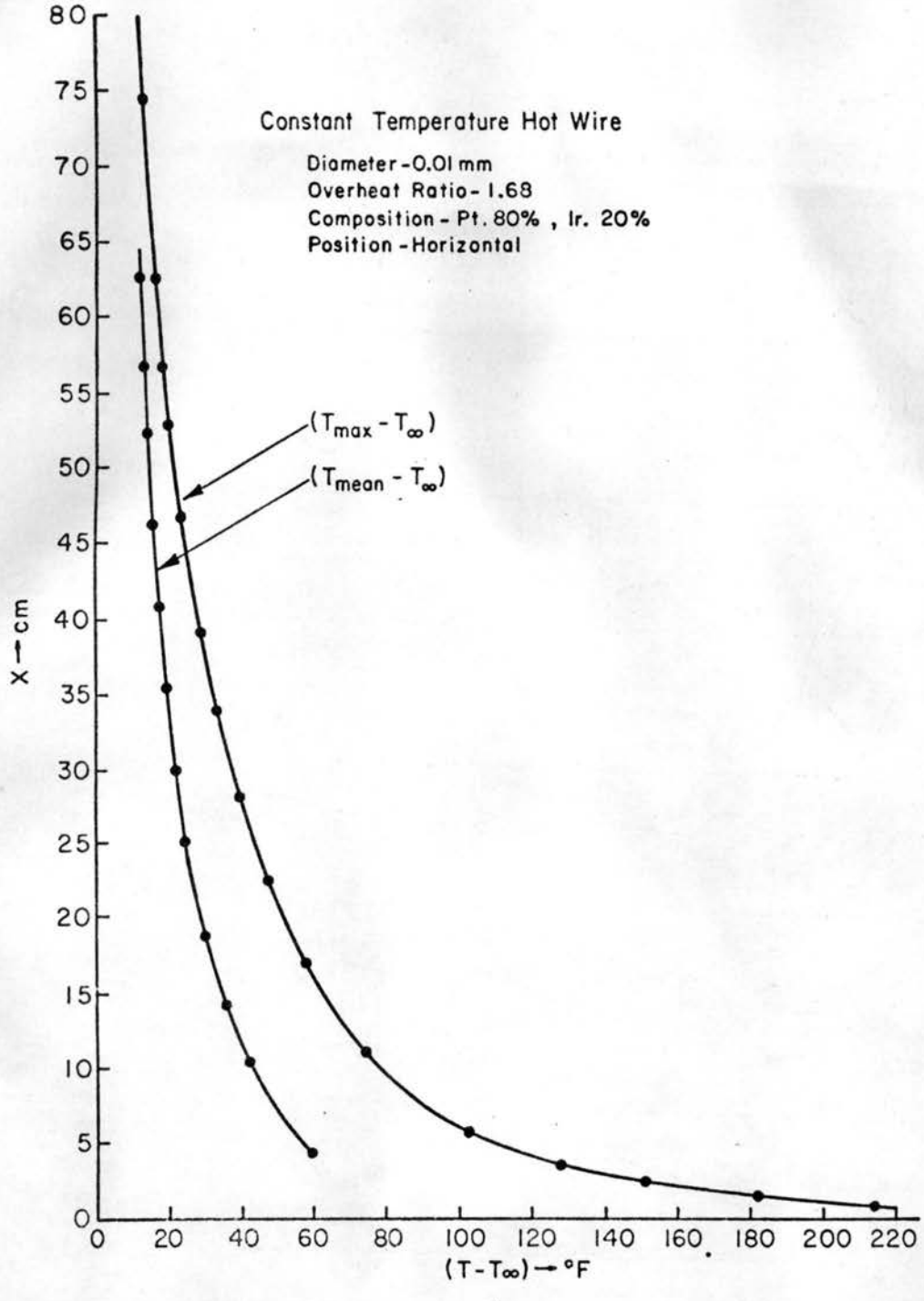

b) distribution of peak and mean temperature

Fig. 2. (Concluded) Survey of temperature in the rising plume of free convection from horizontal constant temperature cylinder; d = 0.01 mm, γ = 1.68.

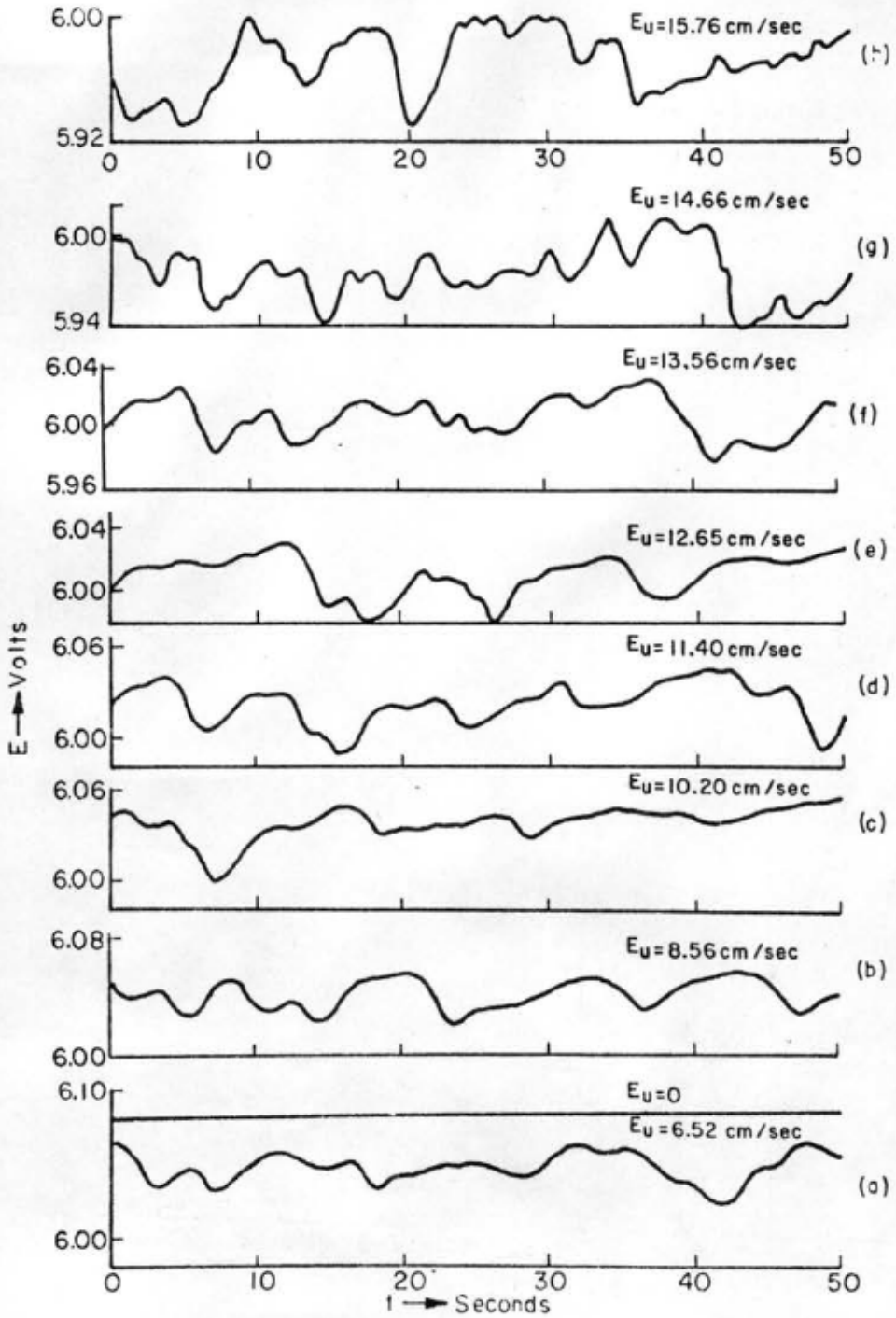

a - h

Fig. 3. Constant temperature hot cylinder output voltage as a function of time, d = 0.01 mm, γ = 1.9, $T_\omega - T_\infty$ = 2020°F, ambient flow directly opposing the free convection.

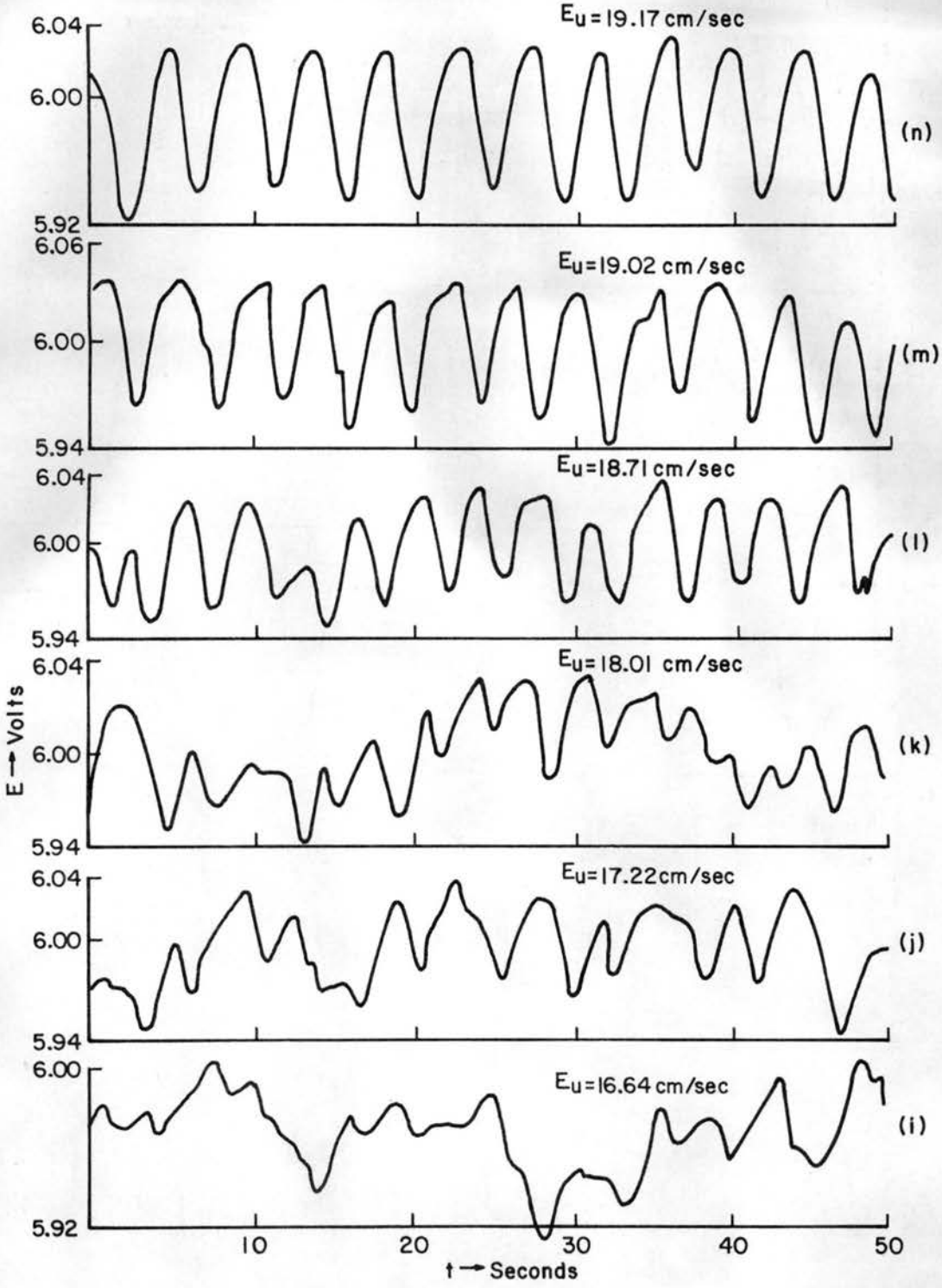

i - n

Fig. 3. (Cont.) Constant temperature hot cylinder output voltage as a function of time, d = 0.01 mm, γ = 1.9, $T_\omega - T_\infty$ = 2020°F, ambient flow directly opposing the free convection.

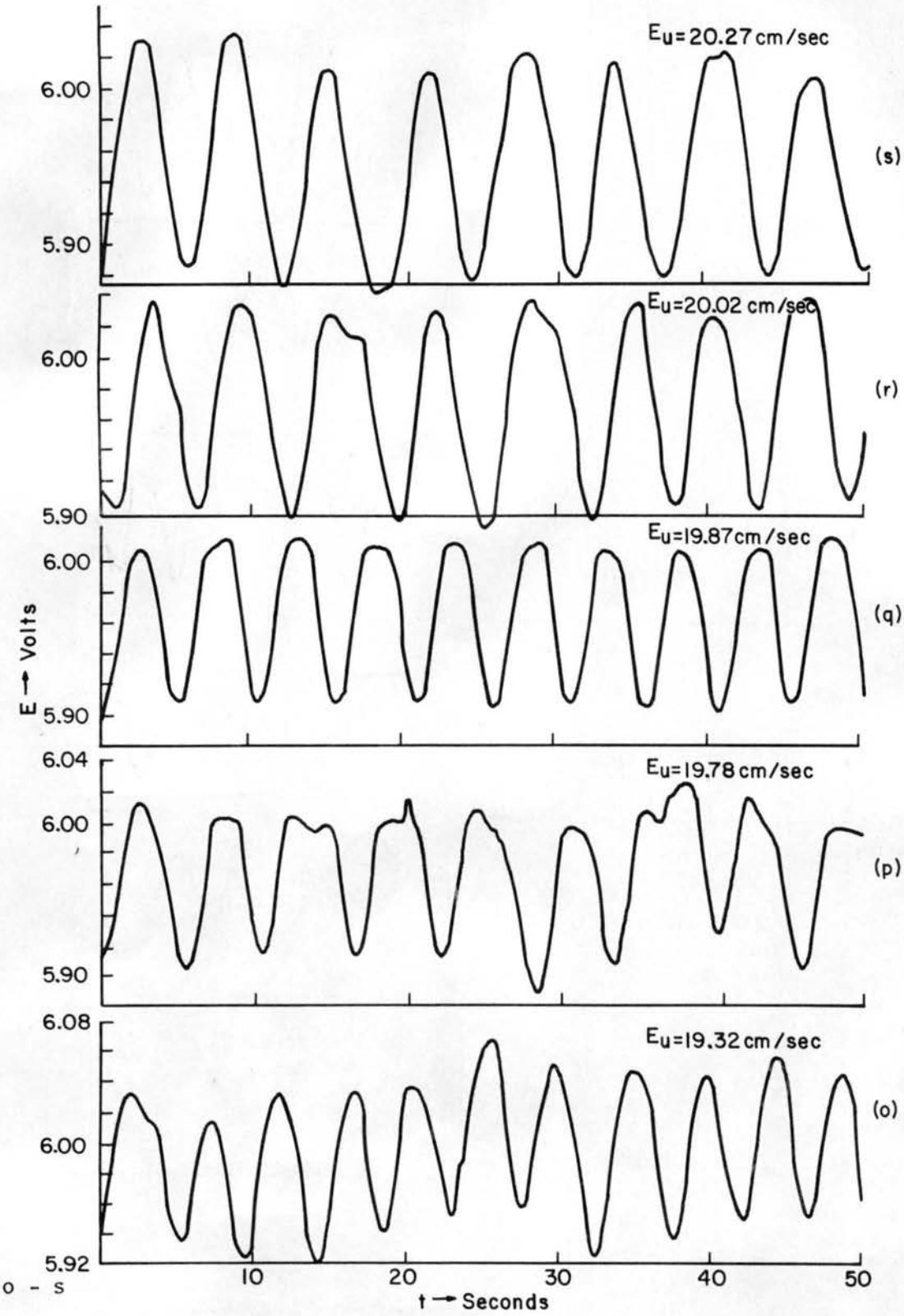

Fig. 3. (Cont.) Constant temperature hot cylinder output voltage as a function of time, d = 0.01 mm, γ = 1.9, $T_\omega - T_\infty$ = 2020°F, ambient flow directly opposing the free convection.

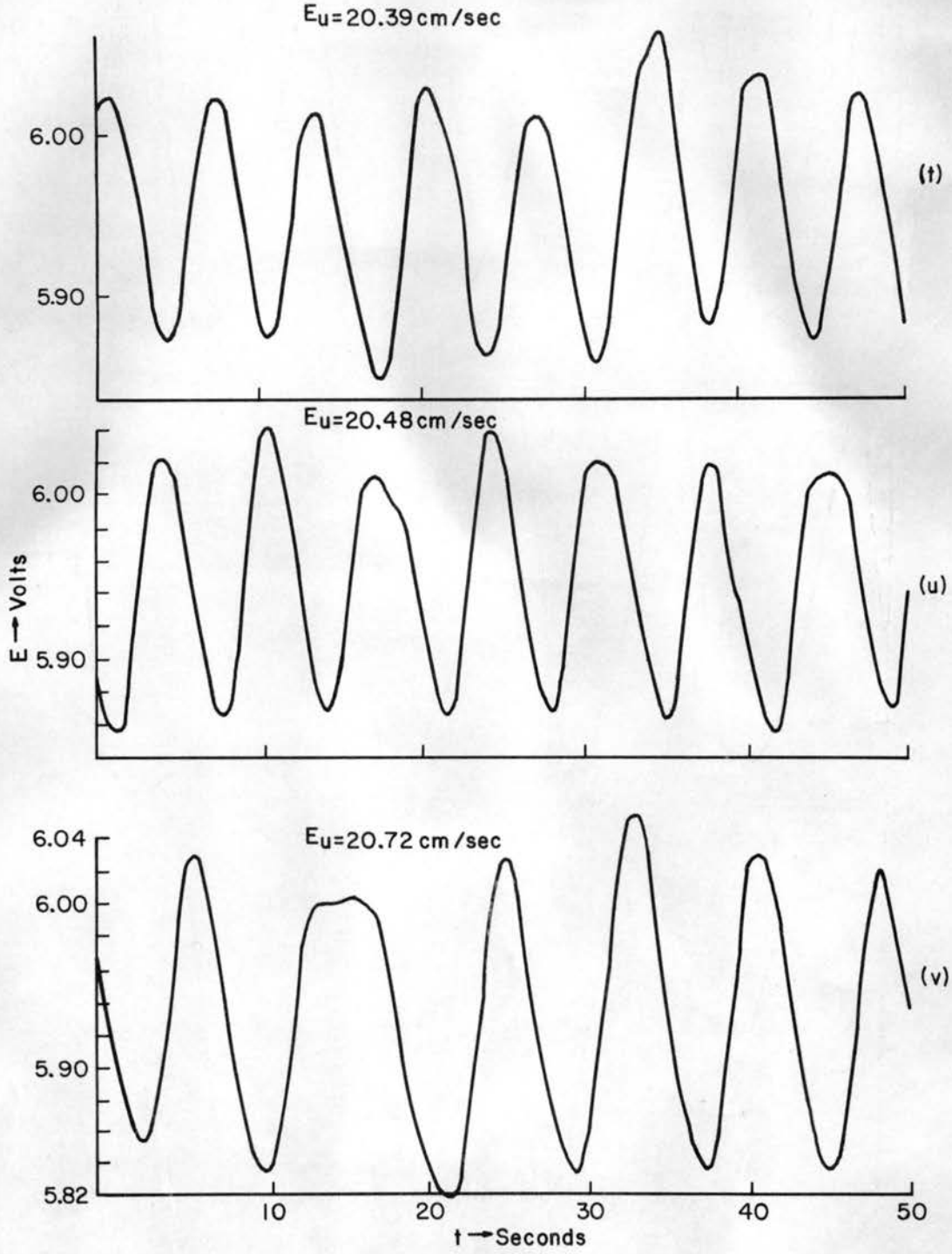

t - v

Fig. 3. (Cont.) Constant temperature hot cylinder output voltage as a function of time, d = 0.01 mm, γ = 1.9, $T_\omega - T_\infty$ = 2020°F, ambient flow directly opposing the free convection.

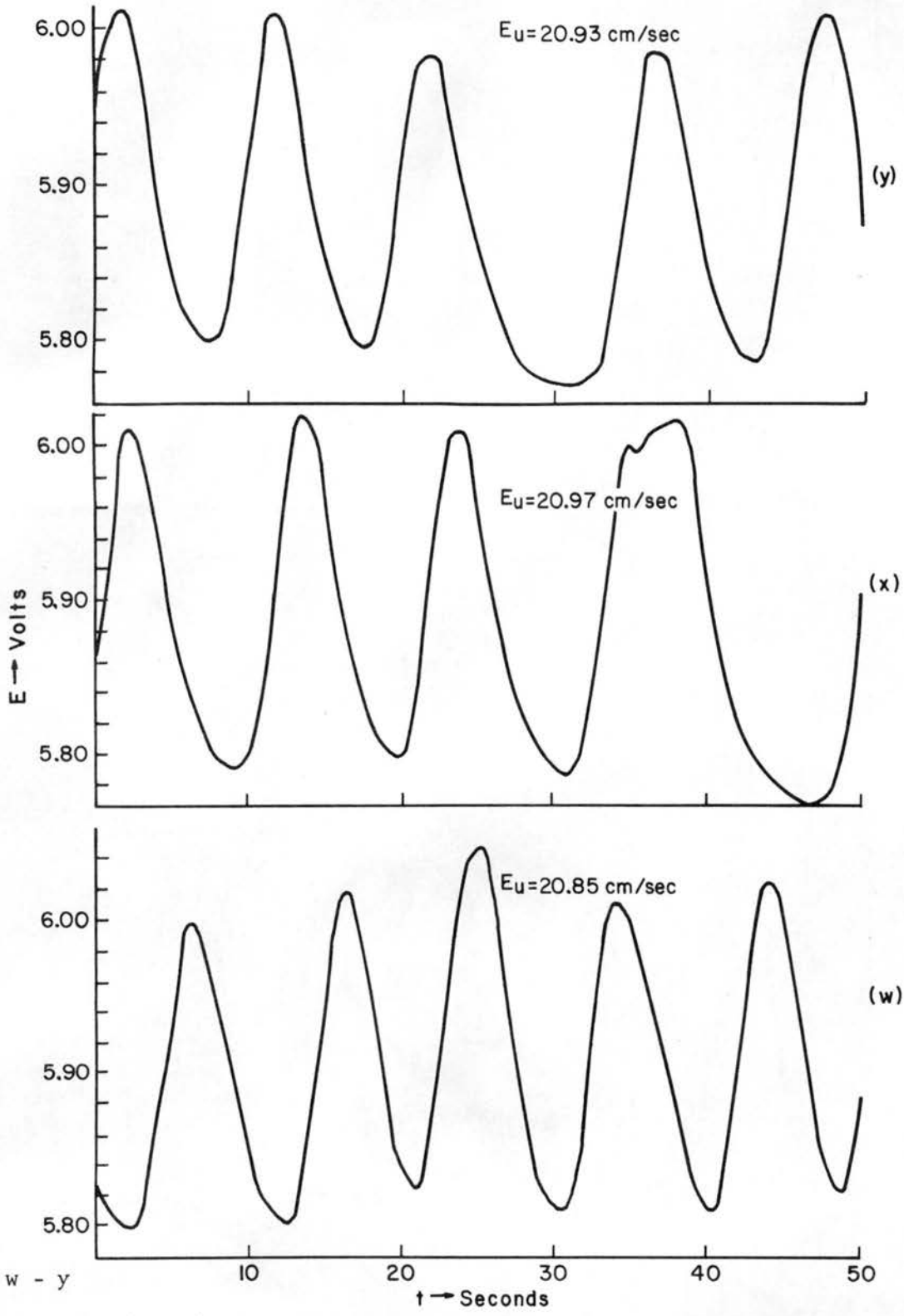

Fig. 3. (Cont.) Constant temperature hot cylinder output voltage as a function of time, d = 0.01 mm, γ = 1.9, $T_\omega - T_\infty$ = 2020°F, ambient flow directly opposing the free convection.

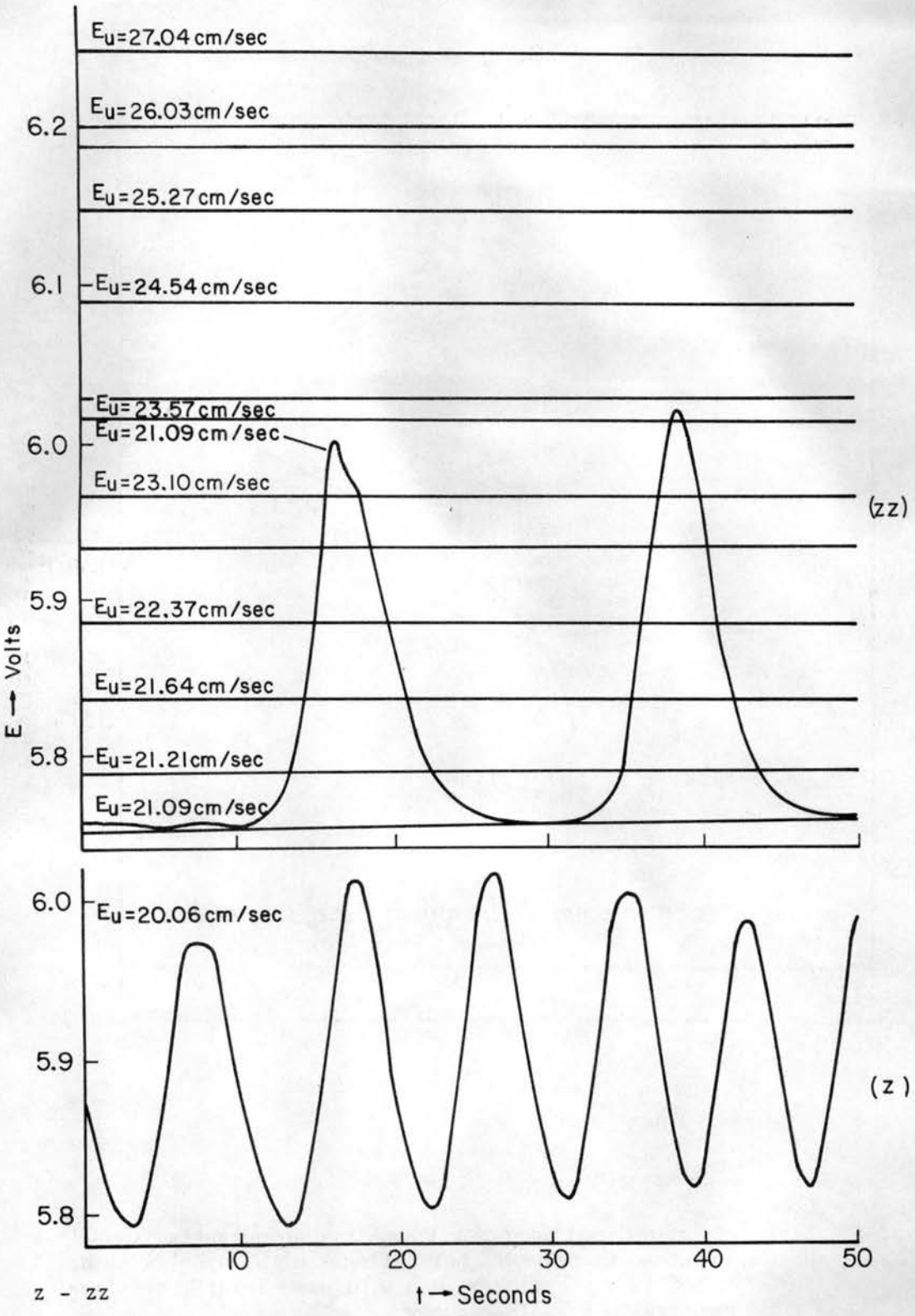

Fig. 3. (Concluded) Constant temperature hot cylinder output voltages as a function of time, d = 0.01 mm, γ = 1.9, $T_\omega - T_\infty$ = 2020°F, ambient flow directly opposing the free convection.

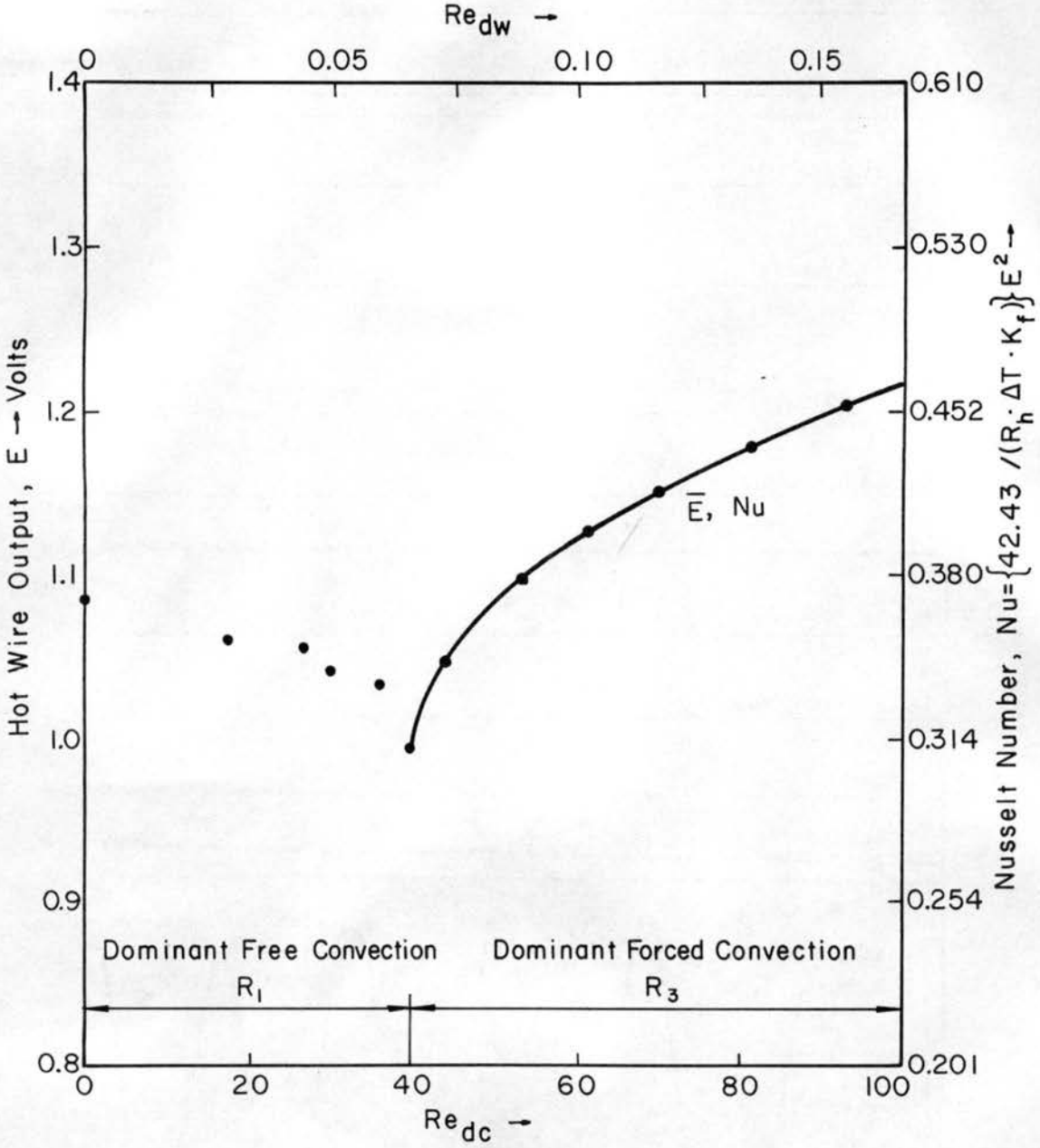

a) $\gamma = 1.1$, $T_\omega - T_\infty = 225°F$, $Gr_{dc} = 2700$

Fig. 4. Variation of Nusselt number and mean bridge output voltage of the constant temperature hot cylinder with Reynolds number for a Pt 80% Ir 20% cylinder, d = 0.01 mm. Insert variation of frequency with Reynolds number.

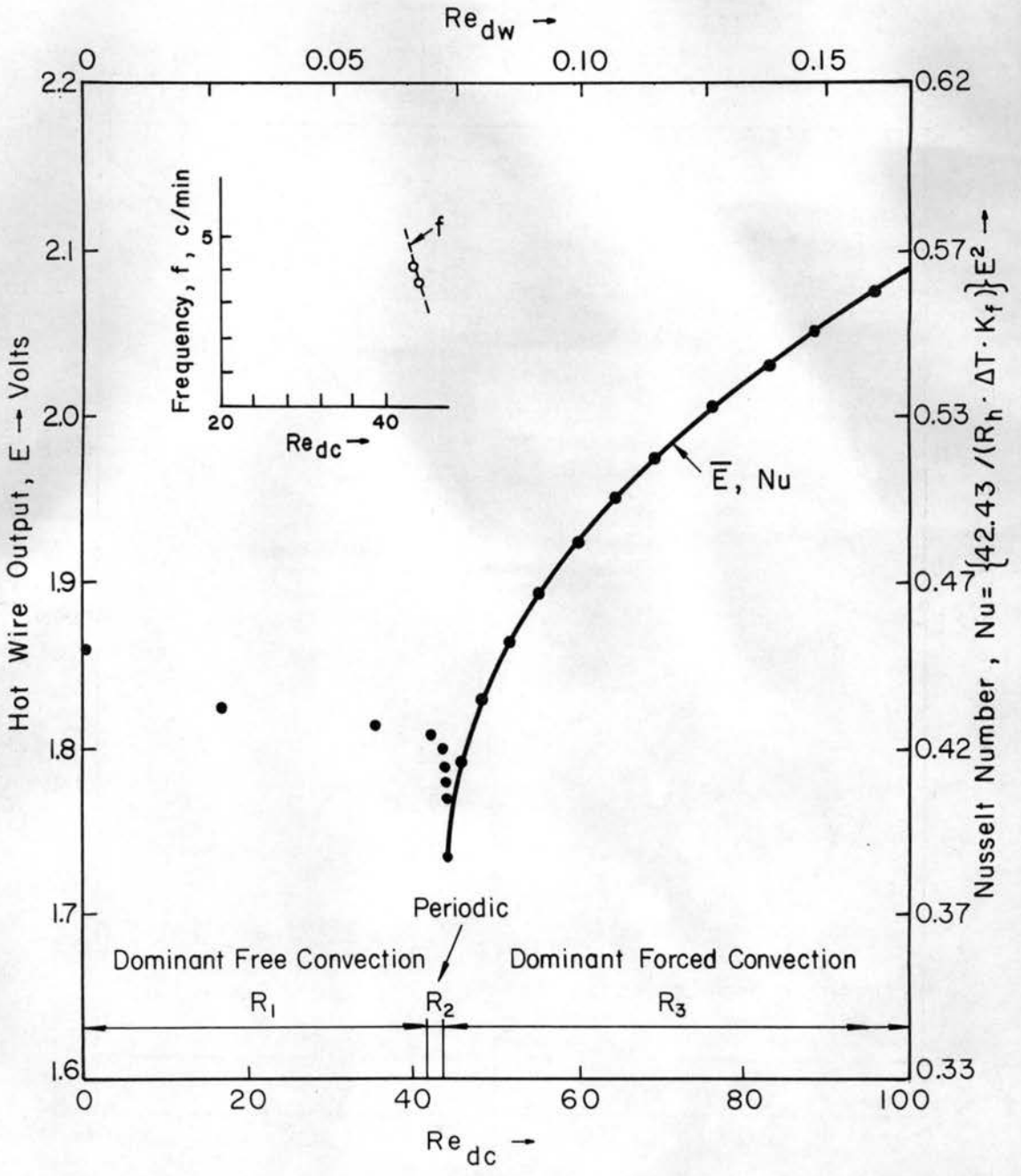

b) $\gamma = 1.2$, $T_\omega - T_\infty = 450°F$, $Gr_{dc} = 5400$

Fig. 4. (Cont.) Variation of Nusselt number and mean bridge output voltage of the constant temperature hot cylinder with Reynolds number for a Pt 80% Ir 20% cylinder, d = 0.01 mm. Insert; variation of frequency with Reynolds number.

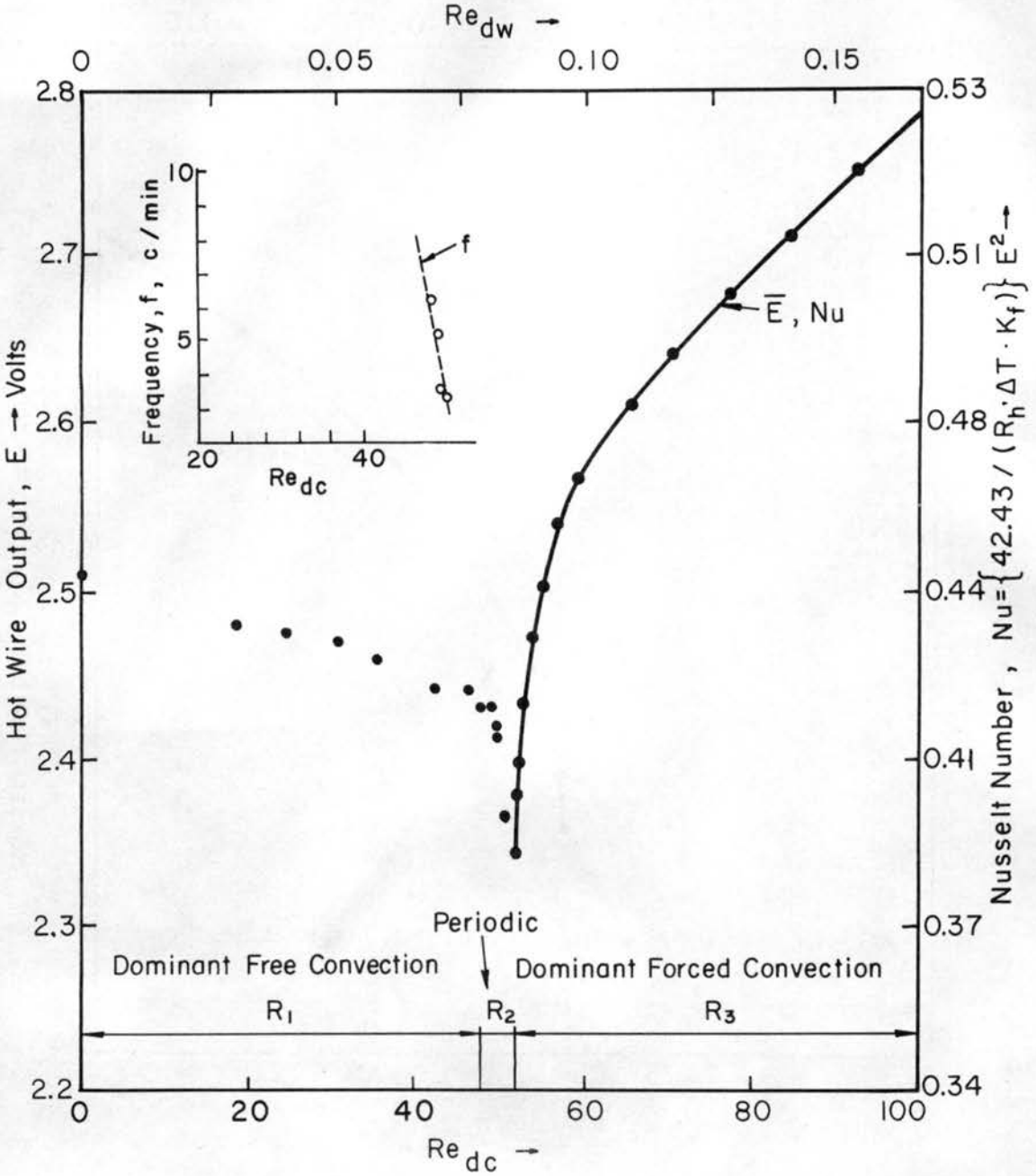

c) $\gamma = 1.3$, $T_\omega - T_\infty = 675°F$, $Gr_{dc} = 8110$

Fig. 4. (Cont.) Variation of Nusselt number and mean bridge output voltage of the constant temperature hot cylinder with Reynolds number for a Pt 80% Ir 20% cylinder, d = 0.01 mm. Insert: variation of frequency with Reynolds number.

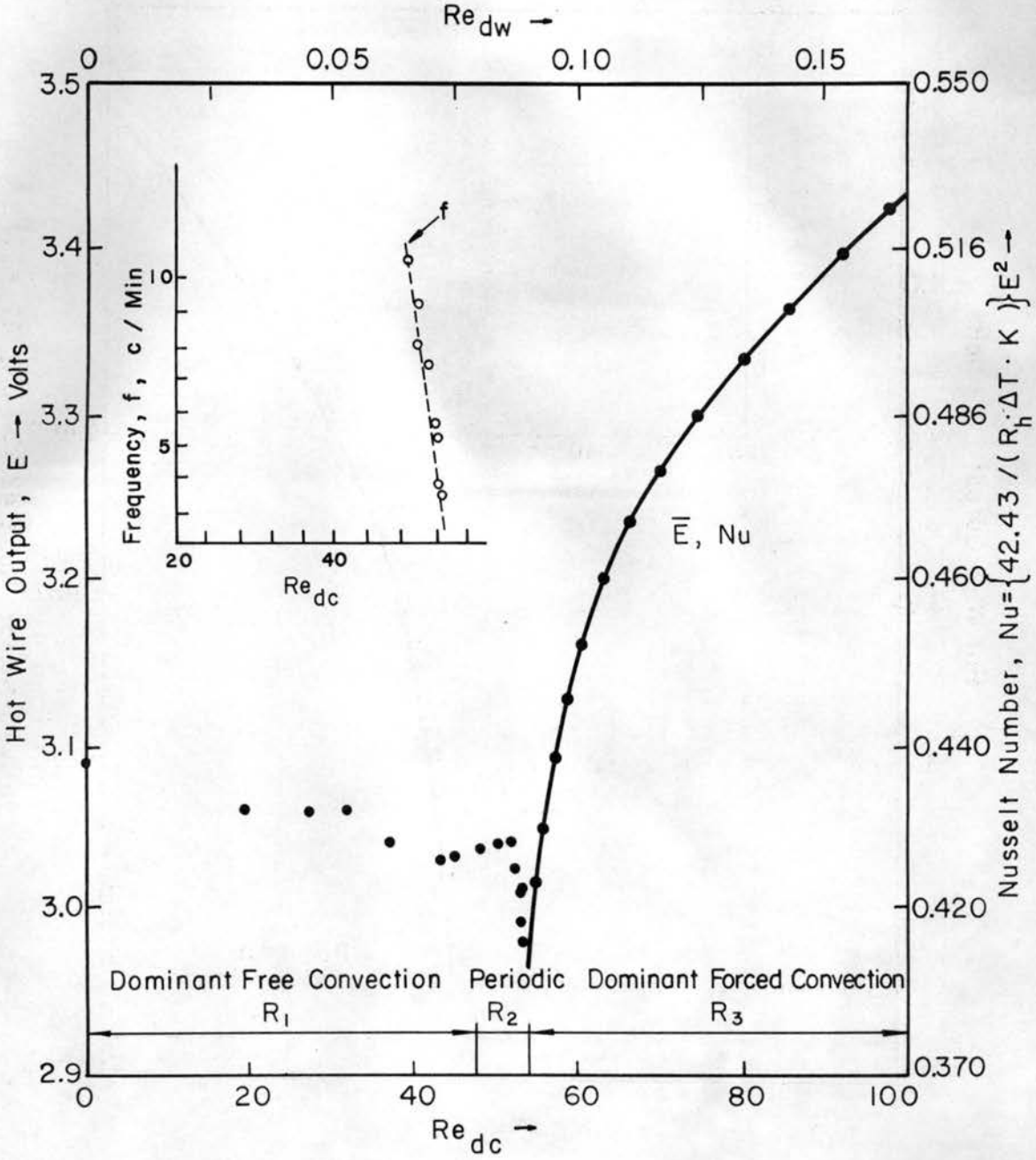

d) $\gamma = 1.4$, $T_\omega - T_\infty = 900°F$, $Gr_{dc} = 10810$

Fig. 4. (Cont.) Variation of Nusselt number and mean bridge output voltage of the constant temperature hot cylinder with Reynolds number for a Pt 80% Ir 20% cylinder, d = 0.01 mm. Insert: variation of frequency with Reynolds number.

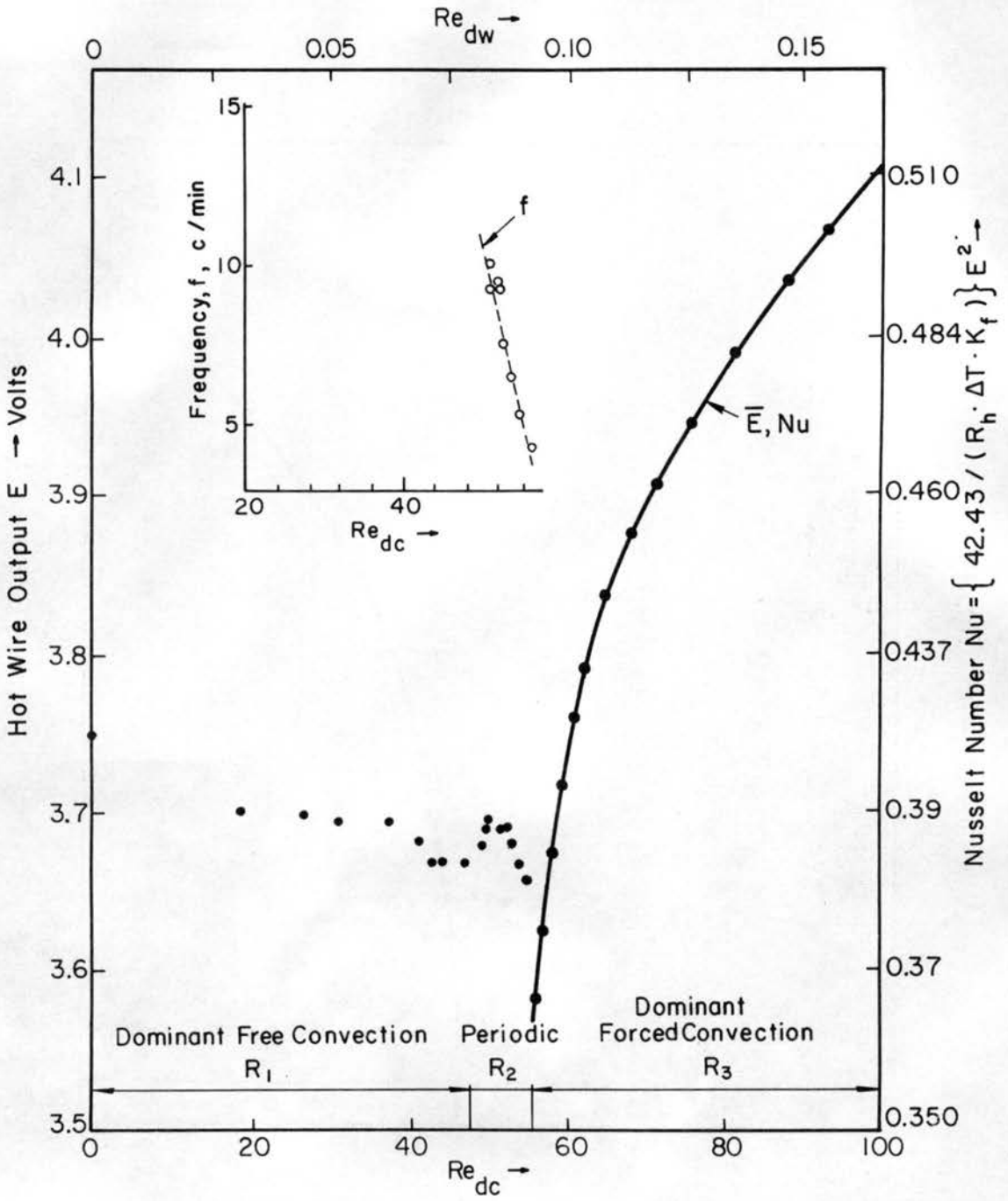

e) $\gamma = 1.5$, $T_\omega - T_\infty = 1125°F$, $Gr_{dc} = 13520$

Fig. 4. (Cont.) Variation of Nusselt number and mean bridge output voltage of the constant temperature hot cylinder with Reynolds number for a Pt 80% Ir 20% cylinder, d = 0.01 mm. Insert: variation of frequency with Reynolds number.

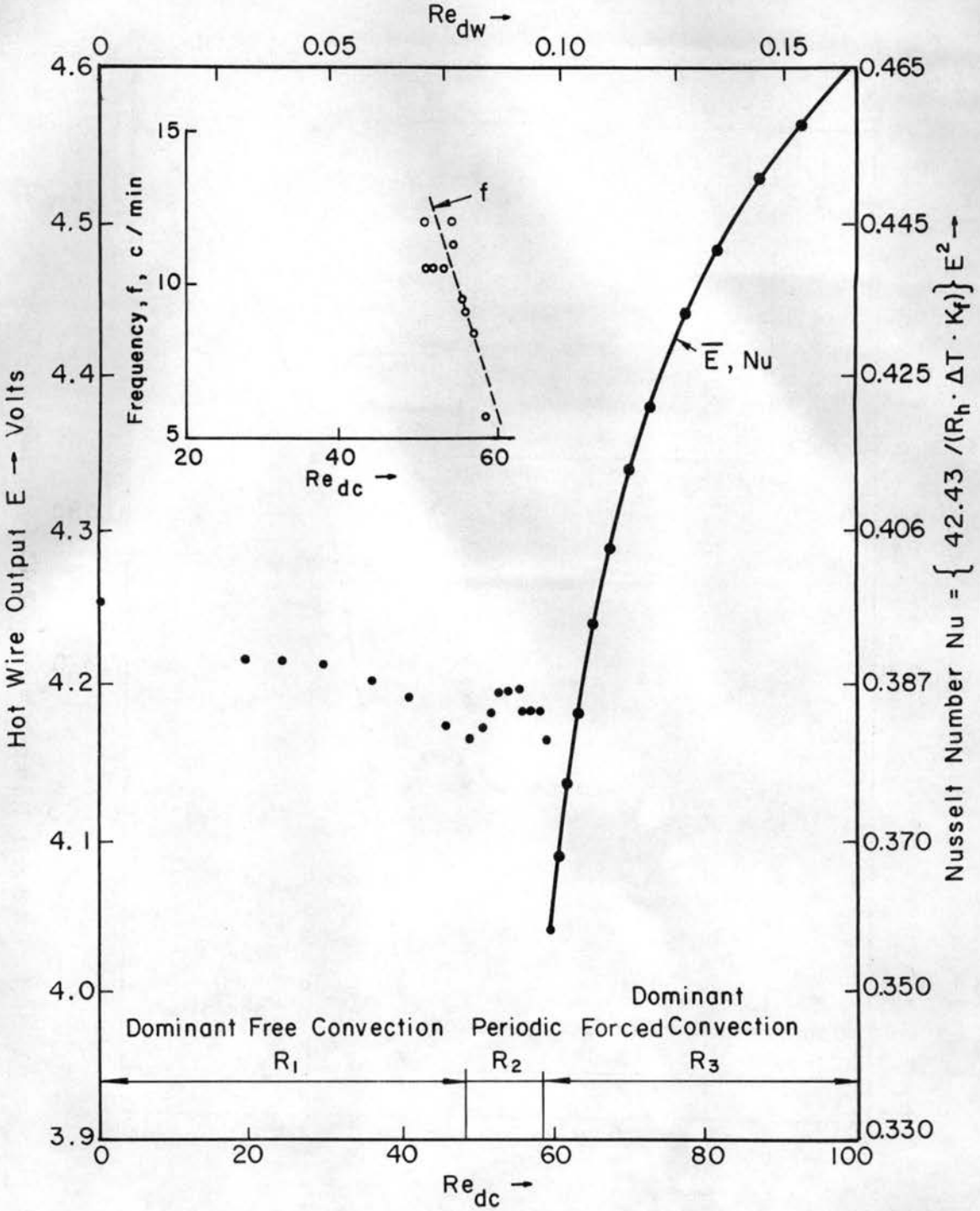

f) $\gamma = 1.6$, $T - T = 1348°F$, $Gr_{dc} = 16220$

Fig. 4. (Cont.) Variation of Nusselt number and mean bridge output voltage of the constant temperature hot cylinder with Reynolds number for a Pt 80% Ir 20% cylinder, d = 0.01 mm. Insert: variation of frequency with Reynolds number.

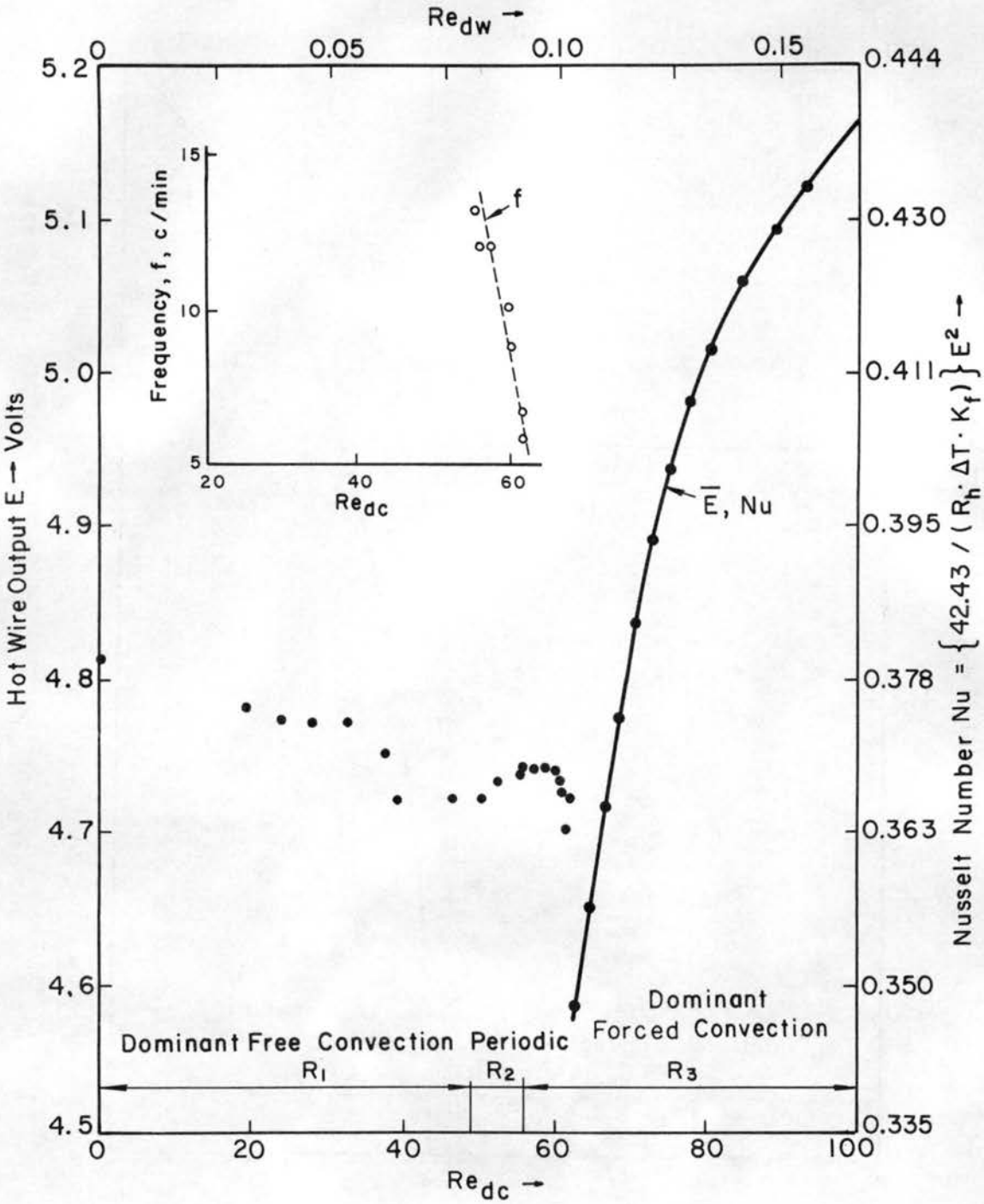

g) $\gamma = 1.7$, $T_\omega - T_\infty = 1575°F$, $Gr_{dc} = 18920$

Fig. 4. (Cont.) Variation of Nusselt number and mean bridge output voltage of the constant temperature hot cylinder with Reynolds number for a Pt 80% Ir 20% cylinder, d = 0.01 mm. Insert: variation of frequency with Reynolds number.

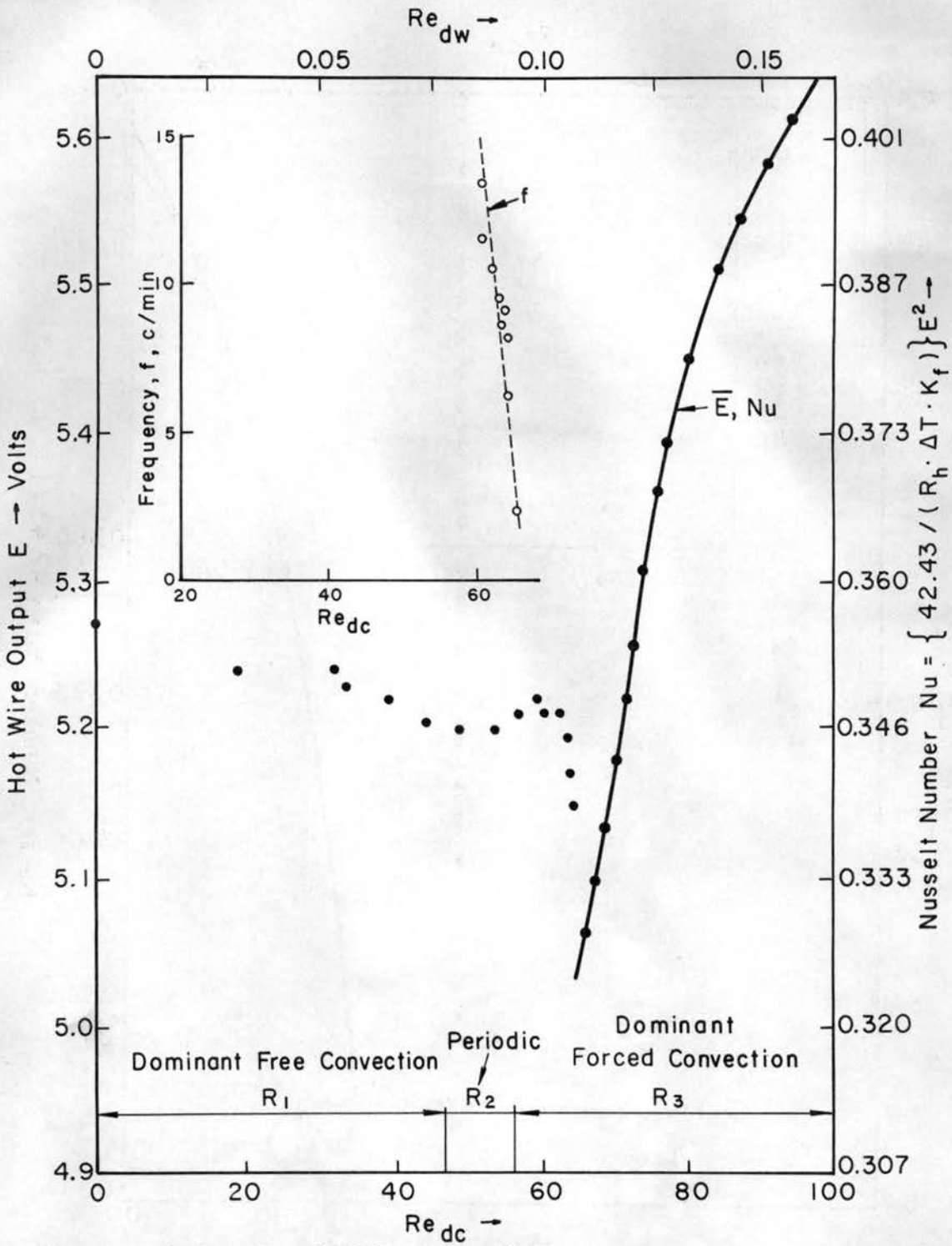

h) $\gamma = 1.8$, $T_\omega - T_\infty = 1800°F$, $Gr_{dc} = 21625$

Fig. 4. (Cont.) Variation of Nusselt number and mean bridge output voltage of the constant temperature hot cylinder with Reynolds number for a Pt 80% Ir 20% cylinder, d = 0.01 mm. Insert: variation of frequency with Reynolds number.

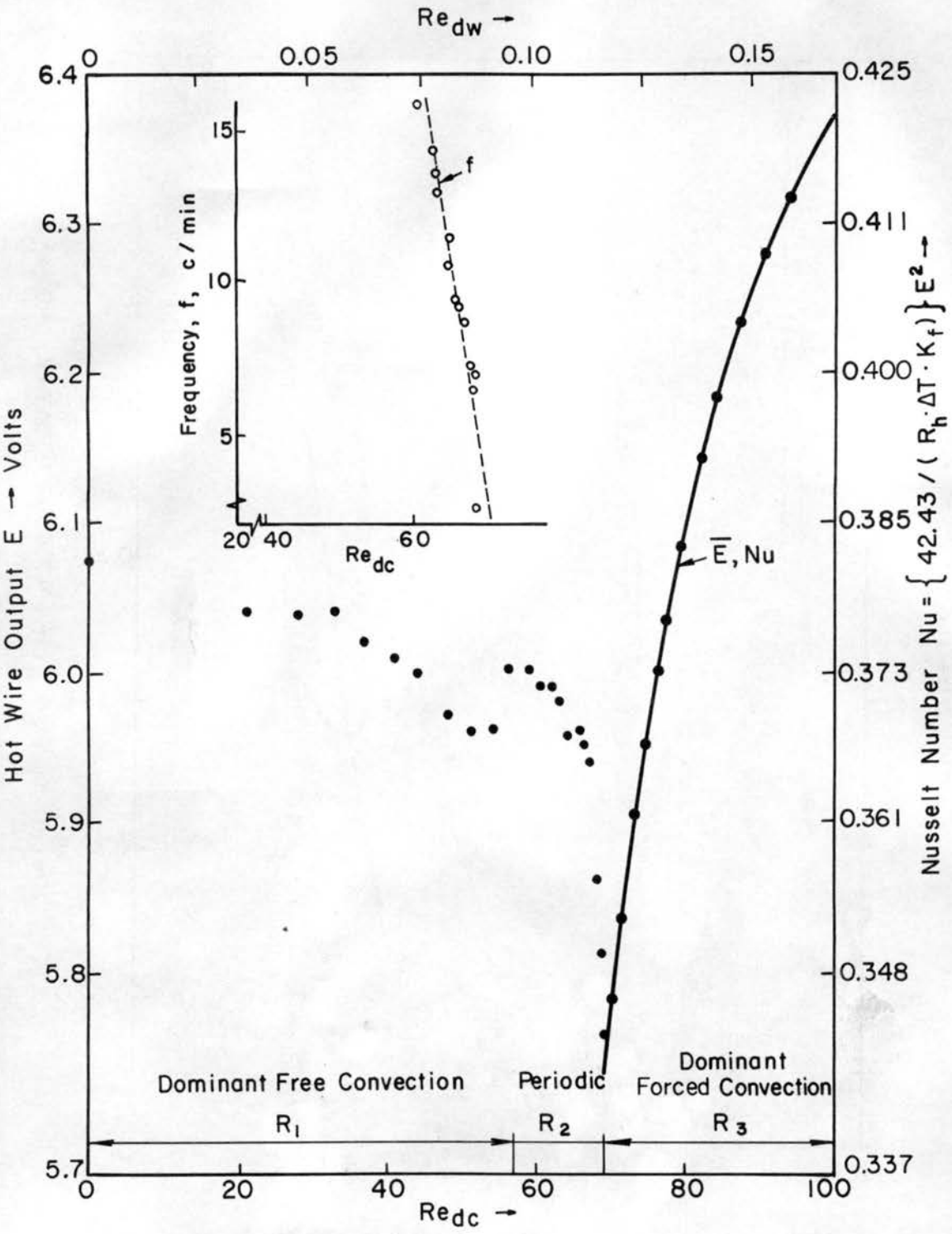

i) $\gamma = 1.9$, $T_\omega - T_\infty = 2020°F$, $Gr_{dc} = 24330$

Fig. 4. (Concluded) Variation of Nusselt number and mean bridge output voltage of the constant temperature hot cylinder with Reynolds number for a Pt 80% Ir 20% cylinder, d = 0.01 mm. Insert: variation of frequency with Reynolds number.

8 16 24 32 40 48 56 64 72 80 88 96 104 112 120 128 186 144 152 160 168 176

Fig. 5. Series of flow visualization pictures showing periodic movement of laminar sheet shrouding the hot cylinder under the influence of directly opposed free and forced convection heat transfer; interval approximately 1/16 second.

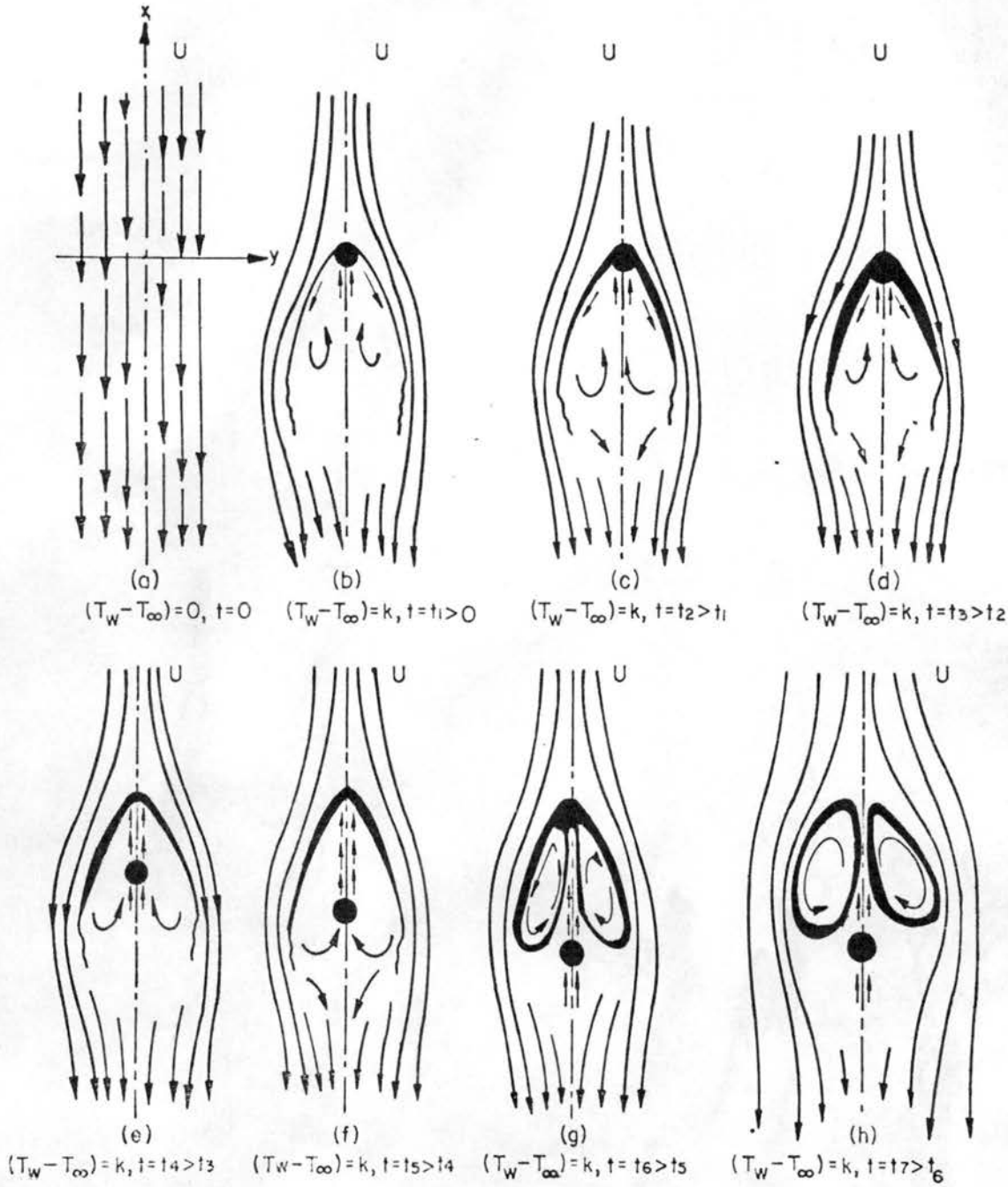

a - h

Fig. 6. Sketches showing the overall mechanism of periodic heat transfer from horizontal heated cylinder during directly opposed equal free and forced convection approximately to full scale.

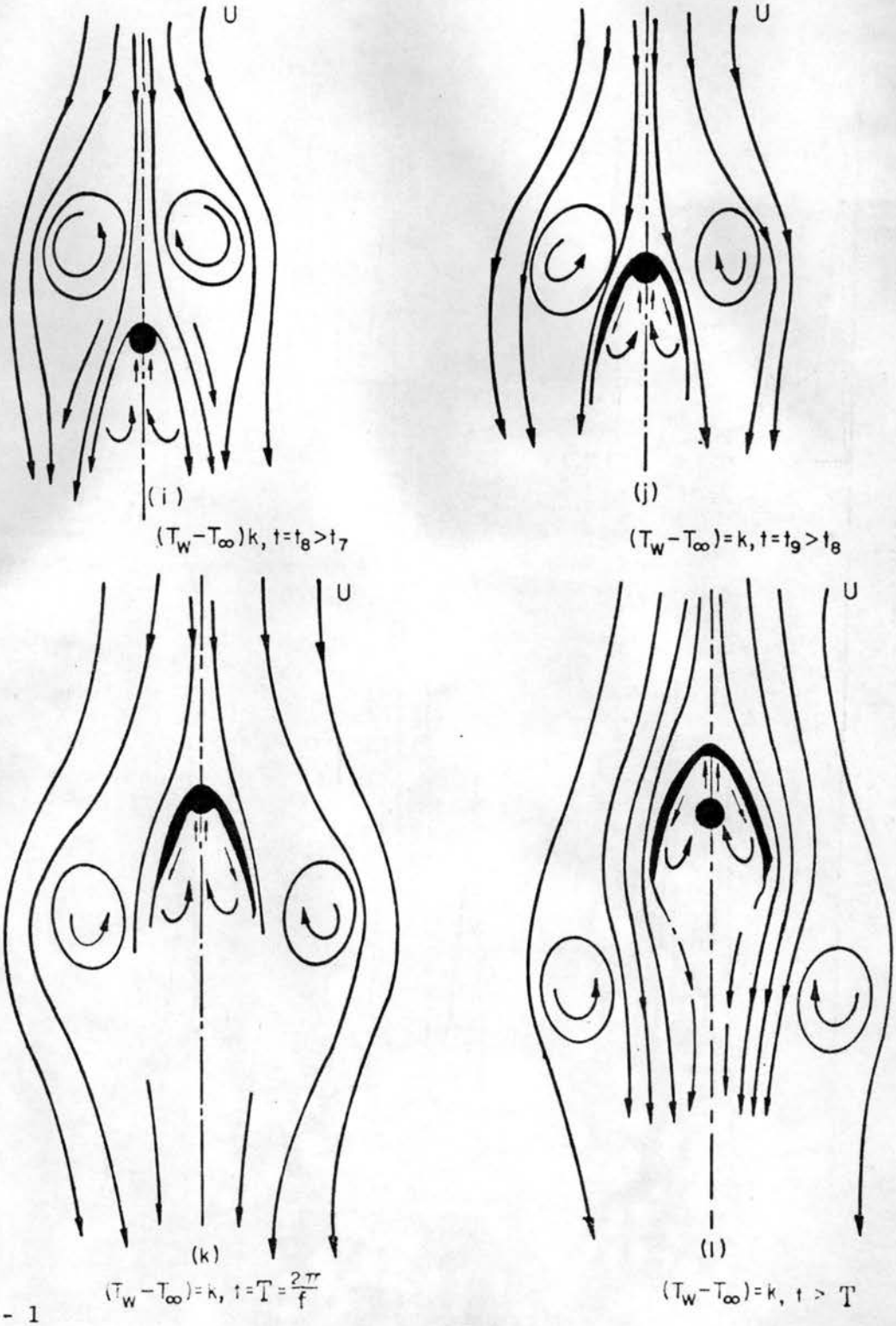

i - 1

Fig. 6. (Concluded) Sketches showing the overall mechanism of periodic heat transfer from horizontal heated cylinder during directly opposed equal free and forced convection approximately to full scale.

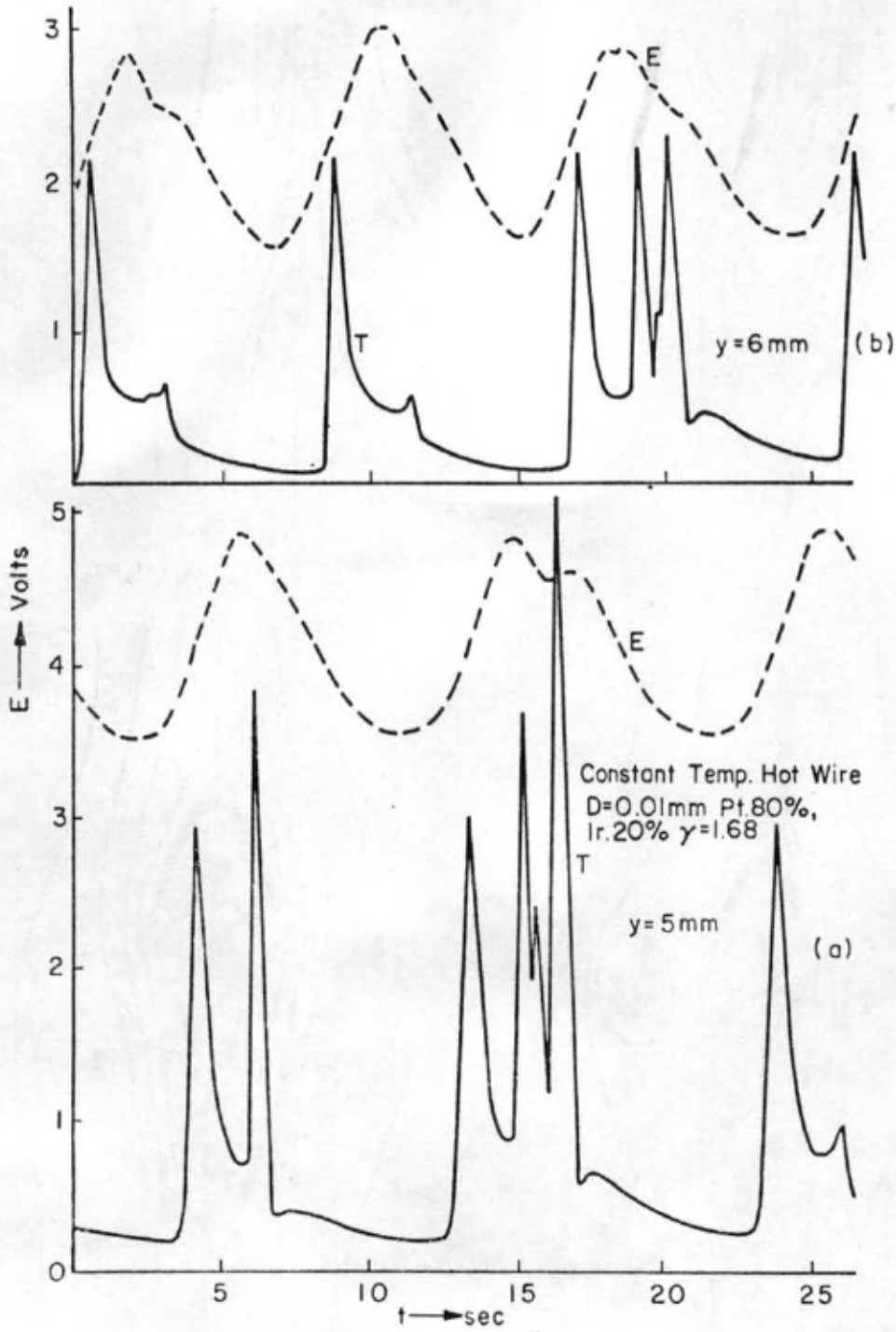

a - b

Fig. 7. Thermals due to constant temperature heating; observation recording the movement of laminar sheet, temperature variation at x = 5.1 mm and corresponding hot cylinder output voltage at a scale of E = 20 mv/cm and T = 5°F/cm.

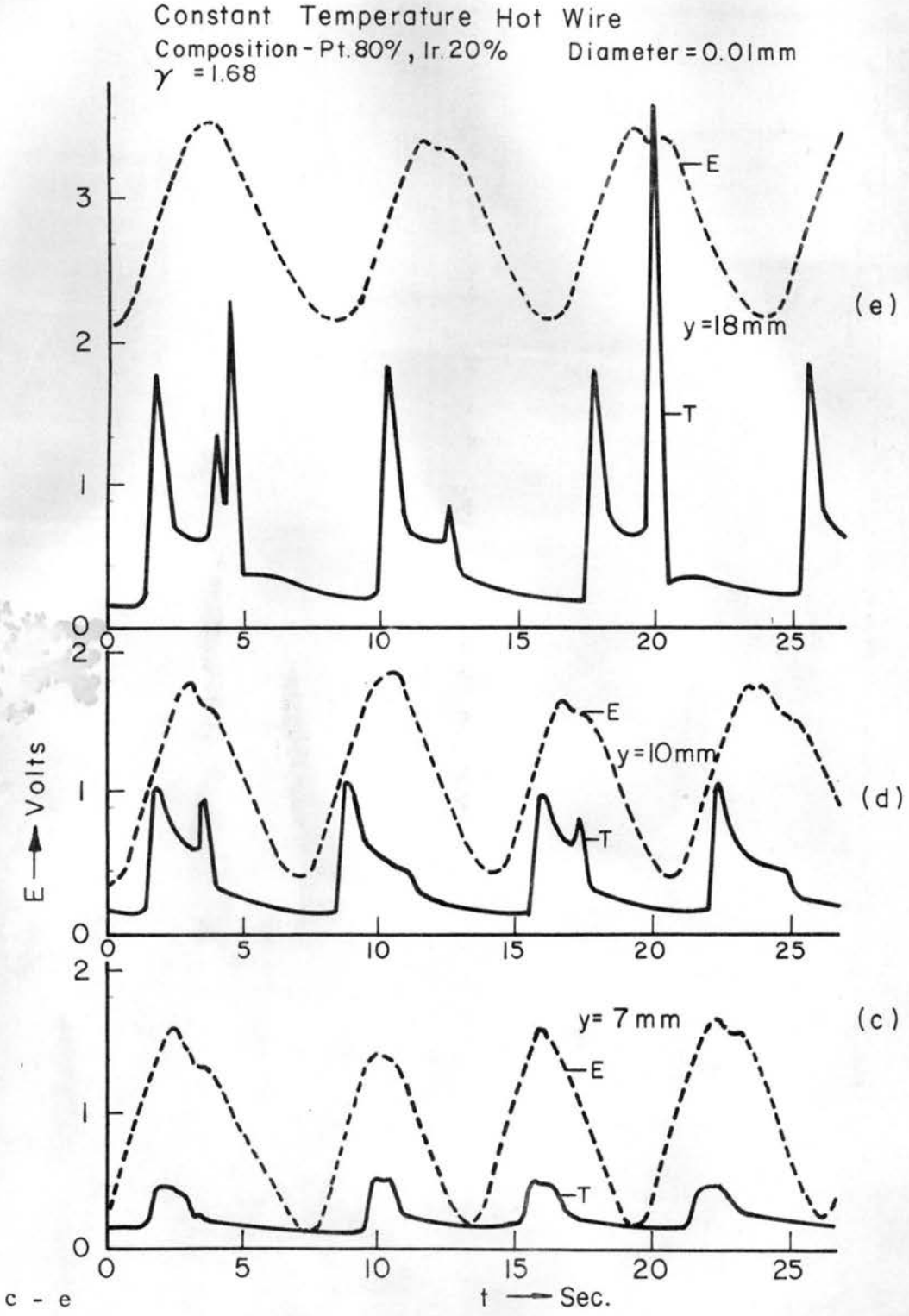

Fig. 7. (Concluded) Thermals due to constant temperature heating; observation recording the movement of laminar sheet, temperature variation at x = 5.1 mm and corresponding hot cylinder output voltage at a scale of E = 20 mv/cm and T = 5°F/cm.

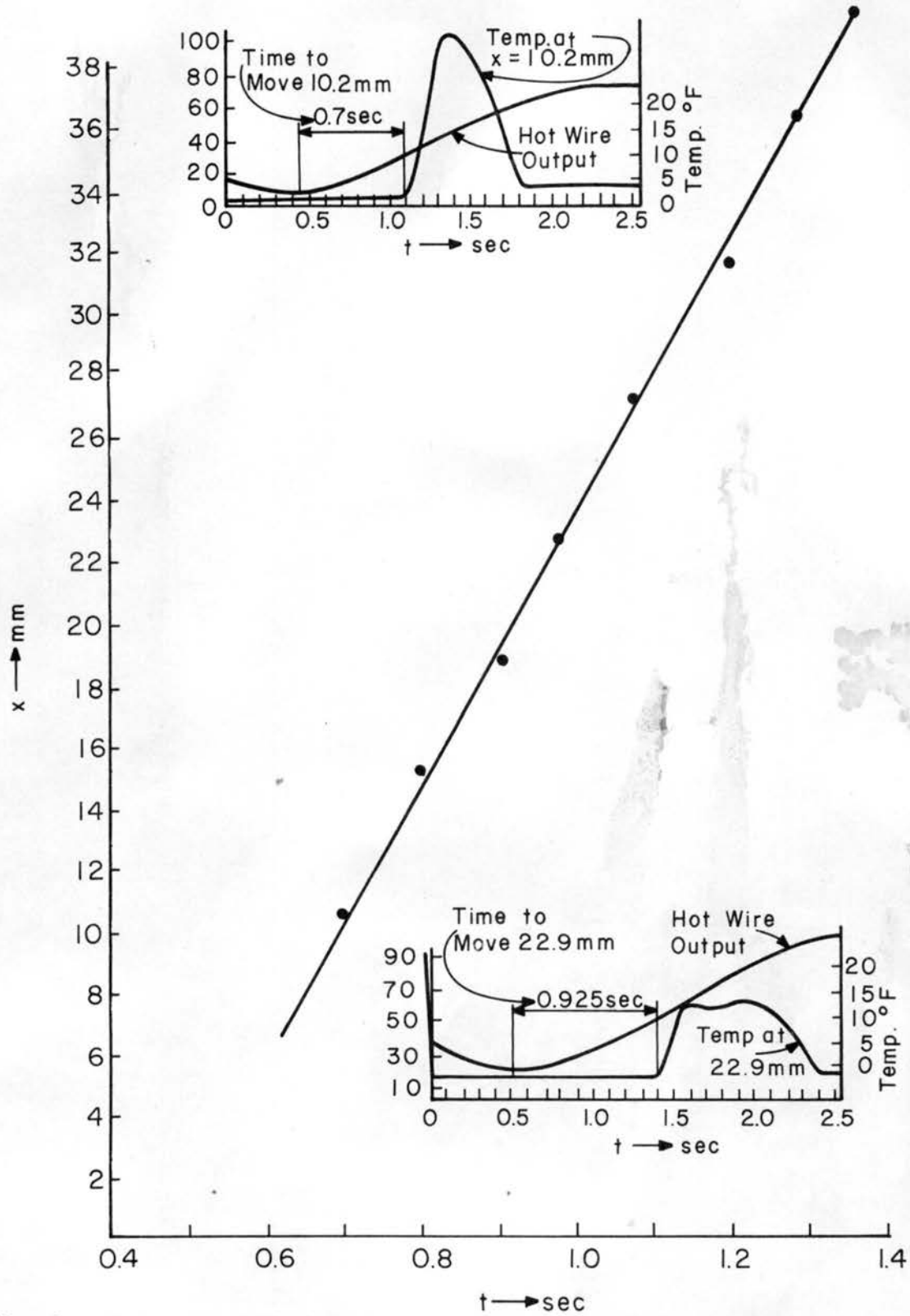

Fig. 8. Time space history of a laminar sheet during its periodic oscillation for Pt 80% Ir 20% cylinder, d = 0.01 mm, γ = 1.68. Inserts: Recordings to show the time taken by the laminar sheet to move 10.2 mm and 22.9 mm.

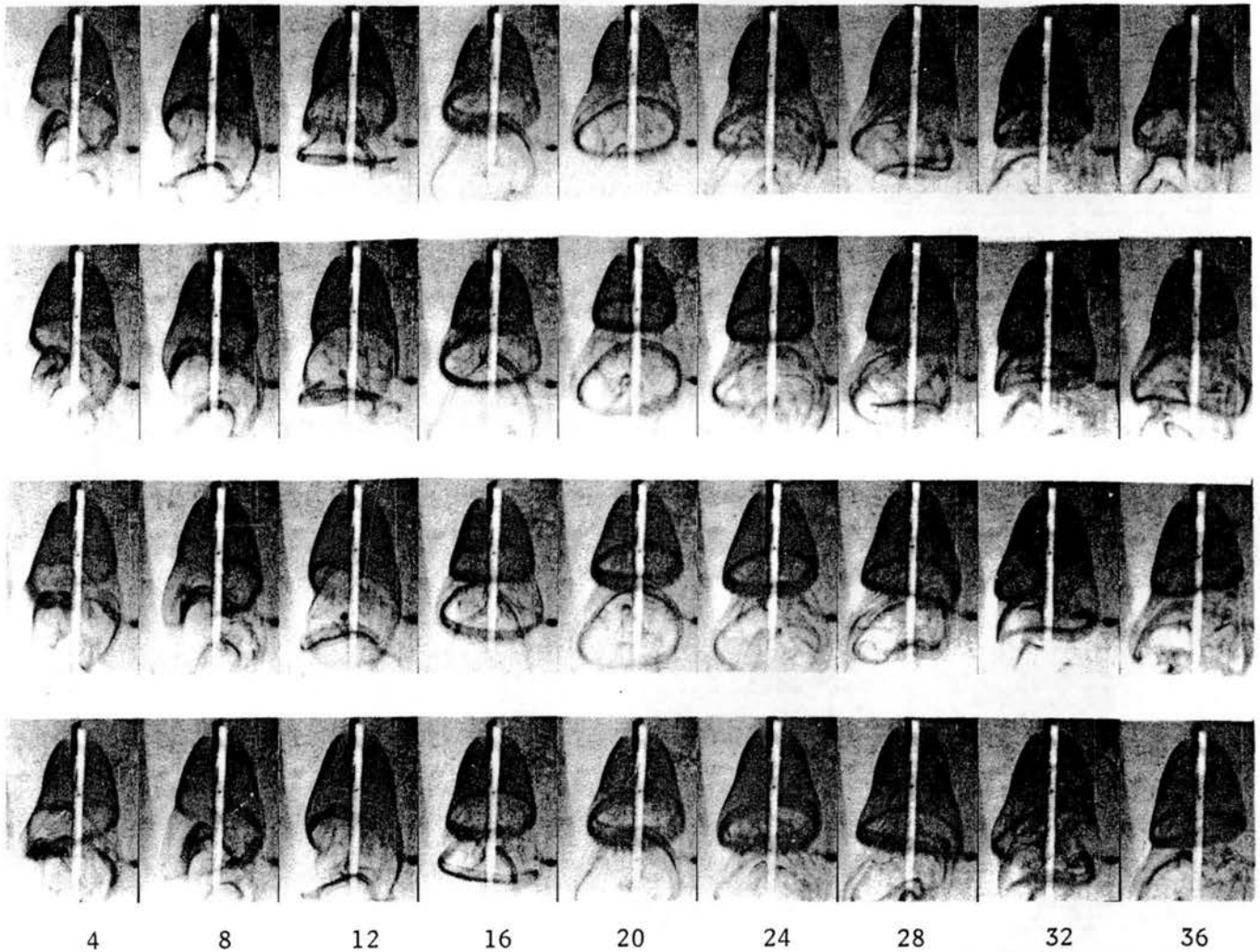

Fig. 9. A series of flow visualization pictures depicting the formation of vortex rings of heated mass at regular intervals for dominant forced convection condition. Interval = 1/16 second.

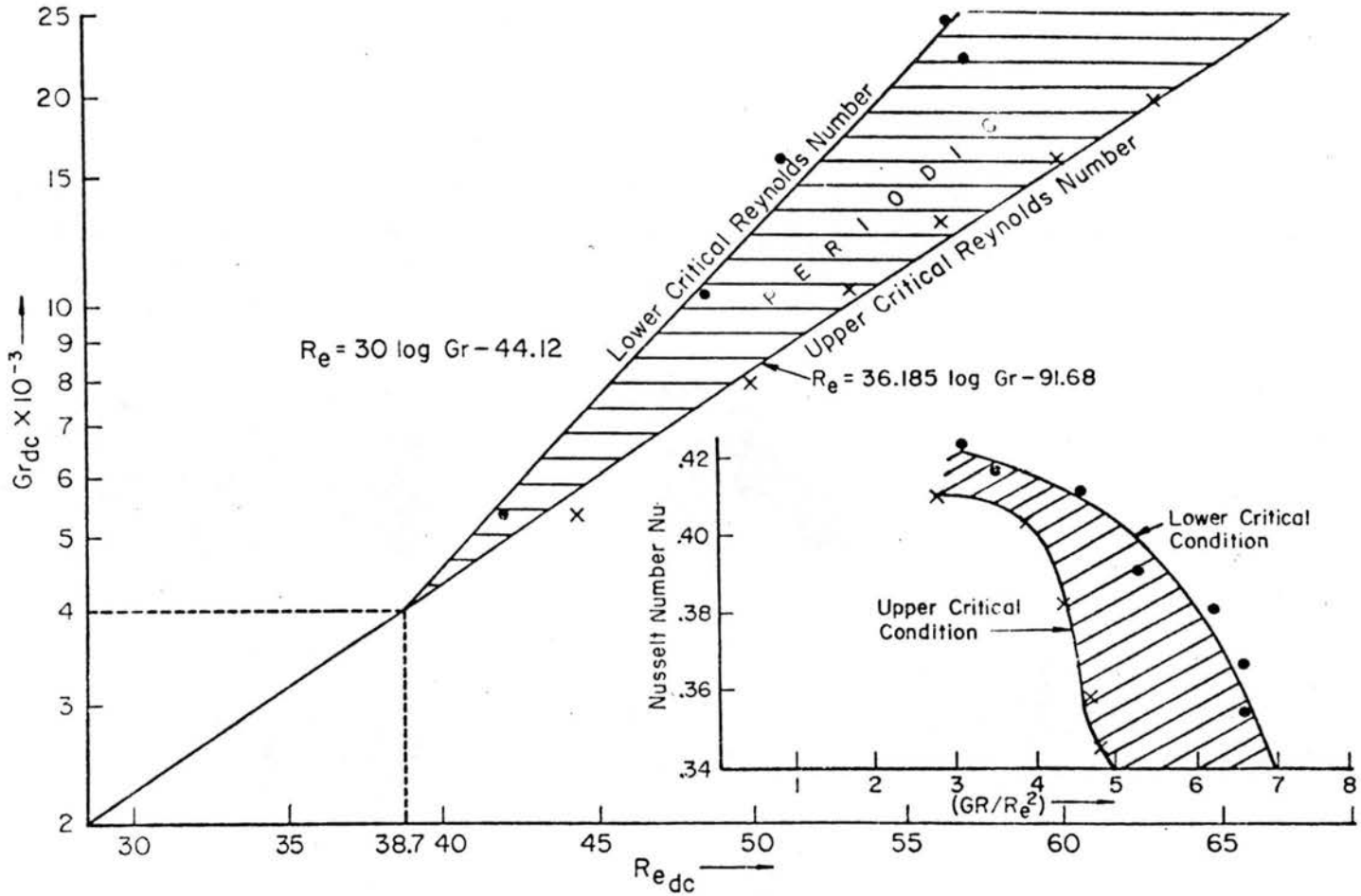

Fig. 10. The region of periodic heat transfer as a function of dimensionless parameters Grashof and Reynolds numbers. Insert: The region of periodic heat transfer correlated with parameters Gr/Re^2 and Re. Pt 80% Ir 20% cylinder d = 0.01 mm, l = 8 mm, α = 0.000445/°F.

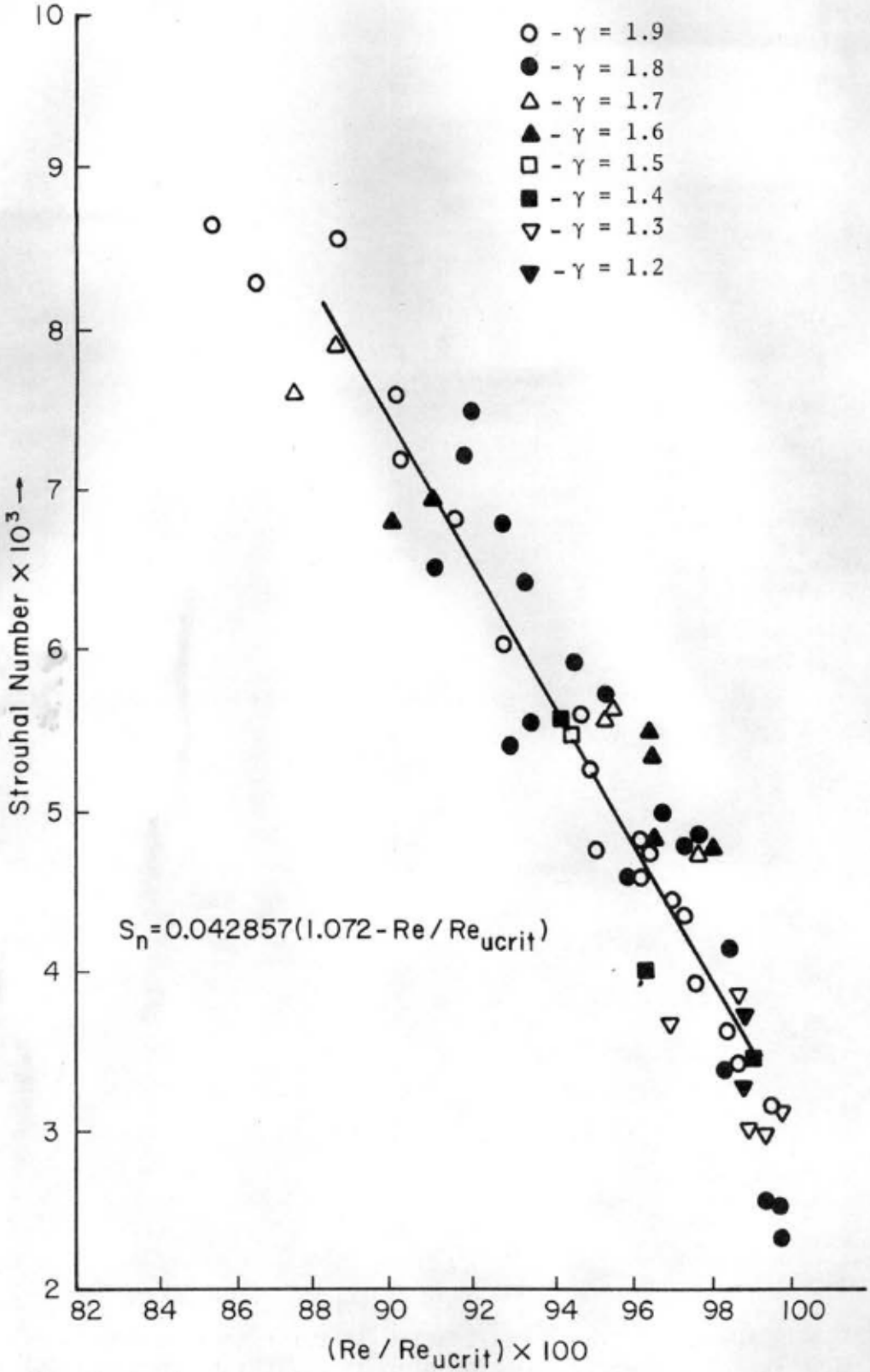

Fig. 11. Variation of Strouhal number with the ratio of Re/Re_{Ucrit} for Pt 80% Ir 20% cylinder, d = 0.01 mm, l = 8 mm, α = 0.000445/°F.

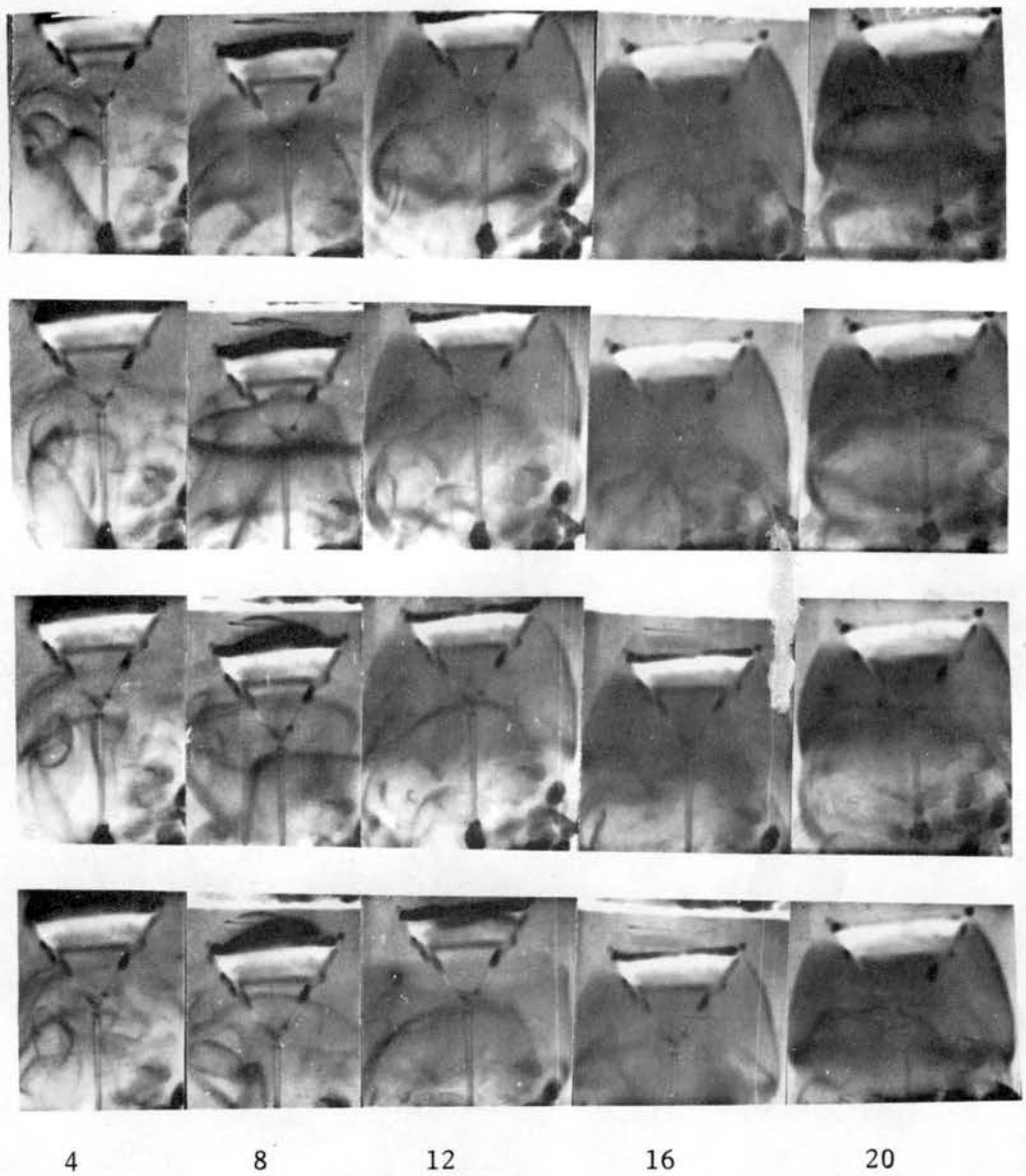

Fig. 12. A series of flow visualization pictures showing overall two dimensionality of the process. Nichrome wire d = 0.4 mm 1 = 75 mm with vertical wide sheet of thin paper along the wire; A.C. heating, 8.0 V at 2.5 amps.

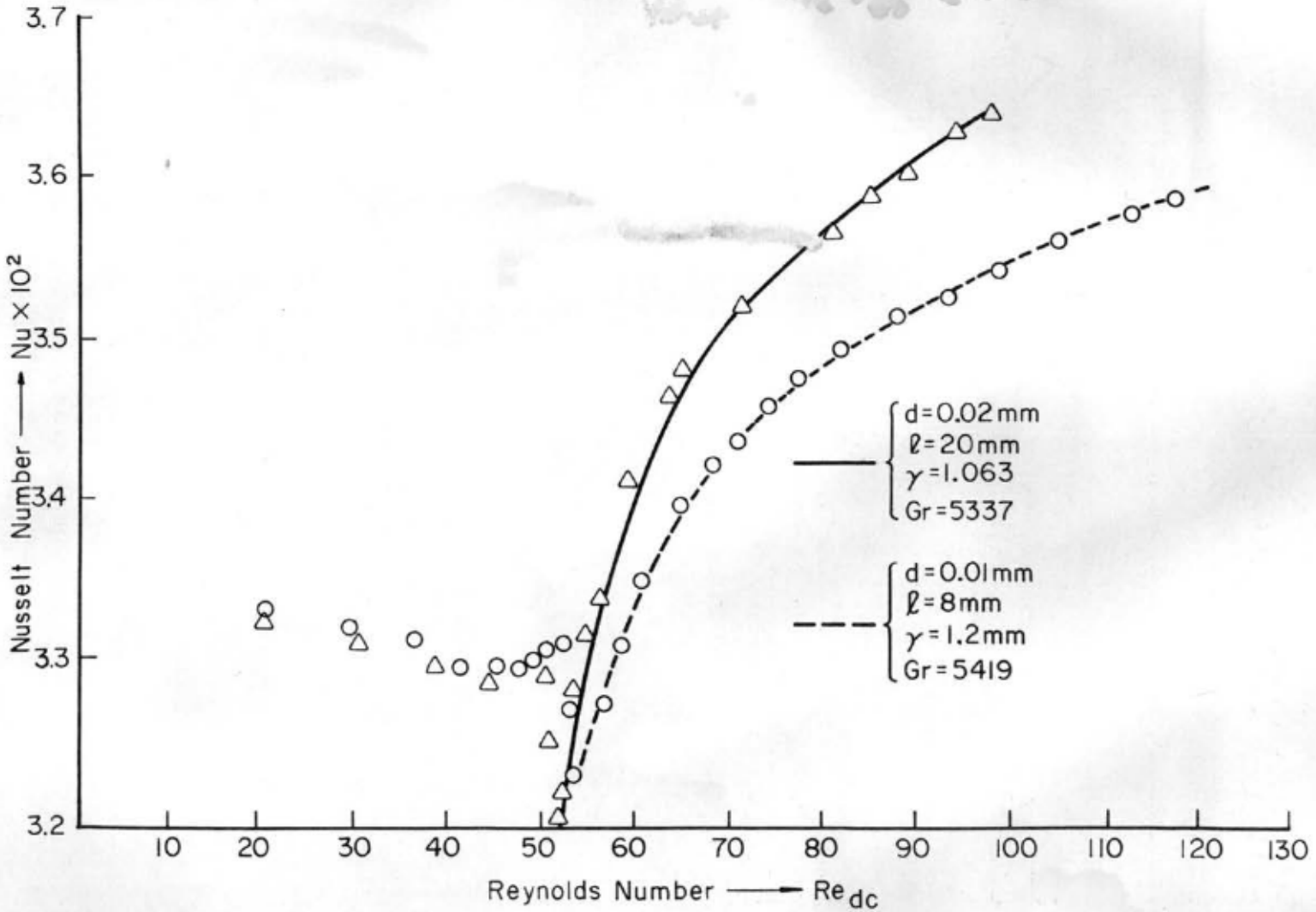

Fig. 13. Effect of diameter of cylinder on Nusselt number variation with Reynolds number for approximately the same Grashof number.

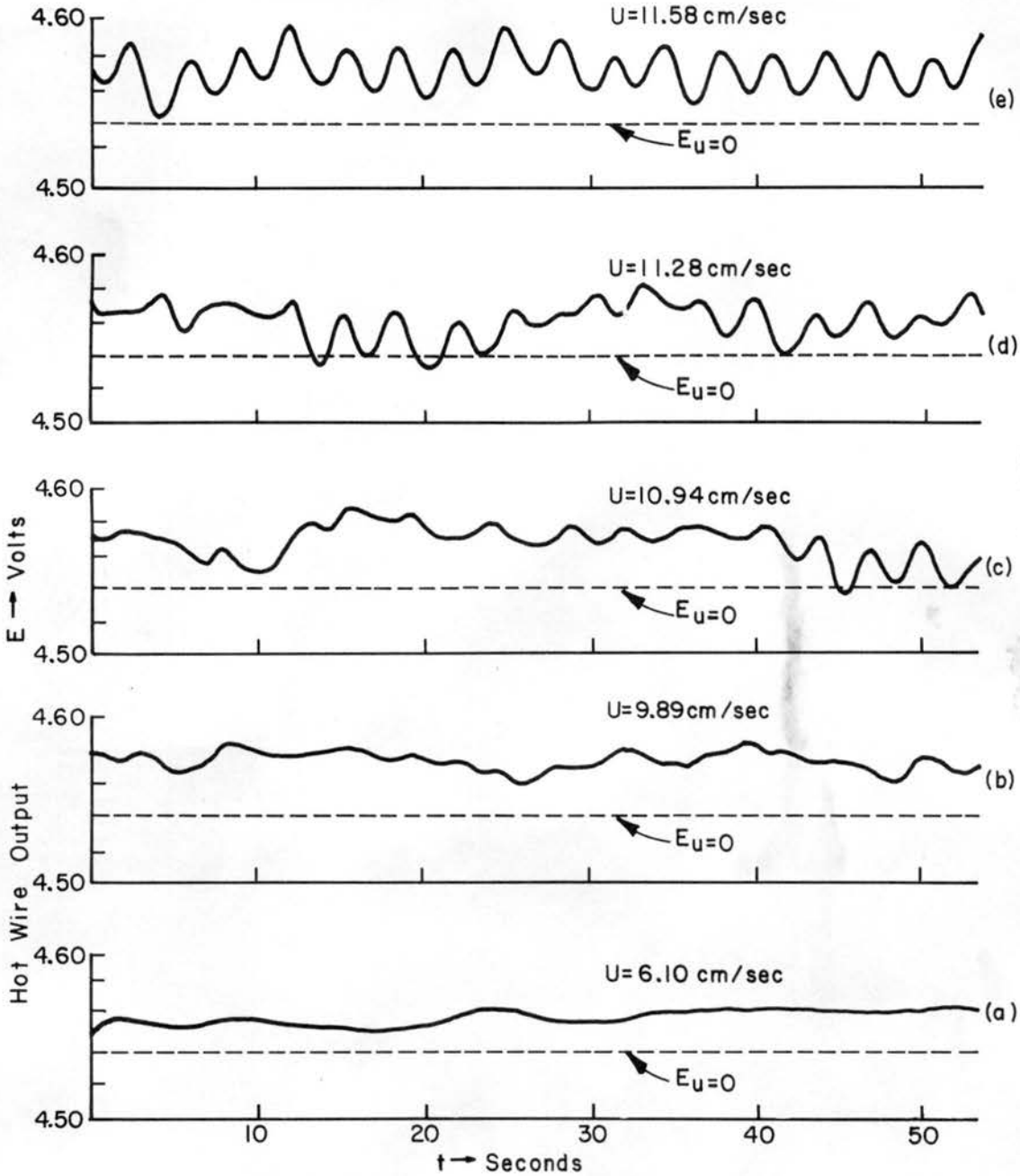

a - e

Fig. 14. Constant current hot cylinder output voltage as a function of time for directly opposed free and forced convection; strain gauge wire, Pt 94% Tung 6%, d = 0.02 mm, l = 8 mm, I = 800 MA.

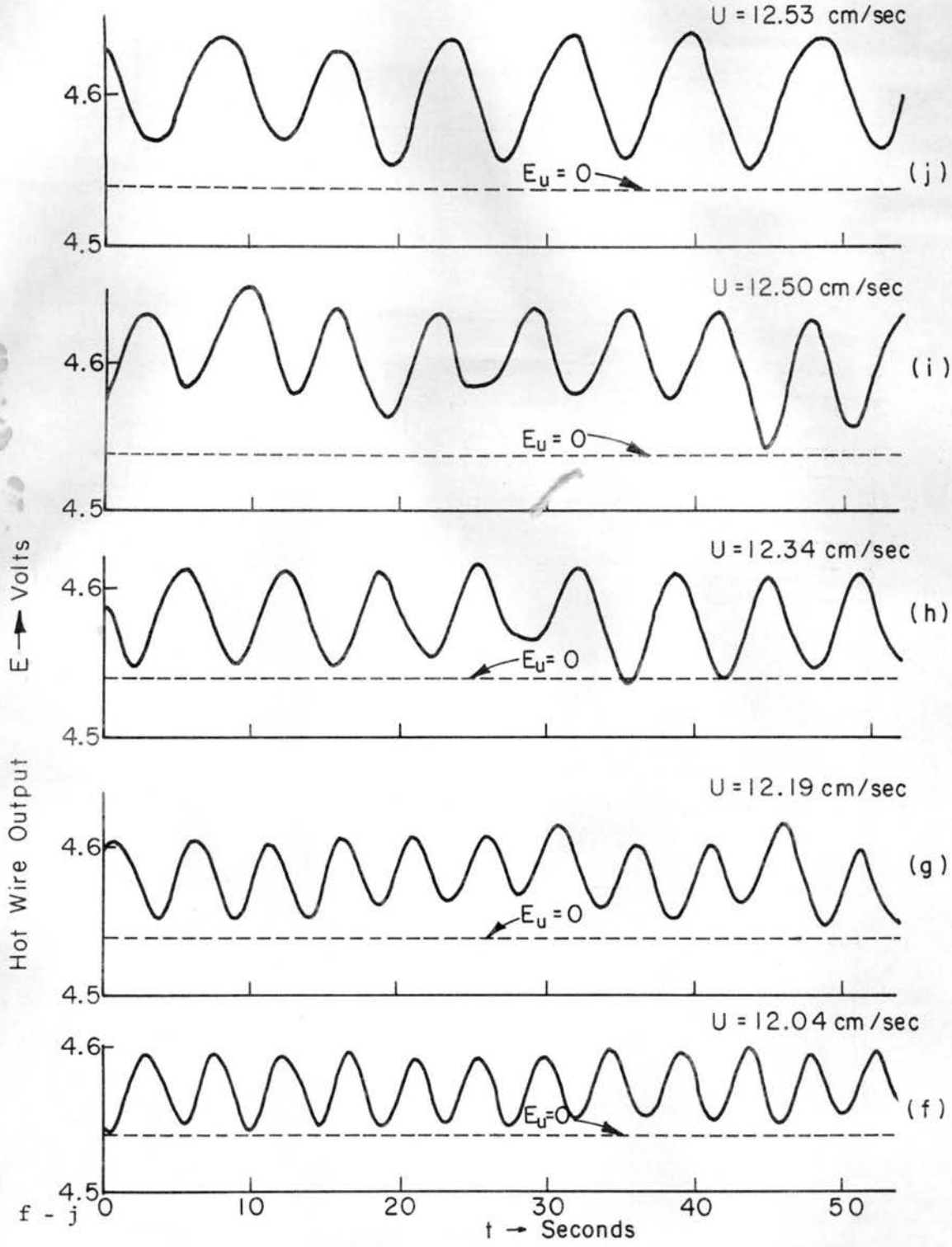

Fig. 14. (Cont.) Constant current hot cylinder output voltage as a function of time for directly opposed free and forced convection; strain gauge wire, Pt 94% Tung 6%, d = 0.02 mm, l = 8 mm, I = 800 MA.

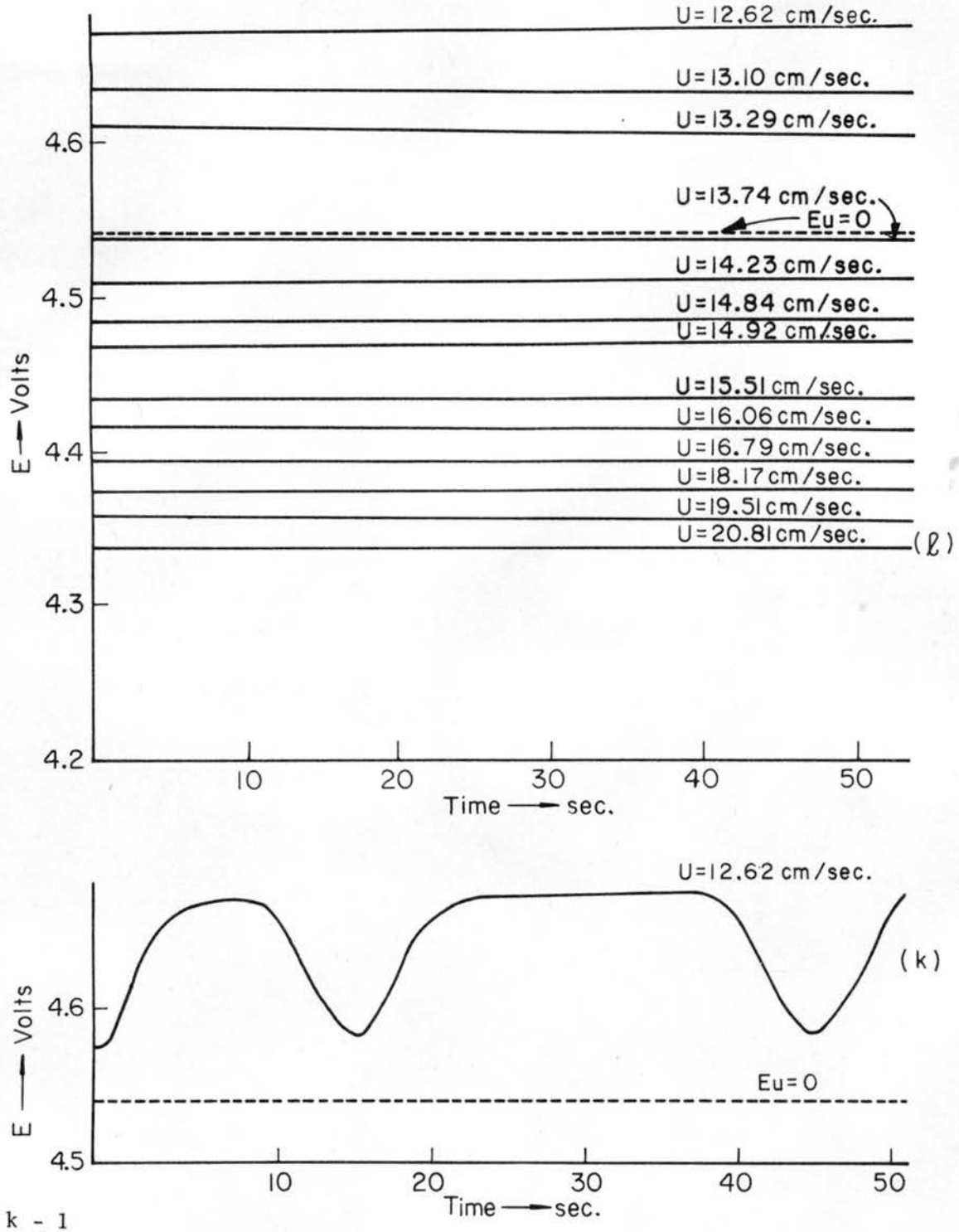

k - 1

Fig. 14. (Concluded) Constant current hot cylinder output voltage as a function of time for directly opposed free and forced convection; strain gauge wire, Pt 94% Tung 6%, d = 0.02 mm, l = 8 mm, I = 800 MA.

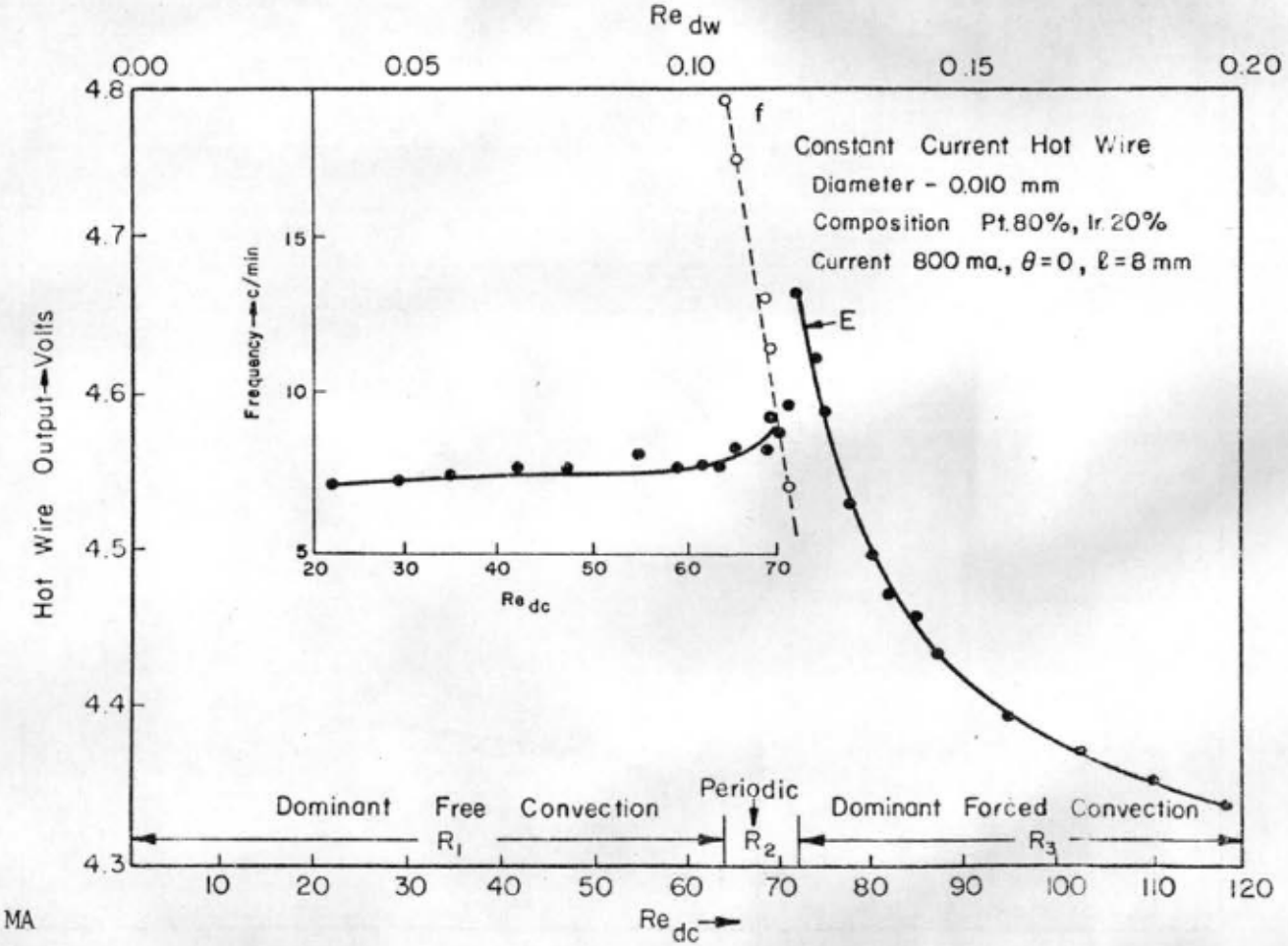

a) Current = 800 MA

Fig. 15. Constant current hot cylinder mean output with Reynolds number for directly opposed free and forced convection for Pt 80% Ir 20% cylinder, d = 0.01 mm, 1 = 8 mm. Insert: Variation of frequency with Reynolds number.

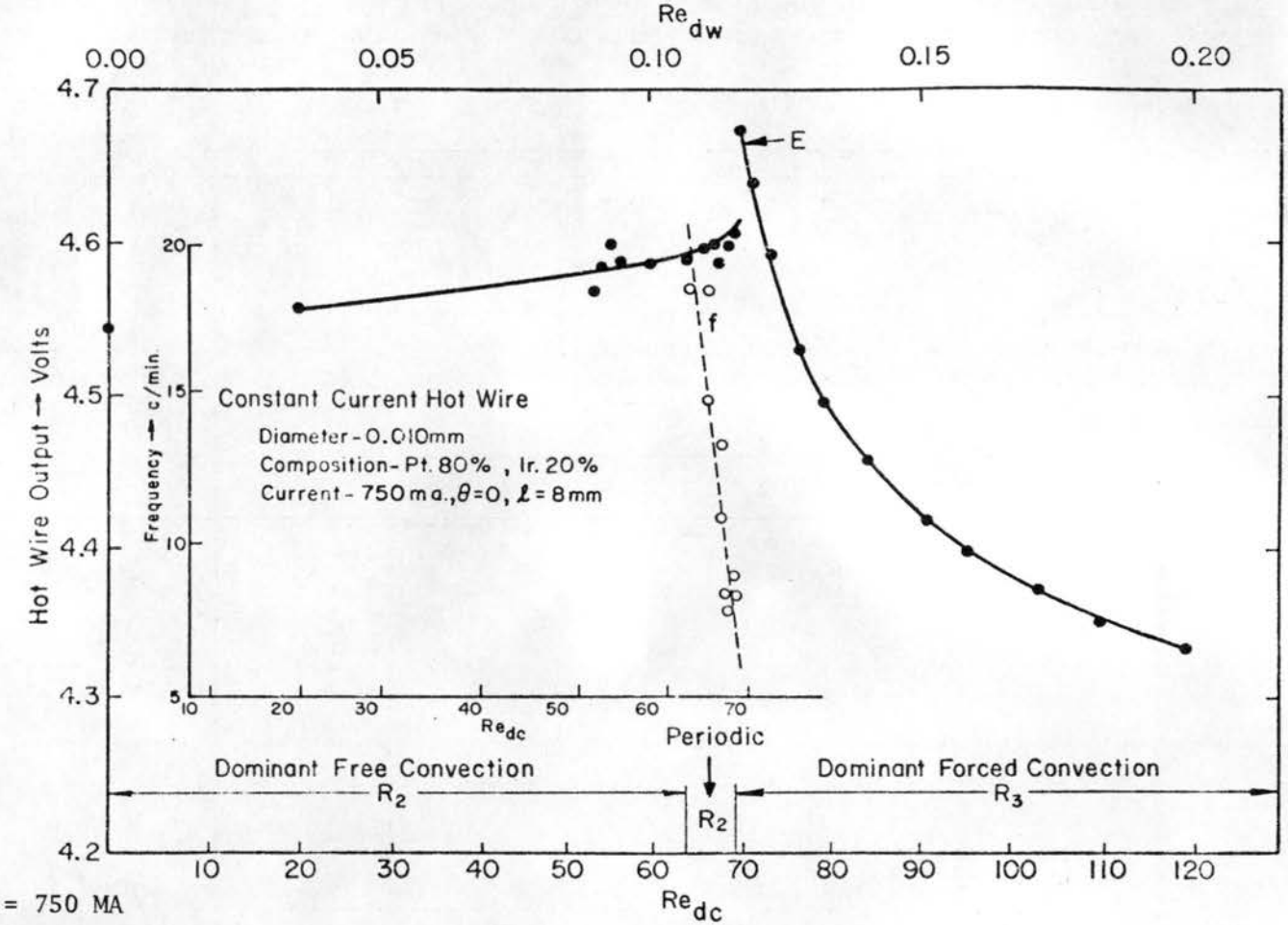

b) Current = 750 MA

Fig. 15. Constant current hot cylinder mean output with Reynolds number for directly opposed free and forced convection for Pt 80% Ir 20% cylinder, d = 0.01 mm, 1 = 8 mm. Insert: Variation of frequency with Reynolds number.

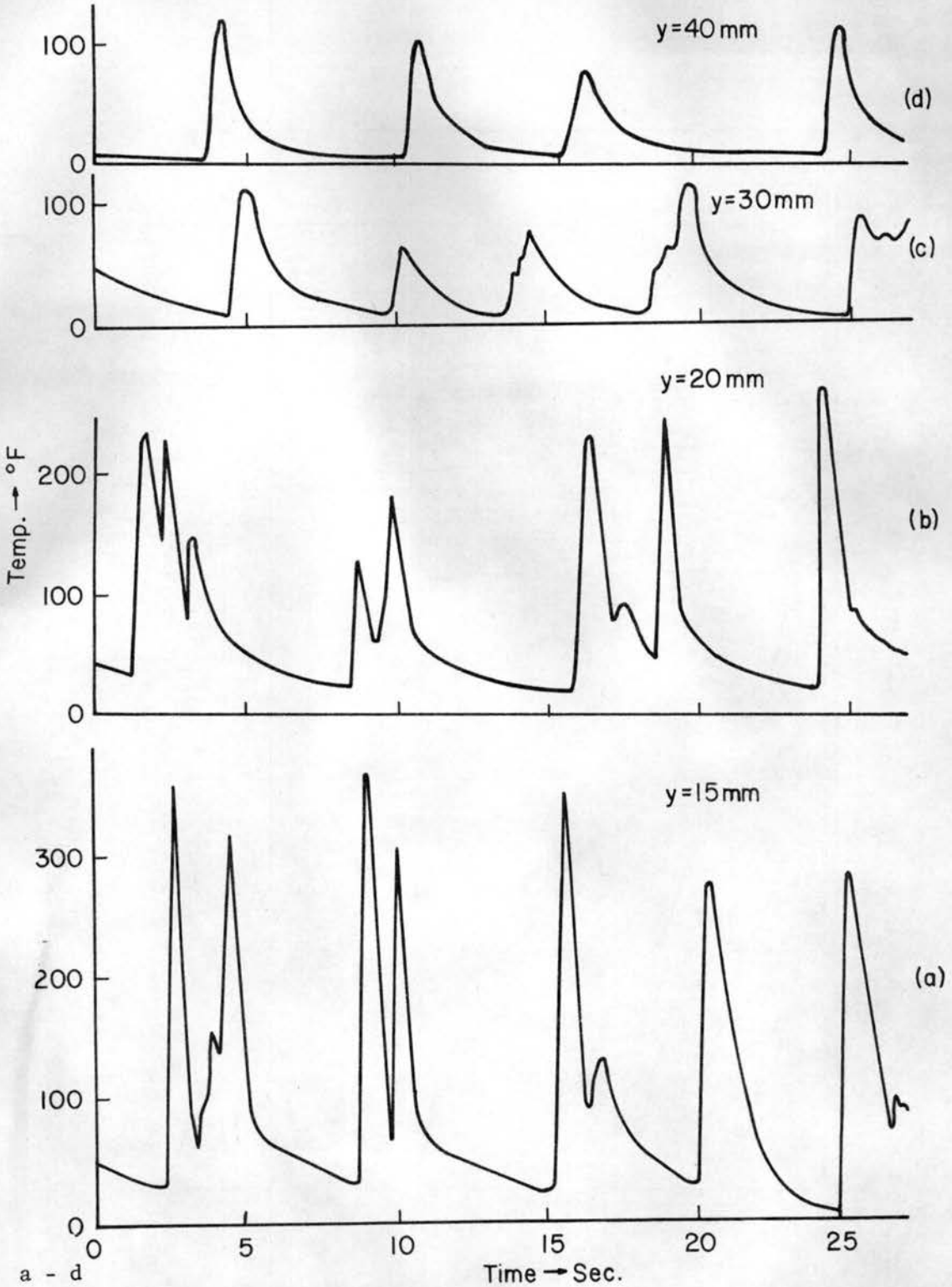

Fig. 16. Thermals due to A.C. heating; observations recording the movement of laminar sheet, temperature variation at x = 10.2 mm. A.C. heating by 9V at 2.5 A, d = 0.4 mm Nichrome cylinder.

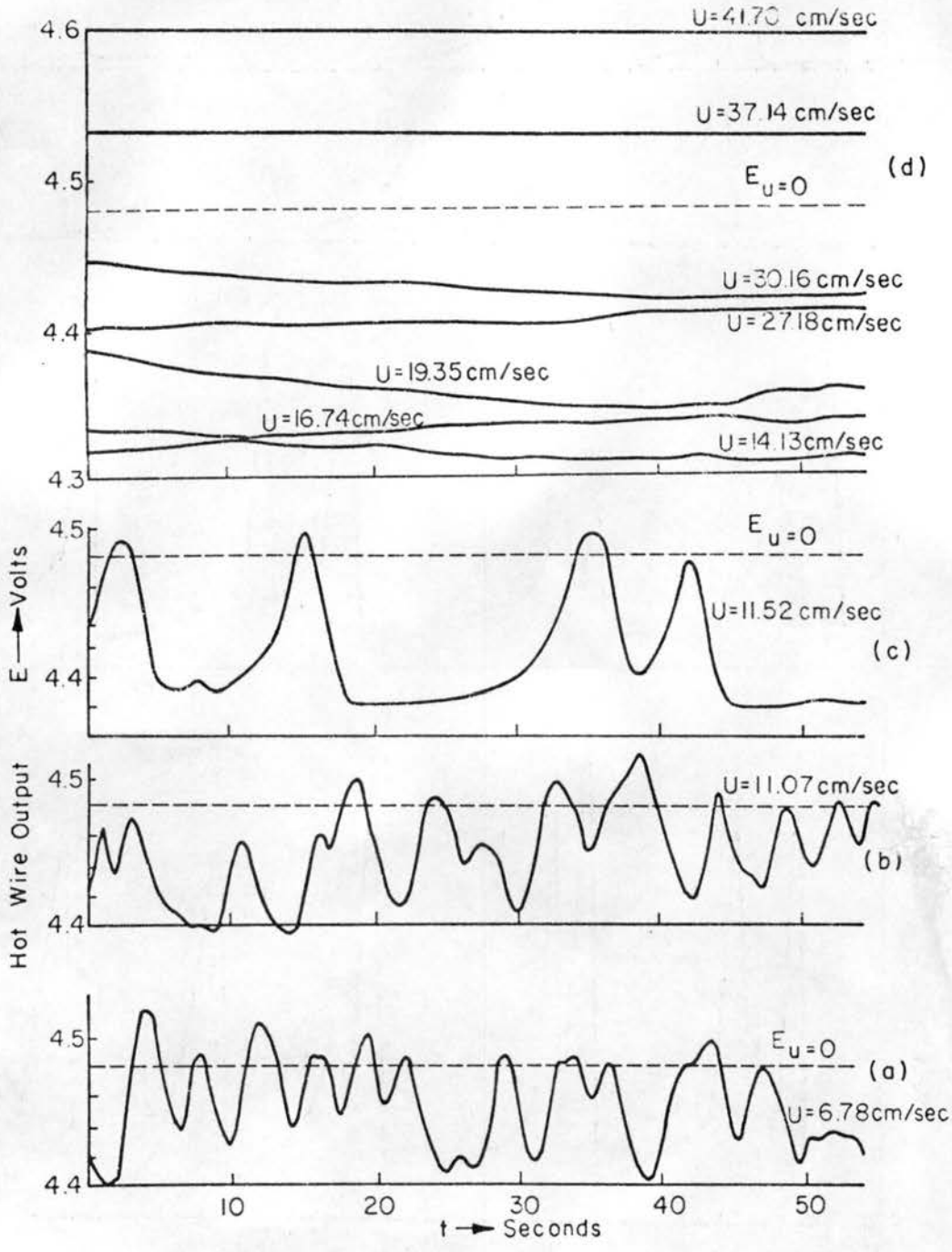

a - d

Fig. 17. Effect of angularity of freestream; constant temperature hot cylinder output as a function of time for freestream at 15° to the gravity. Strain gauge wire, d = 0.02 mm, 1 = 8 mm, γ = 1.3.

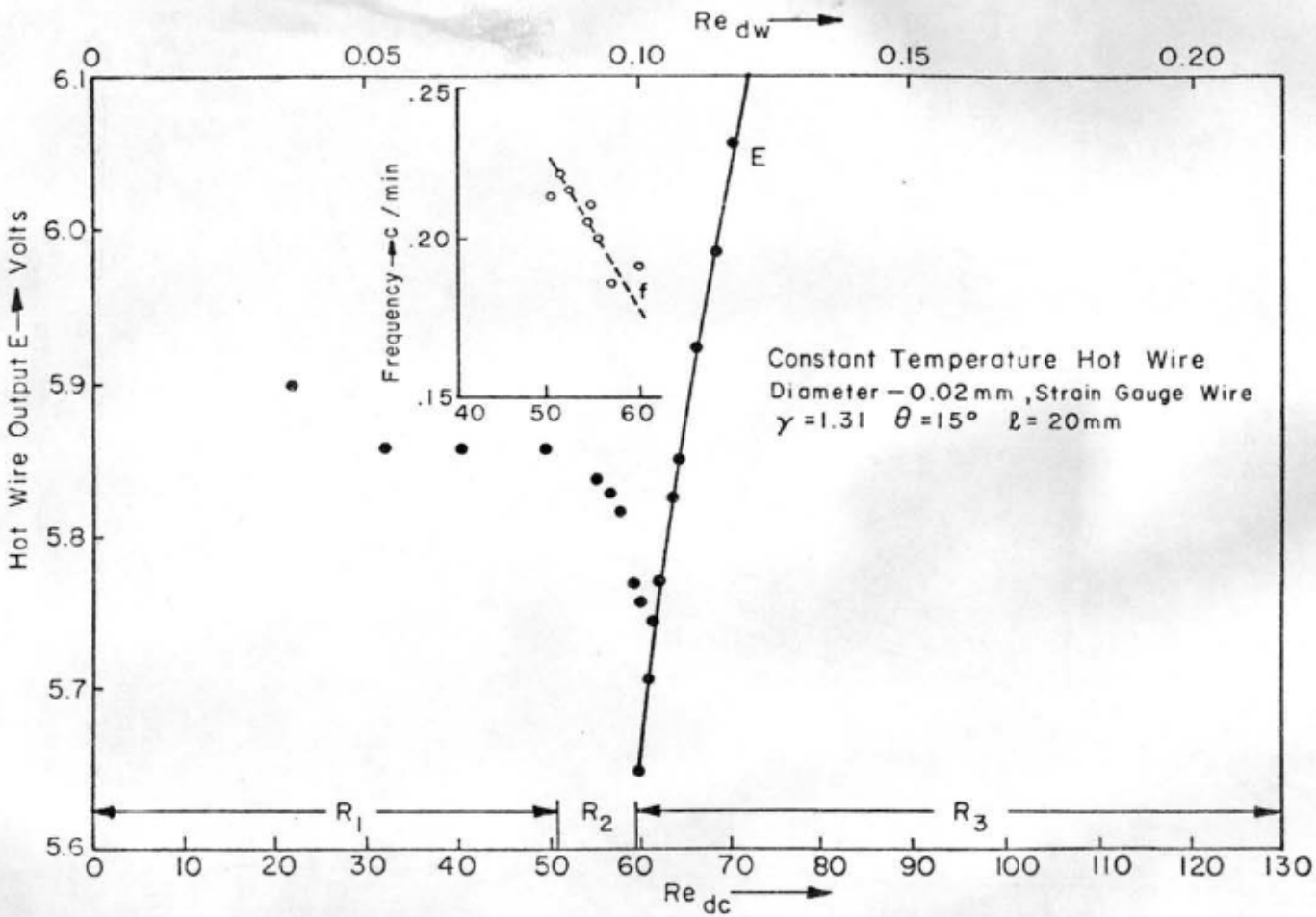

Fig. 18. Effect of angularity of free stream velocity; constant temperature hot cylinder mean output as a function of Reynolds number. Insert: Variation of frequency with Reynolds number for strain gauge cylinder, d = 0.02 mm, l = 8 mm, γ = 1.3.

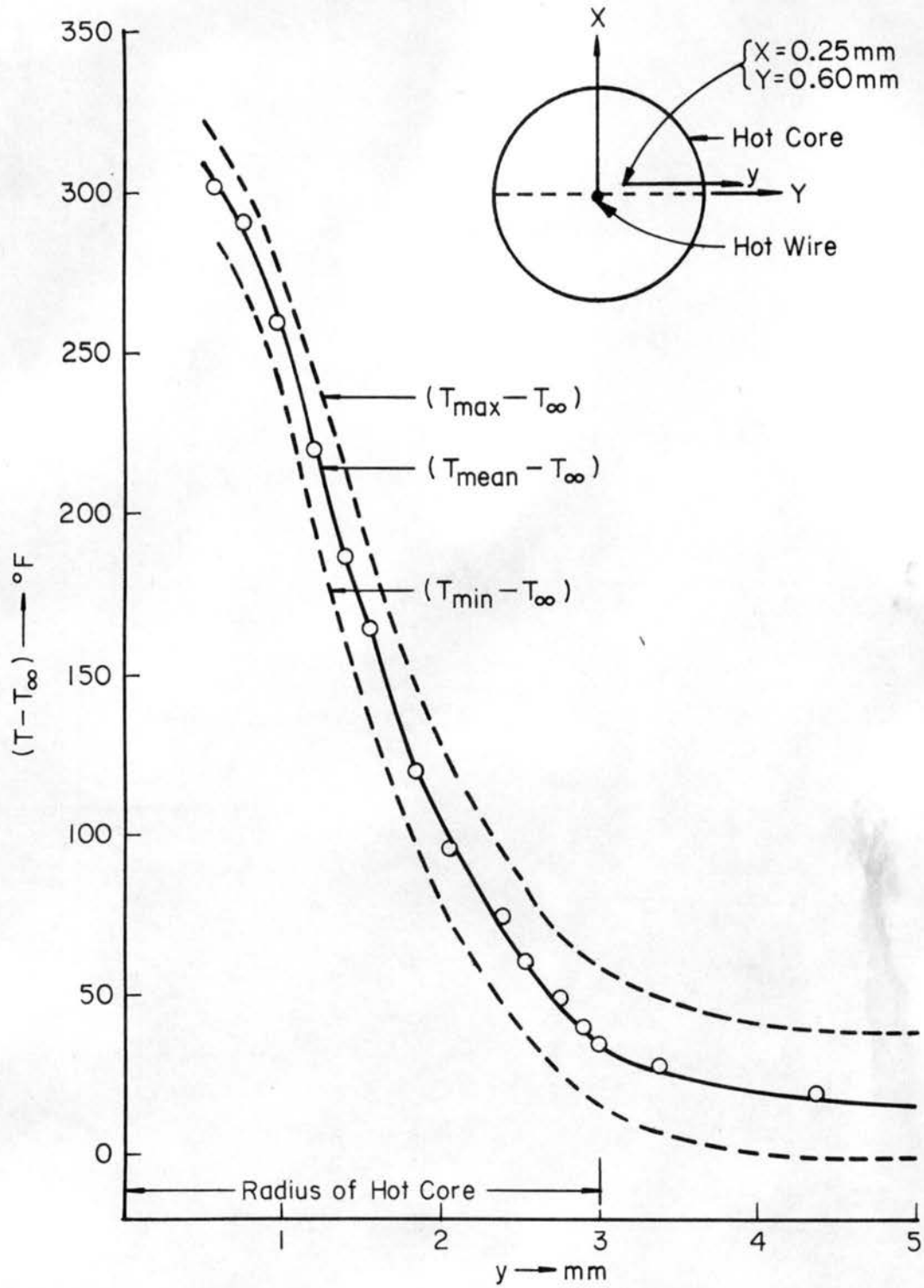

Fig. 19. A typical plot showing the limits of variation of temperature in the hot core during the periodic variations for Pt 80% Ir 20% cylinder, d = 0.01 mm, γ = 1.8, $T_\omega - T_\infty$ = 1812°F, Re = 52.3

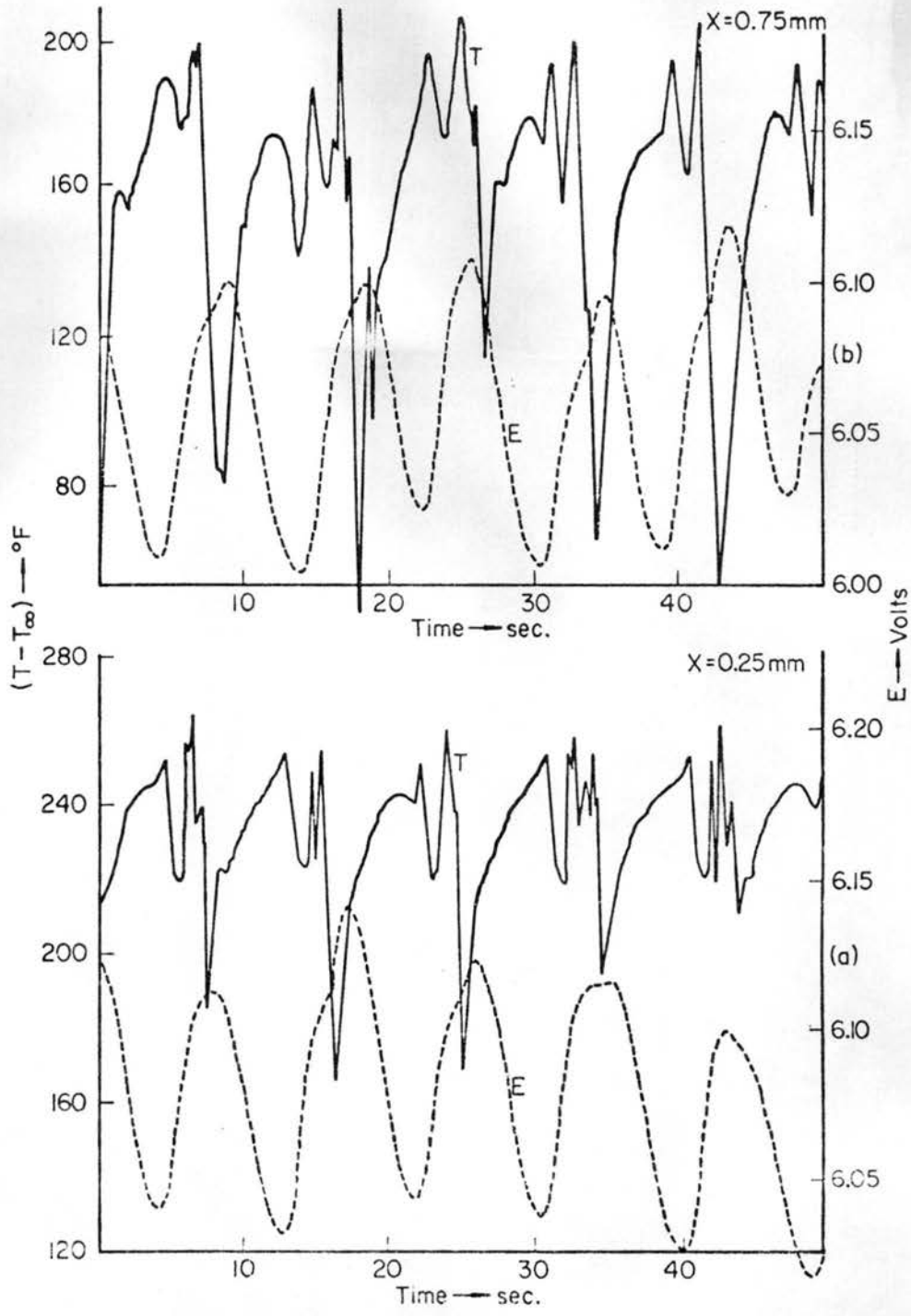

a - b

Fig. 20. Variation of temperature within the hot core during periodic behavior for constant temperature Pt 80% Ir 20% cylinder, d = 0.01 mm, 1 = 8 mm, Re = 44, γ = 1.4, y = 0.

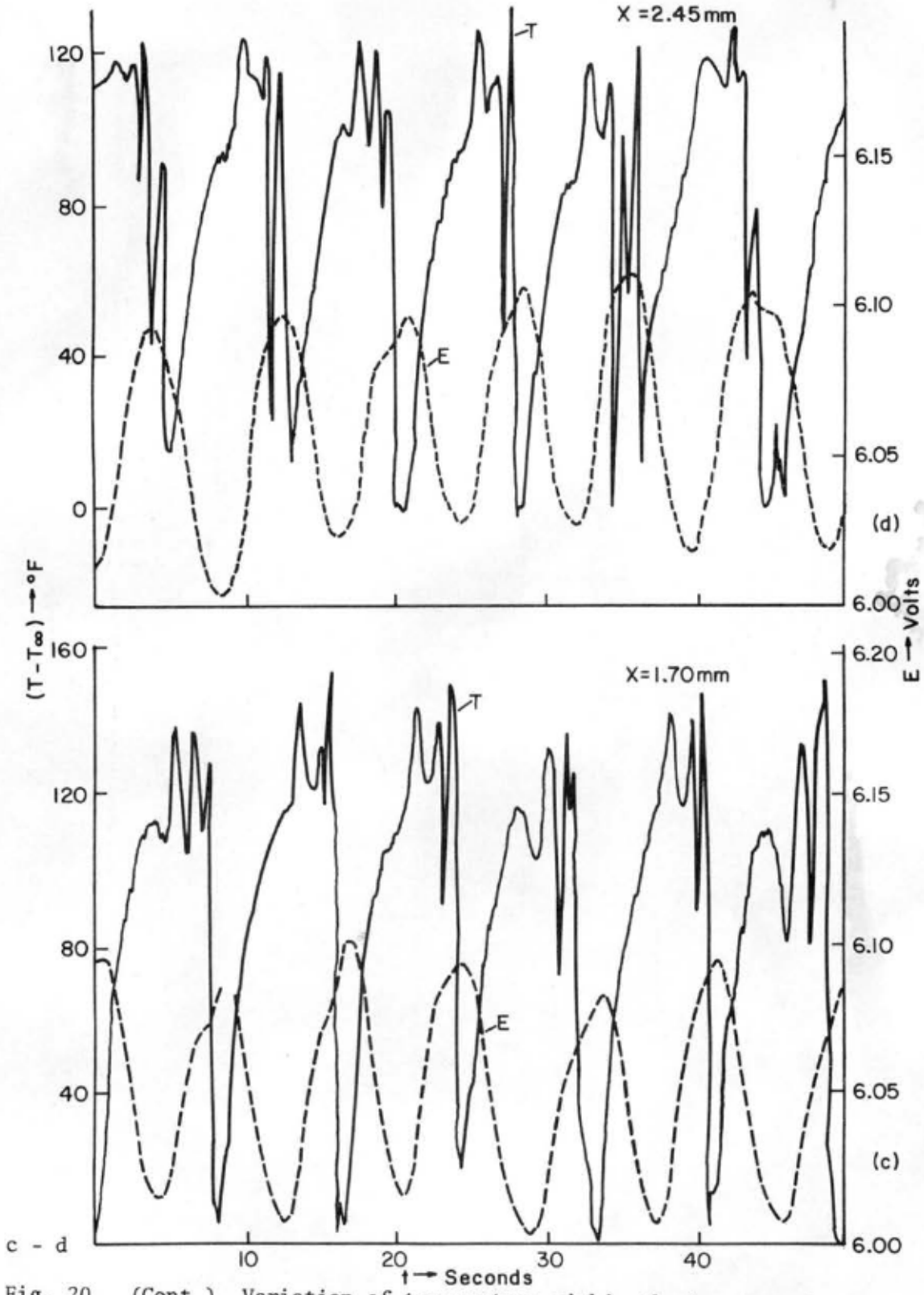

Fig. 20. (Cont.) Variation of temperature within the hot core during periodic behavior for constant temperature Pt 80% Ir 20% cylinder, d = 0.01 mm, 1 = 8 mm, Re = 44, γ = 1.4, y = 0.

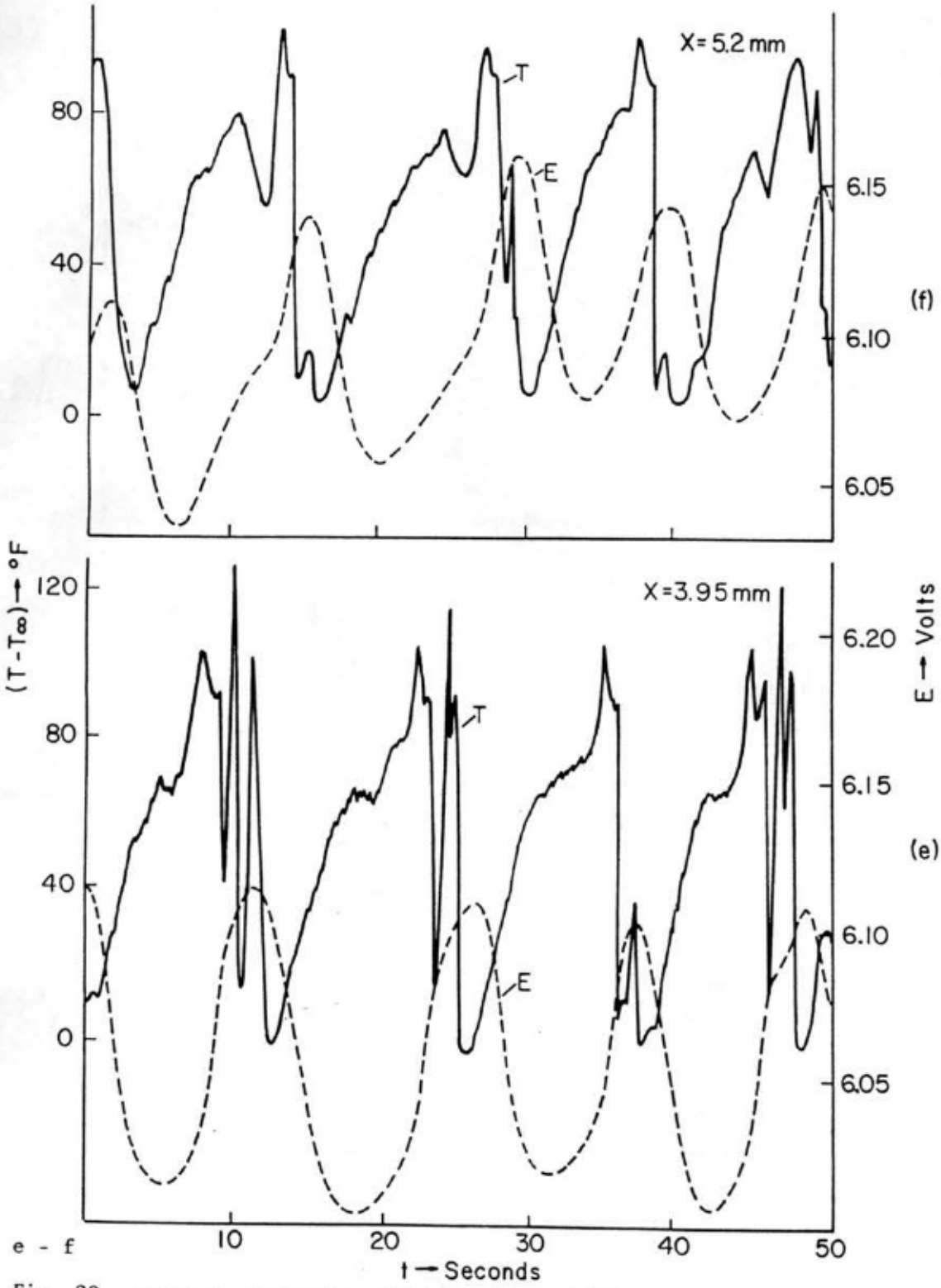

Fig. 20. (Cont.) Variation of temperature within the hot core during periodic behavior for constant temperature Pt 80% Ir 20% cylinder, d = 0.01 mm, l = 8 mm, Re = 44, γ = 1.4, y = 0.

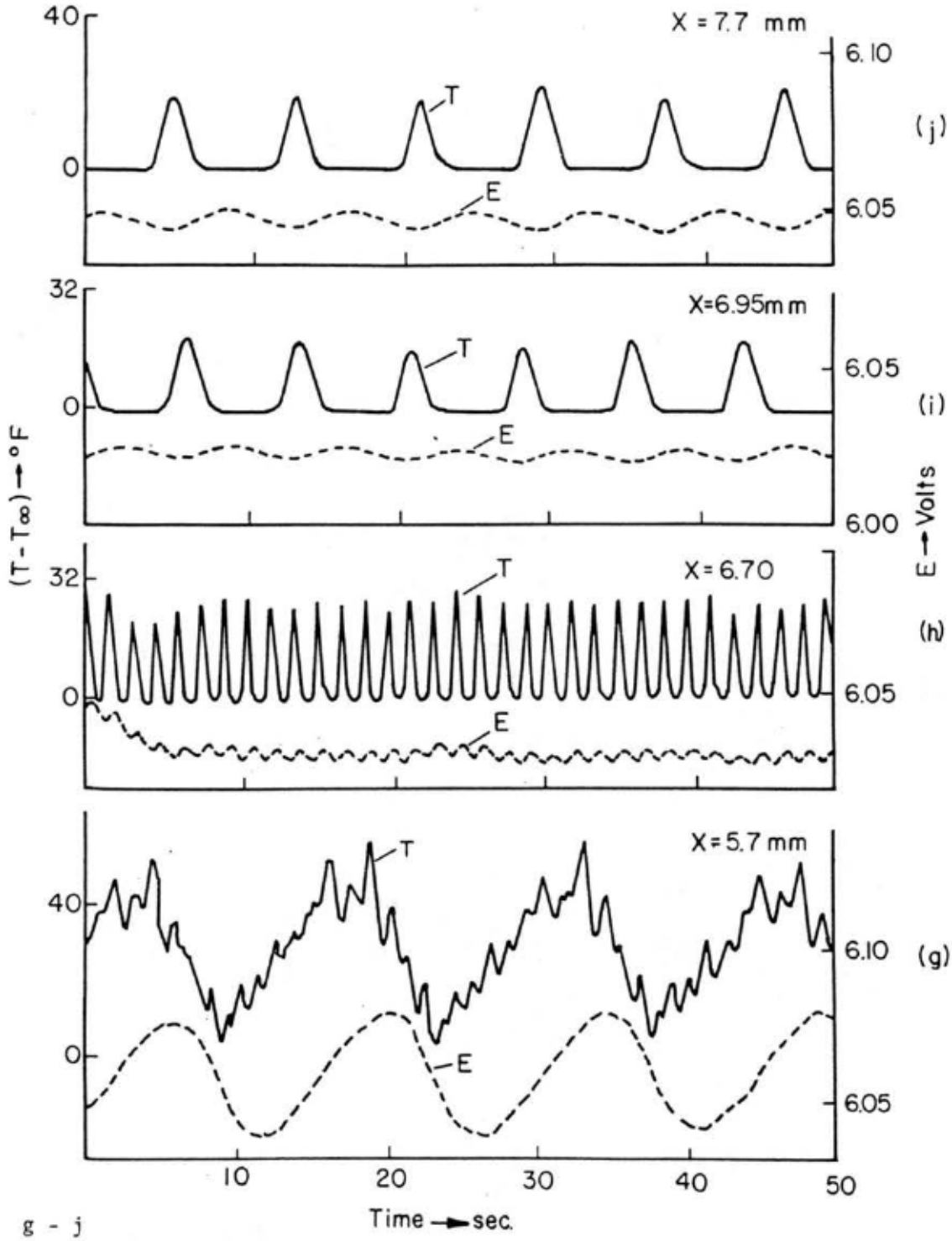

Fig. 20. (Cont.) Variation of temperature within the hot core during periodic behavior for constant temperature Pt 80% Ir 20% cylinder, d = 0.01 mm, l = 8 mm, Re = 44, γ = 1.4, y = 0.

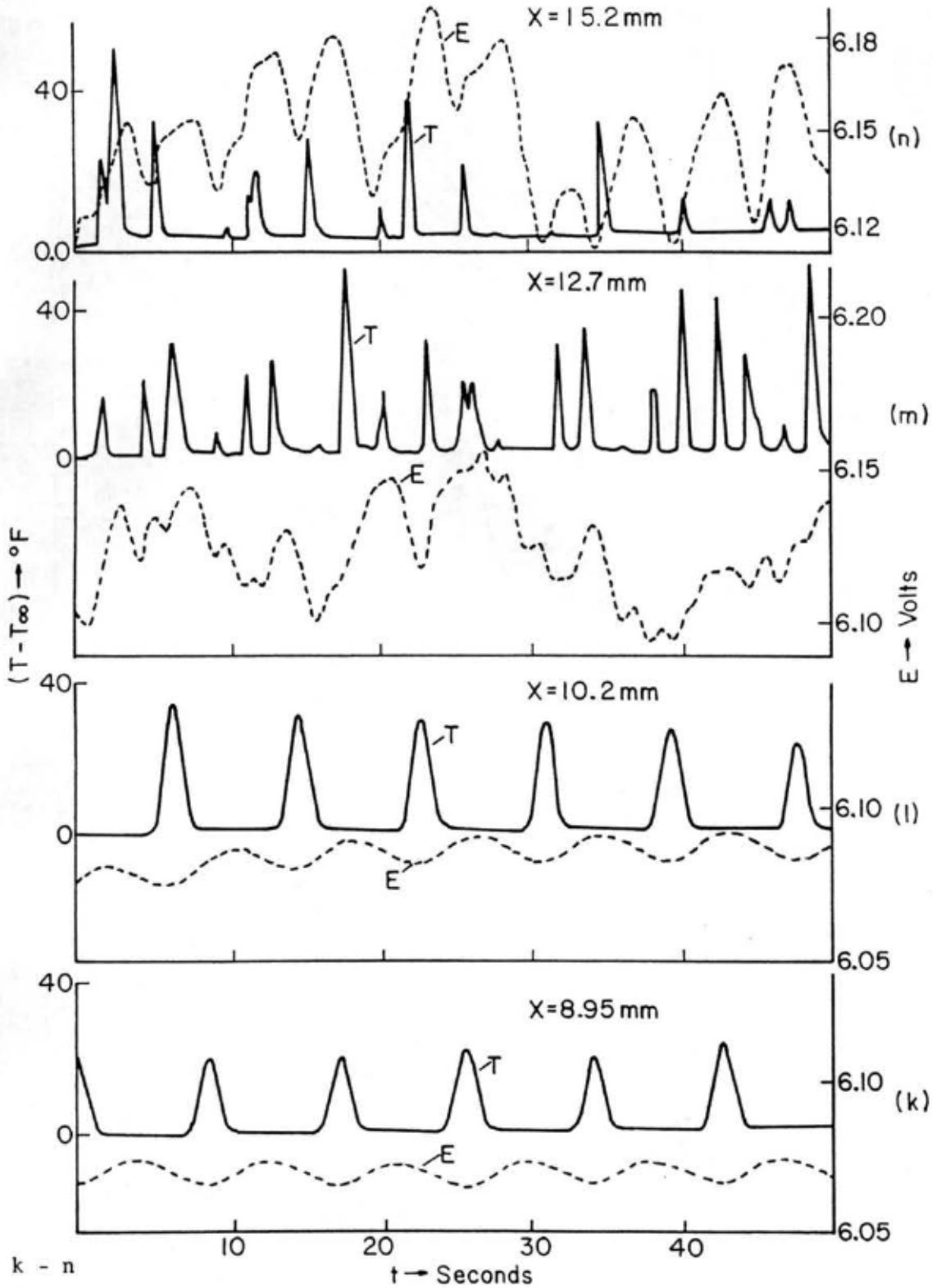

Fig. 20. (Concluded) Variation of temperature within the hot core during periodic behavior for constant temperature Pt 80% Ir 20% cylinder, d = 0.01 mm, l = 8 mm, Re = 44, γ = 1.4, y = 0.

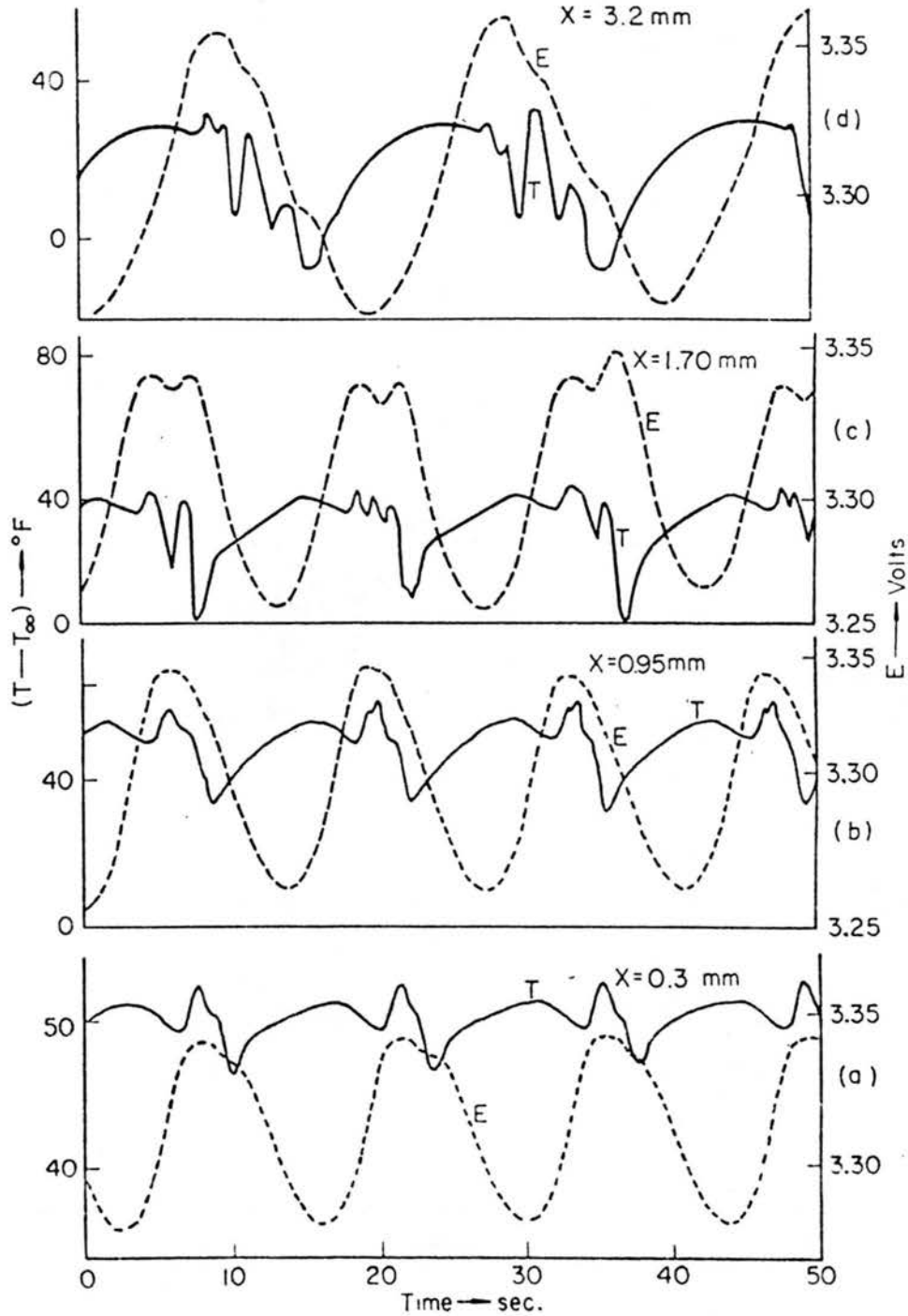

a - d

Fig. 21. Variation of temperature within the hot core during periodic behavior for constant temperature, Pt 80% Ir 20% cylinder, d = 0.01 mm, d = 8 mm, Re = 40, γ = 1.2, y = 0.

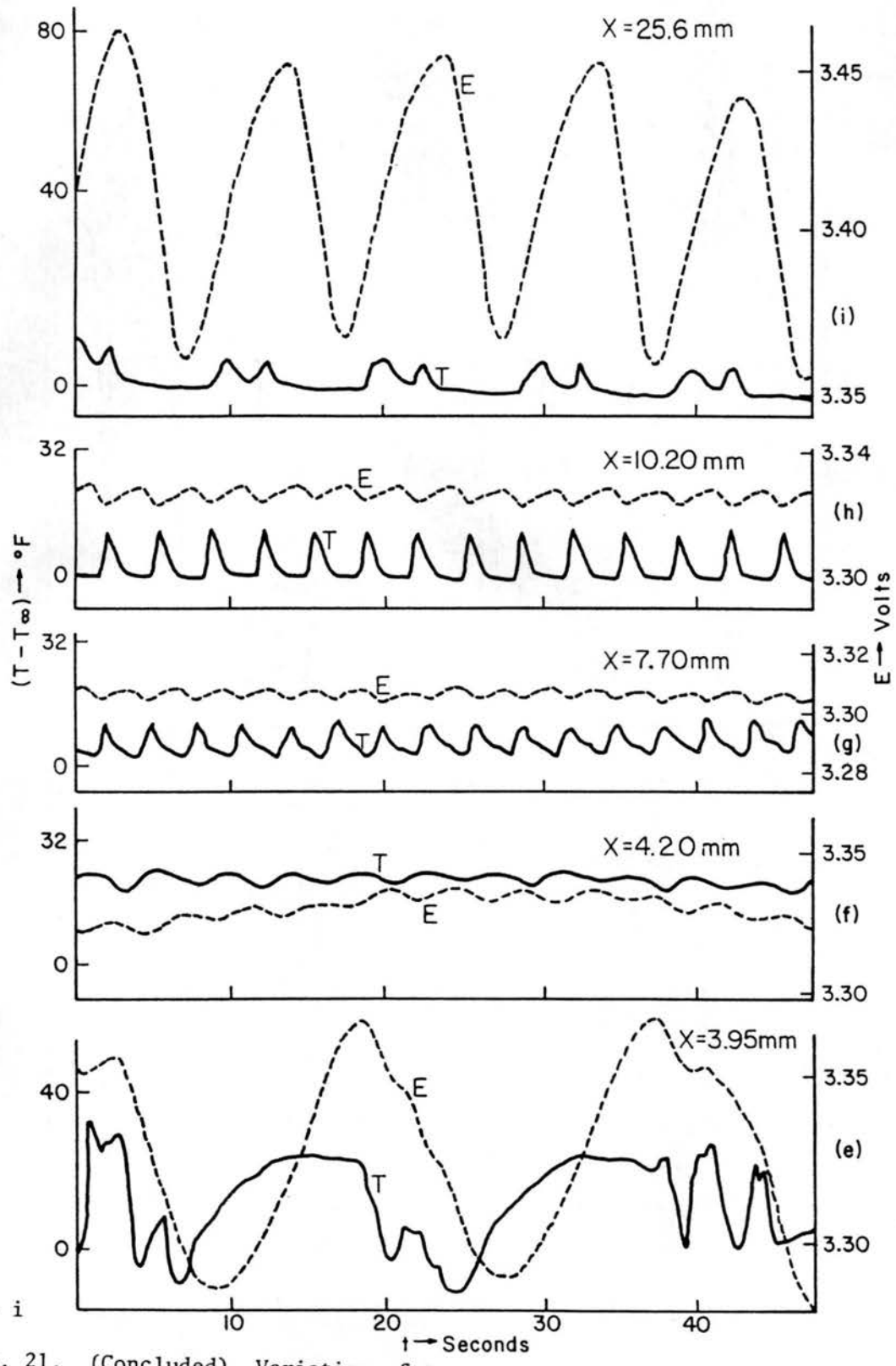

Fig. 21. (Concluded) Variation of temperature within the hot core during periodic behavior for constant temperature Pt 80% Ir 20% cylinder, d = 0.01, d = 8 mm, Re = 40, γ = 1.2, y = 0.

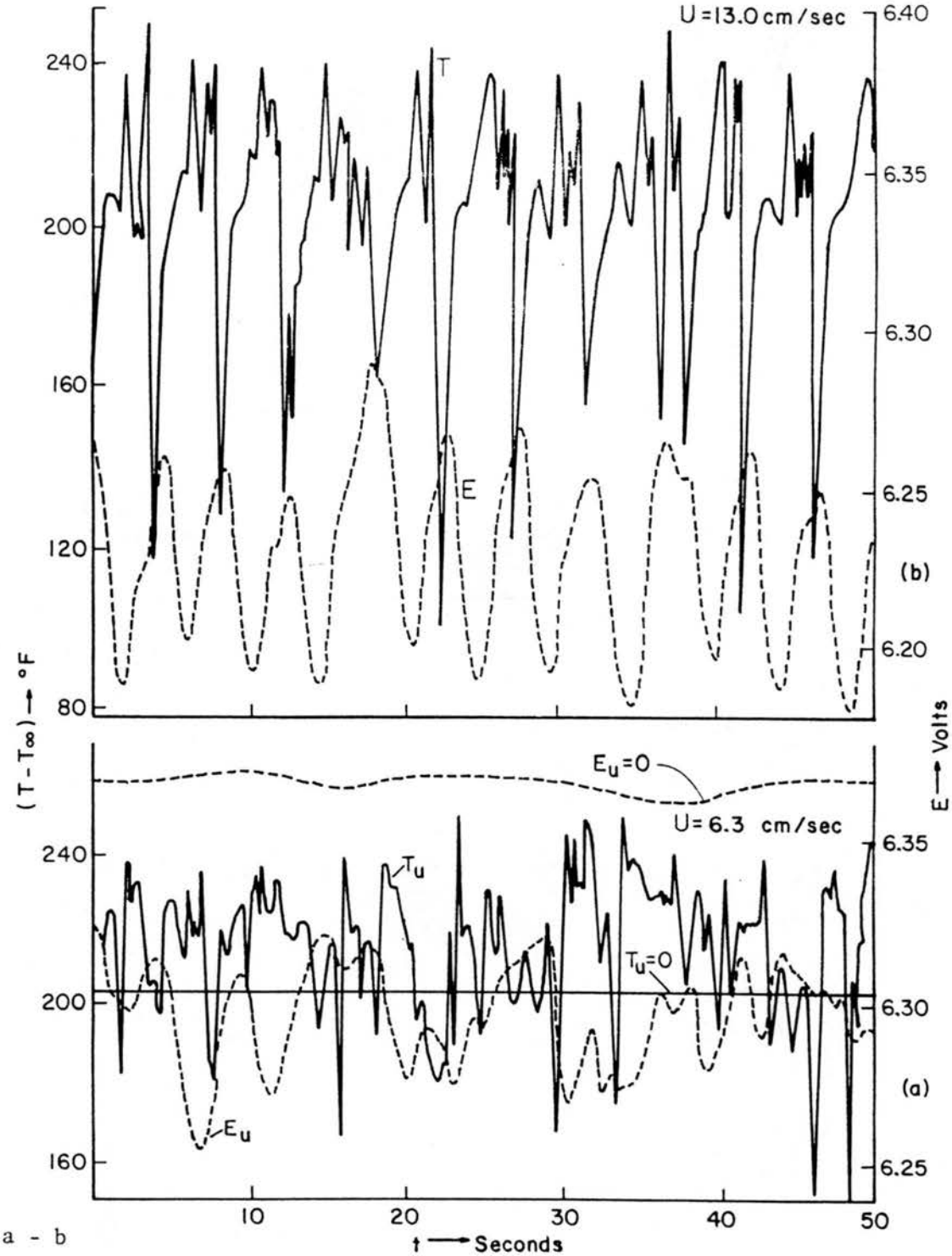

a - b

Fig. 22. Effect of ambient velocity on the variation of temperature within the hot core for directly opposed free and forced convection from constant temperature horizontal cylinder; Pt 80% Ir 20% cylinder, d = 0.01 mm, l = 15 mm, γ = 1.35, u = 0.25 mm, y = 0.

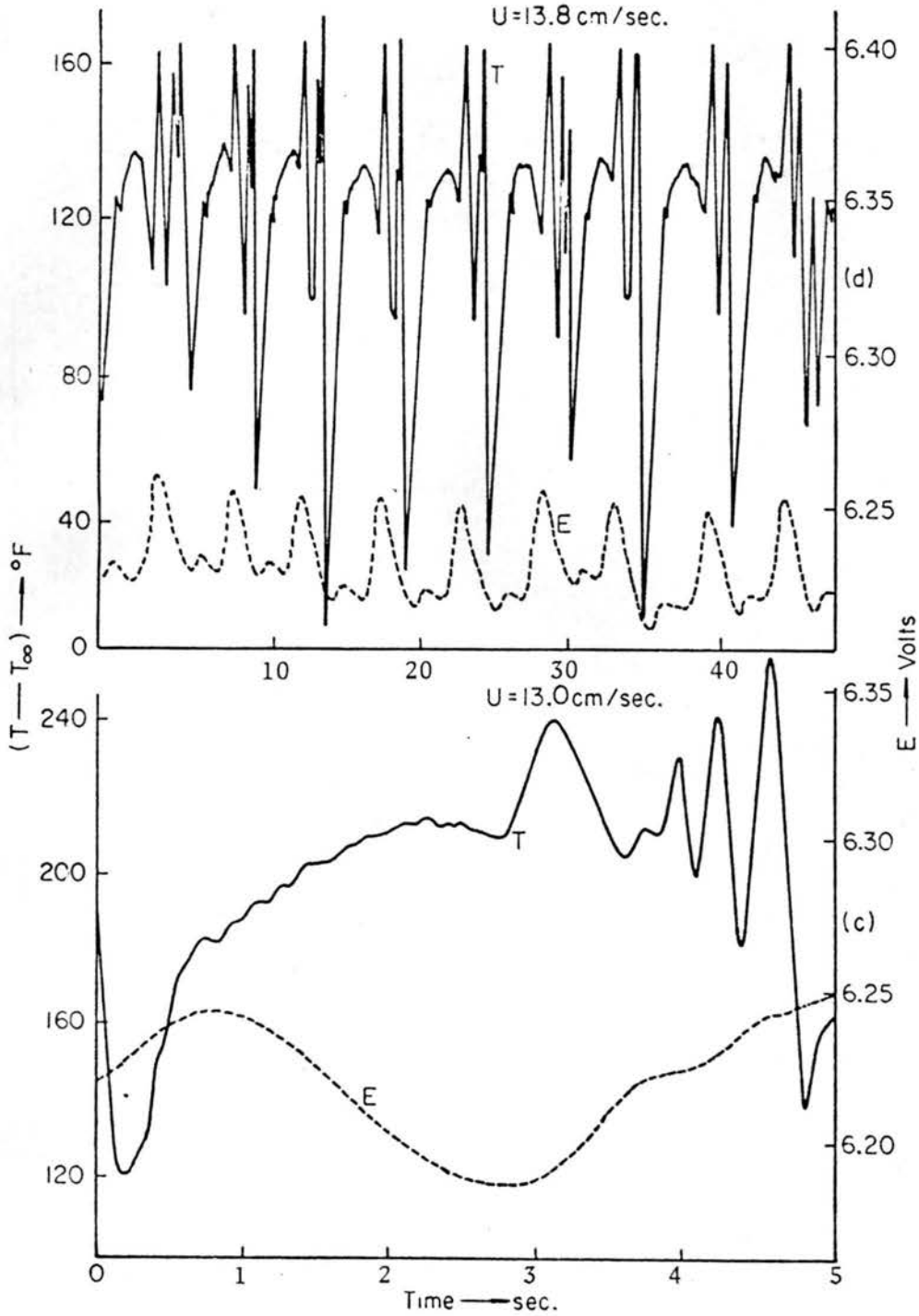

c - d

Fig. 22. (Cont.) Effect of ambient velocity on the variation of temperature within the hot core for directly opposed free and forced convection from constant temperature horizontal cylinder; Pt 80% Ir 20% cylinder, d = 0.01 mm, l = 15 mm, γ = 1.35, u = 0.25 mm, y = 0.

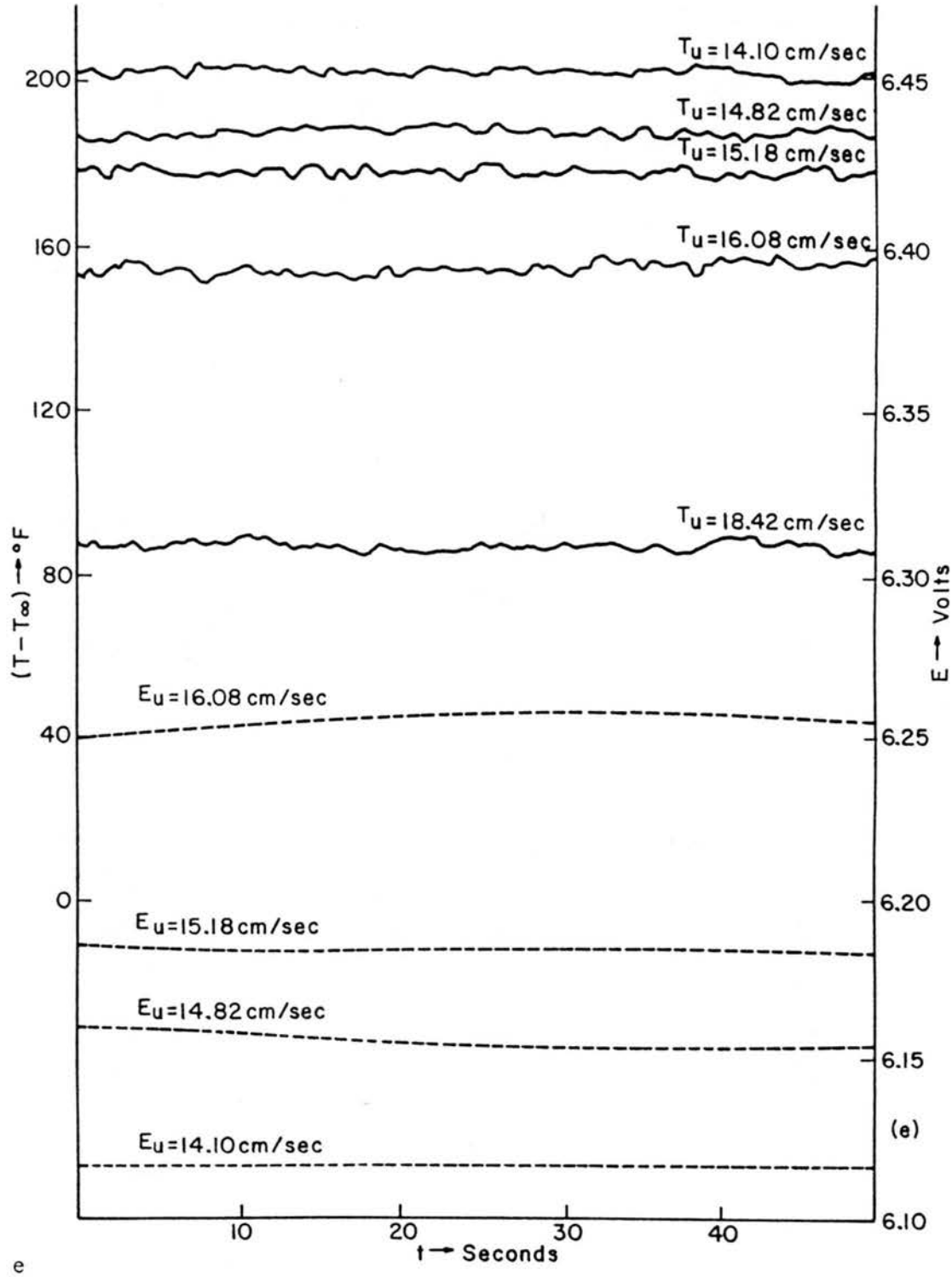

e

Fig. 22. (Concluded) Effect of ambient velocity on the variation of temperature within the hot core for directly opposed free and forced convection from constant temperature horizontal cylinder; Pt 80% Ir 20% cylinder, d = 0.01 mm, l = 15 mm, γ = 1.35, u = 0.25 mm, y = 0.

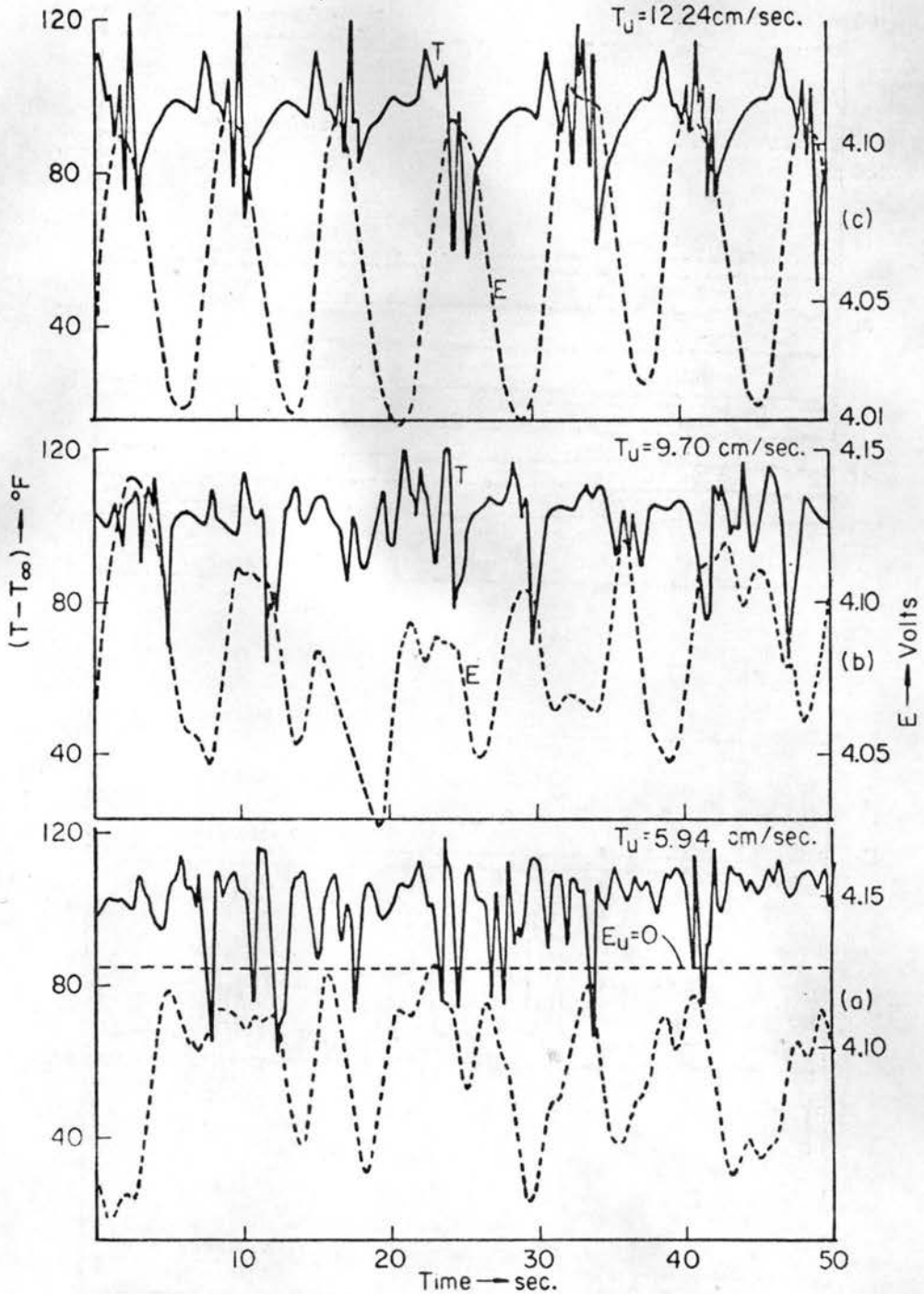

a - c

Fig. 23. Effect of ambient velocity on the variation of temperature within the hot core for directly opposed free and forced convection from constant temperature horizontal cylinder; Pt 80% Ir 20%, d = 0.01 mm, l = 15 mm, γ = 1.2, x = 0.25 mm, y = 0.

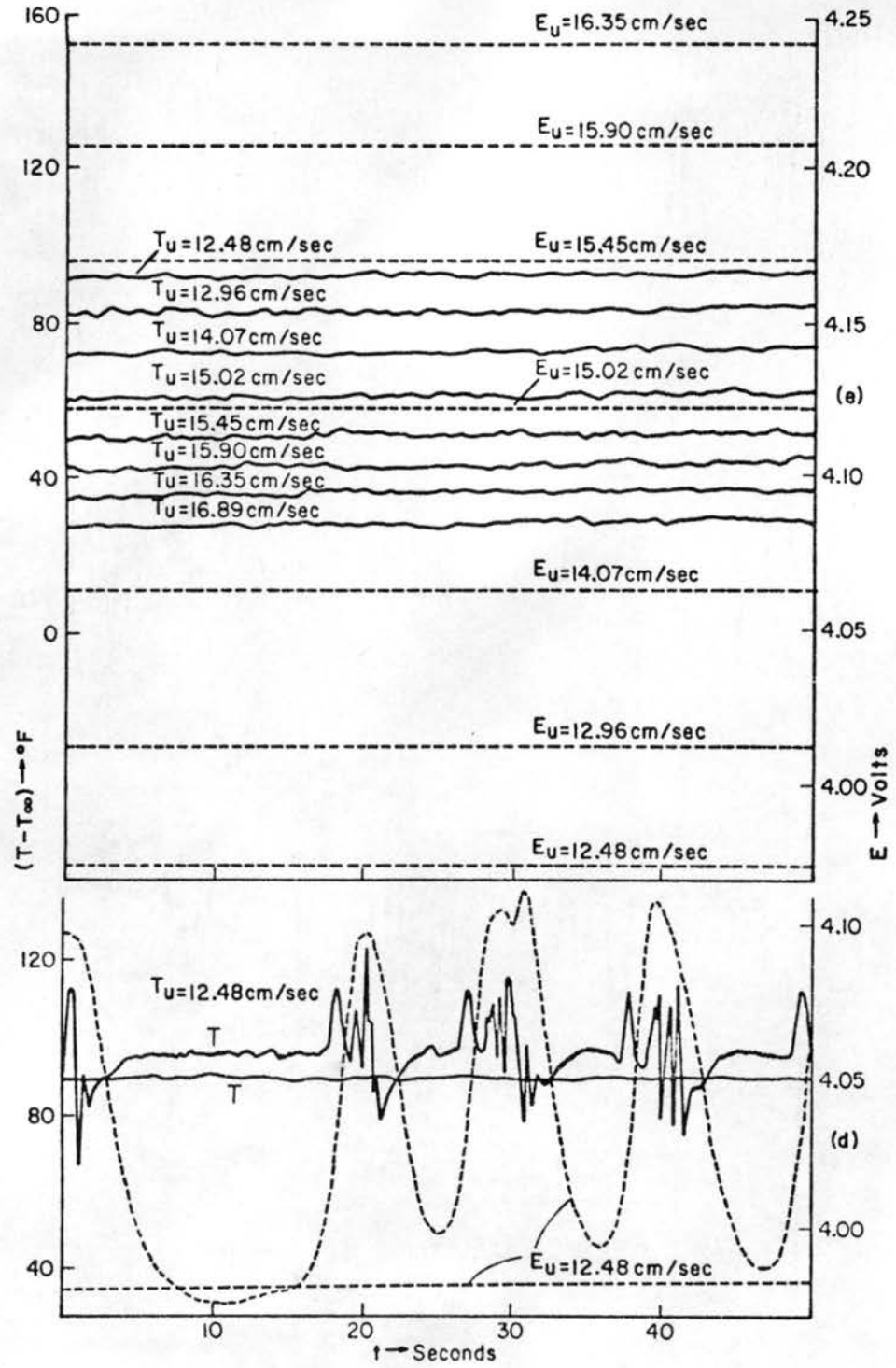

d - e

Fig. 23. (Concluded) Effect of ambient velocity on the variation of temperature within the hot core for directly opposed free and forced convection from constant temperature horizontal cylinder; Pt 80% Ir 20%, d = 0.01 mm, 1 = 15 mm, γ = 1.2, x = 0.25 mm, y = 0.

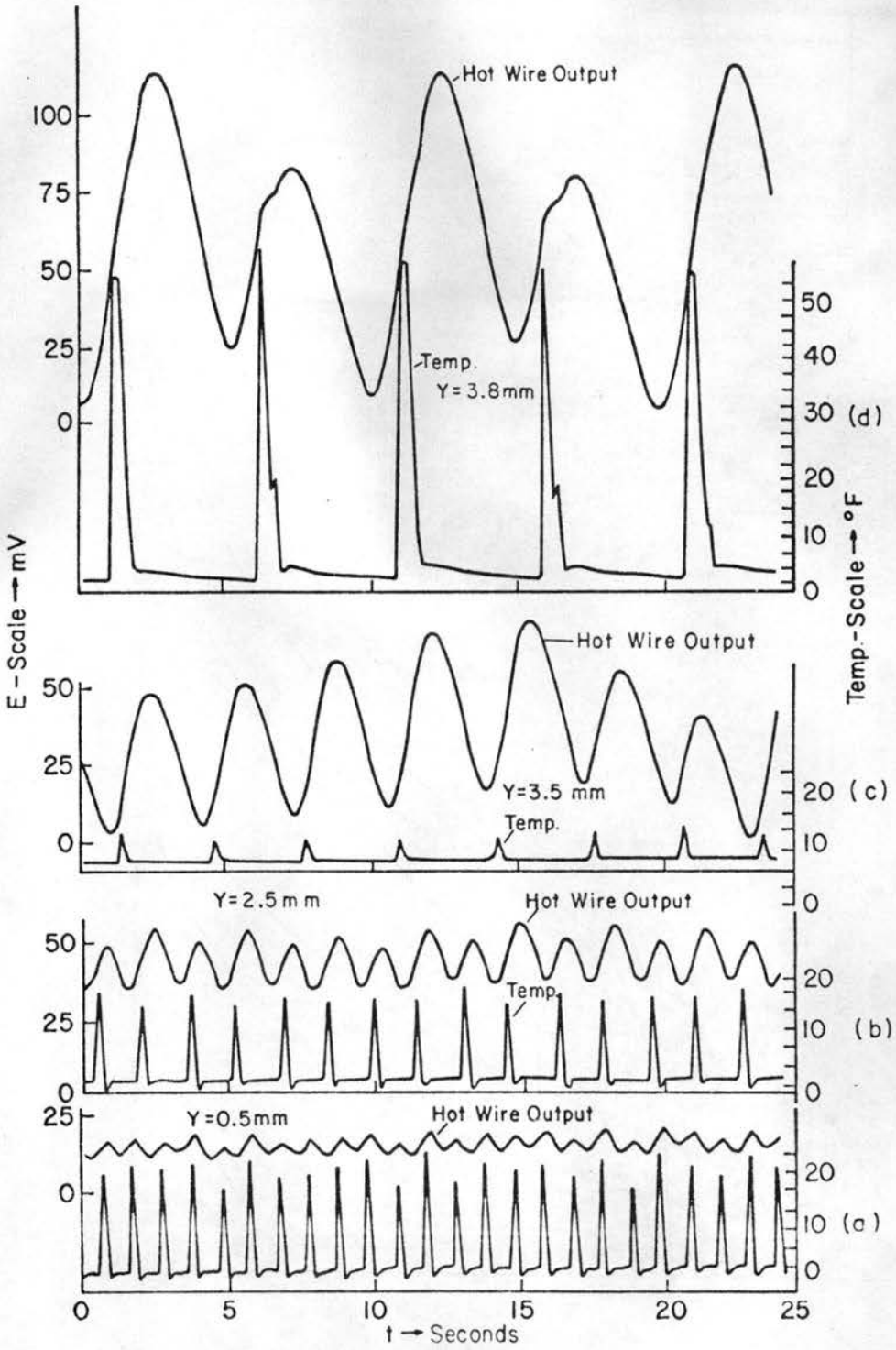

a - d

Fig. 24. Sensitivity of rising plume to local disturbances during periodic behavior constant temperature Pt 80% Ir 20% cylinder, d = 0.01 mm, l = 12 mm, γ = 1.68, Re = 48.6, x = 8 mm.

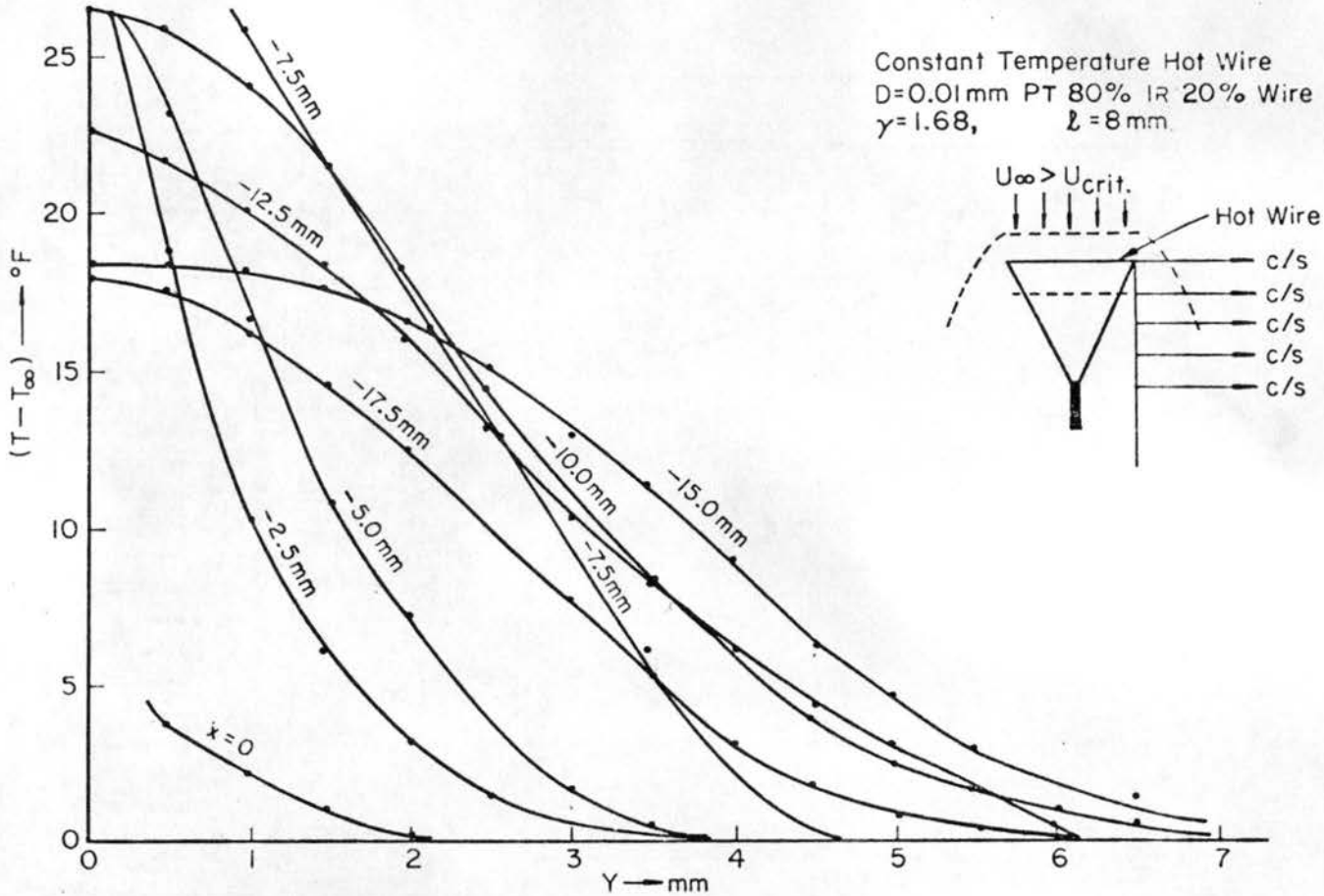

Fig. 25. End effect of the shroud; wake temperature distribution beyond the ends of the hot cylinder during the dominant forced convection. Constant temperature Pt 80% Ir 20% cylinder, d = 0.01 mm, 1 = 8 mm, γ = 1.68, Re = 68.

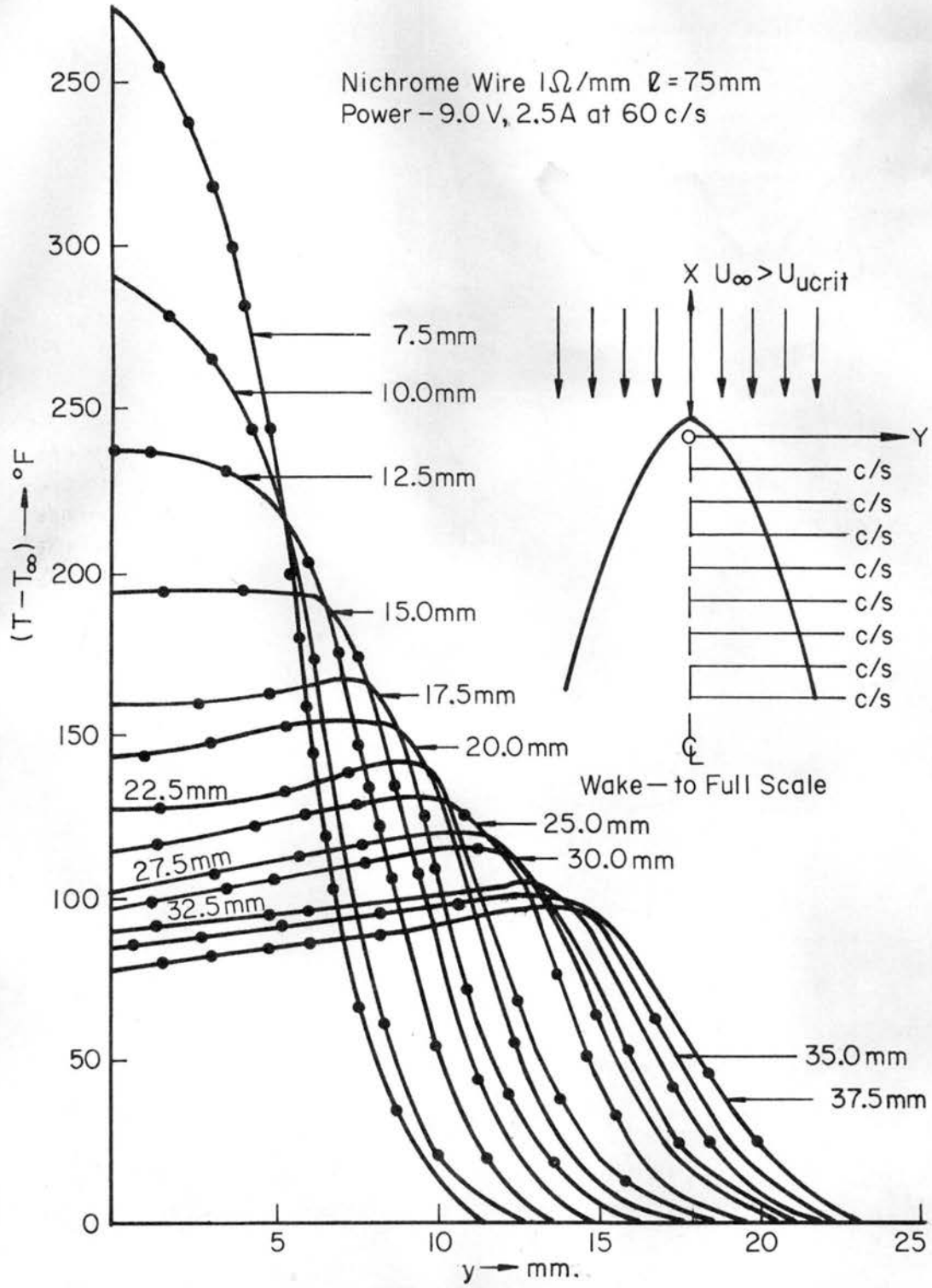

a) A.C. heating by 9V at 2.5 Amp

Fig. 26. Wake temperature distribution under dominant forced convection, Nichrome cylinder, d = 0.4 mm, R = 1 ohm/mm, 1 = 75 mm.

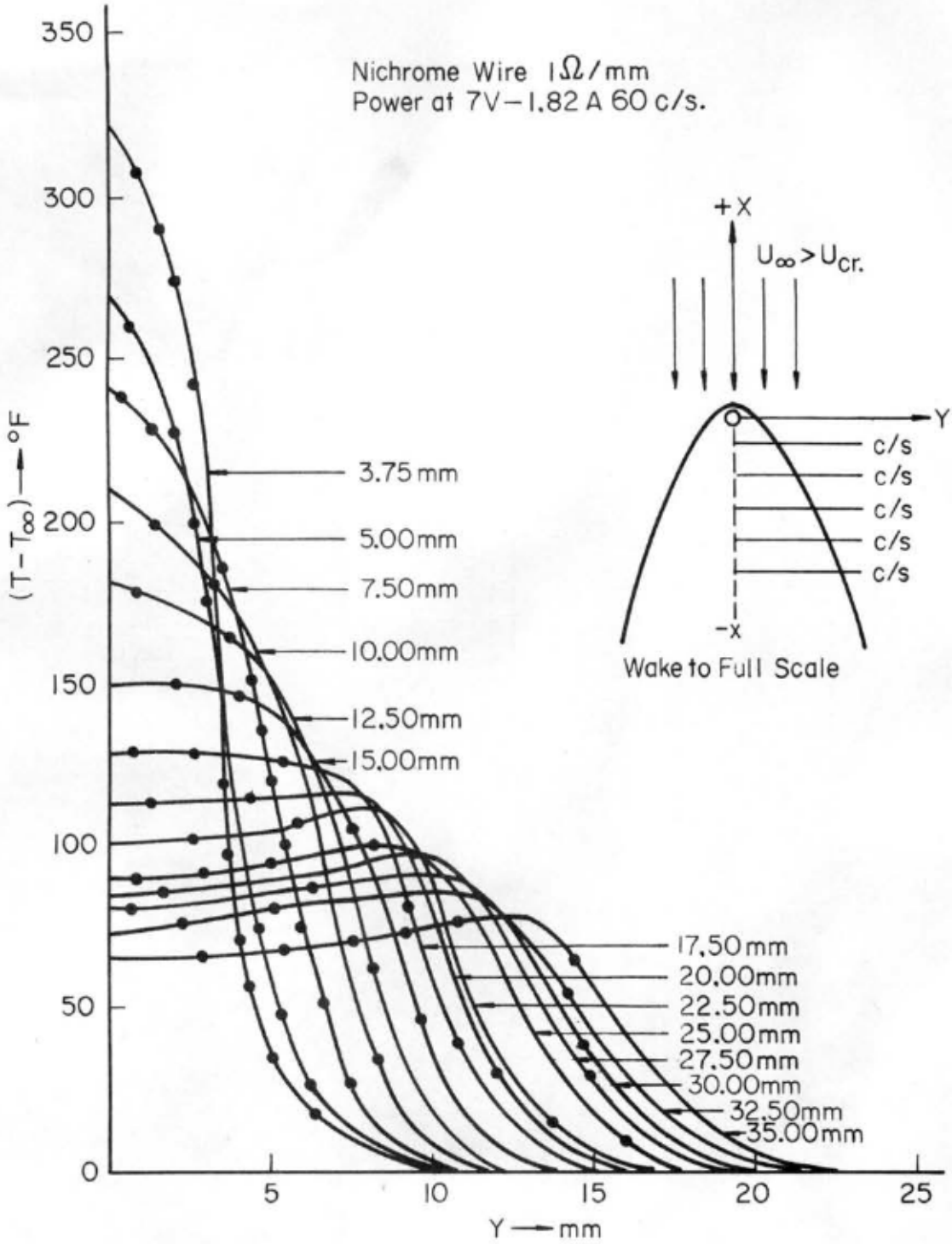

b) A.C. heating by 7V at 1.82 Amp

Fig. 26. (Concluded) Wake temperature distribution under dominant forced convection, Nichrome cylinder, d = 0.4 mm, R = 1 ohm/mm, l = 75 mm.

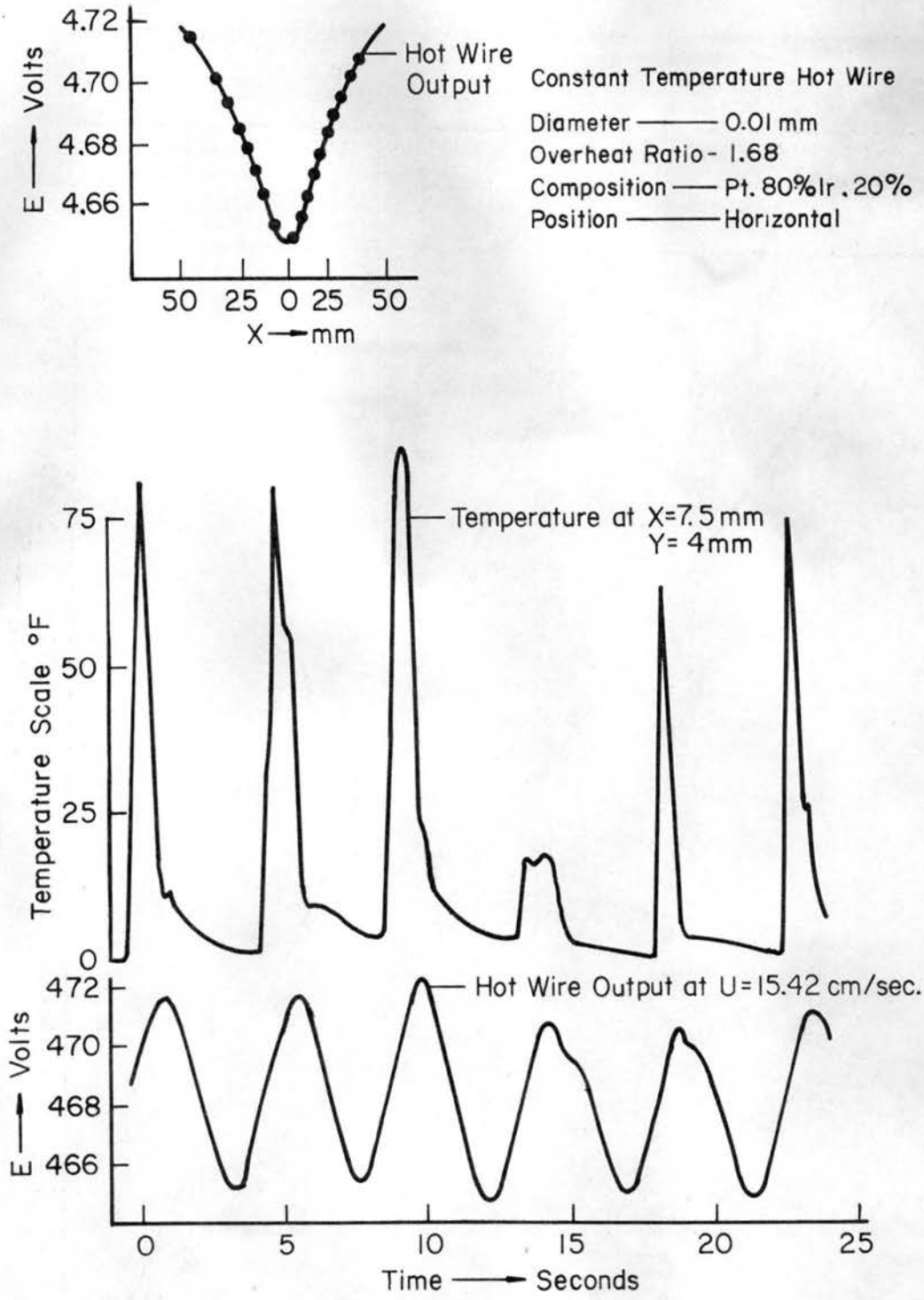

Fig. 27. An observation recording the periodic heat transfer and temperature close to the rising plume for constant temperature Pt 80% Ir 20% cylinder, d = 0.01 mm, l = 12 mm, γ = 1.68, Re = 51.4, x = 75 mm, y = 4 mm. Insert: Corresponding heat transfer from hot cylinder with laminar sheet replaced by thin shield and no ambient velocity.

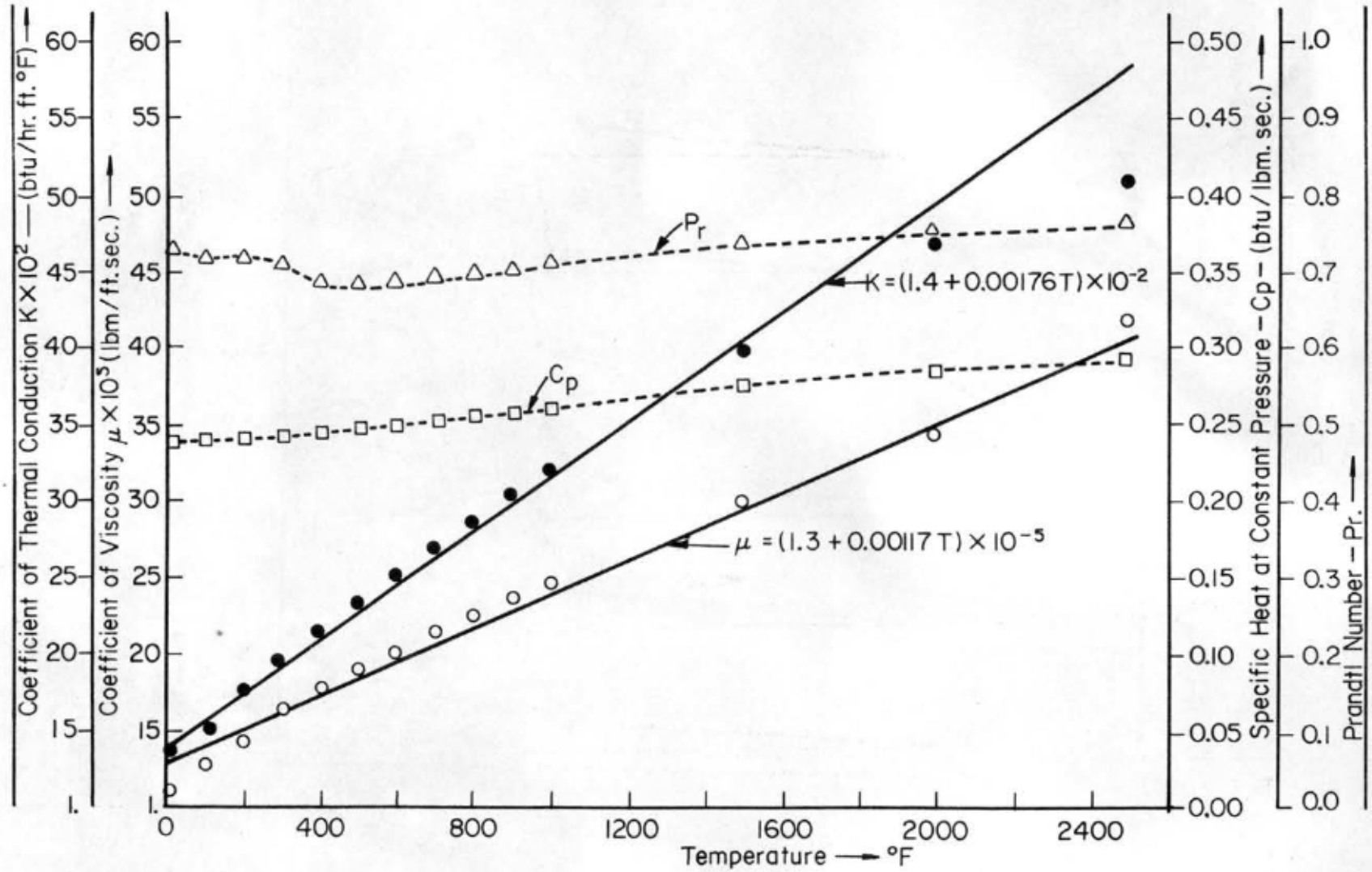

Fig. 28. Variation of K , μ , C_p , and Pr with temperature for air; data from Ref. 19.

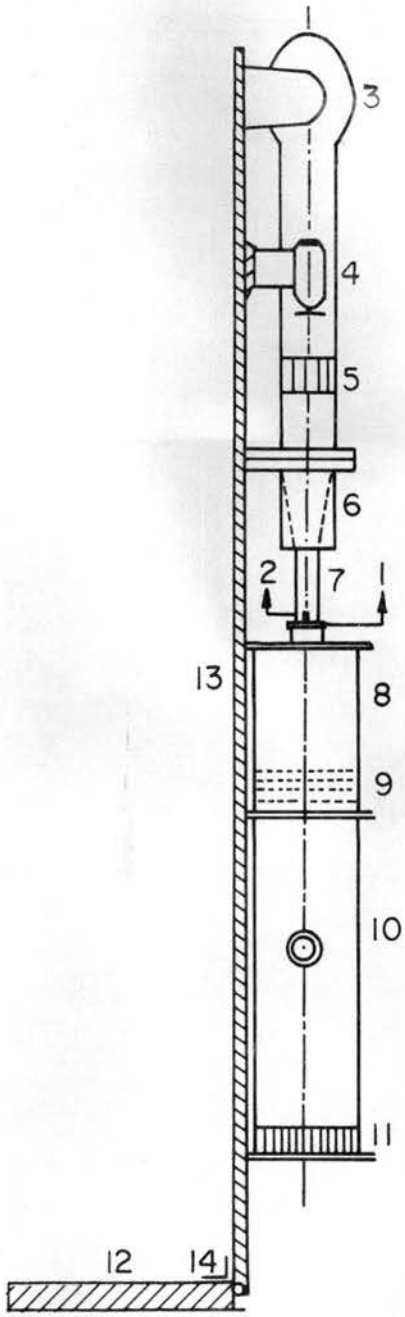

1. Total Head–Outlet
2. Static Head–Outlet
3. Blower A.C.
4. Blower D.C.
5. Honey Comb.
6. Contraction
7. Control–Section
8. Settling Chamber
9. Screens
10. Test Section
11. Honey Comb.
12. Support
13. Flat Plate
14. Hinge

Fig. 29a. Layout of the flow facility.

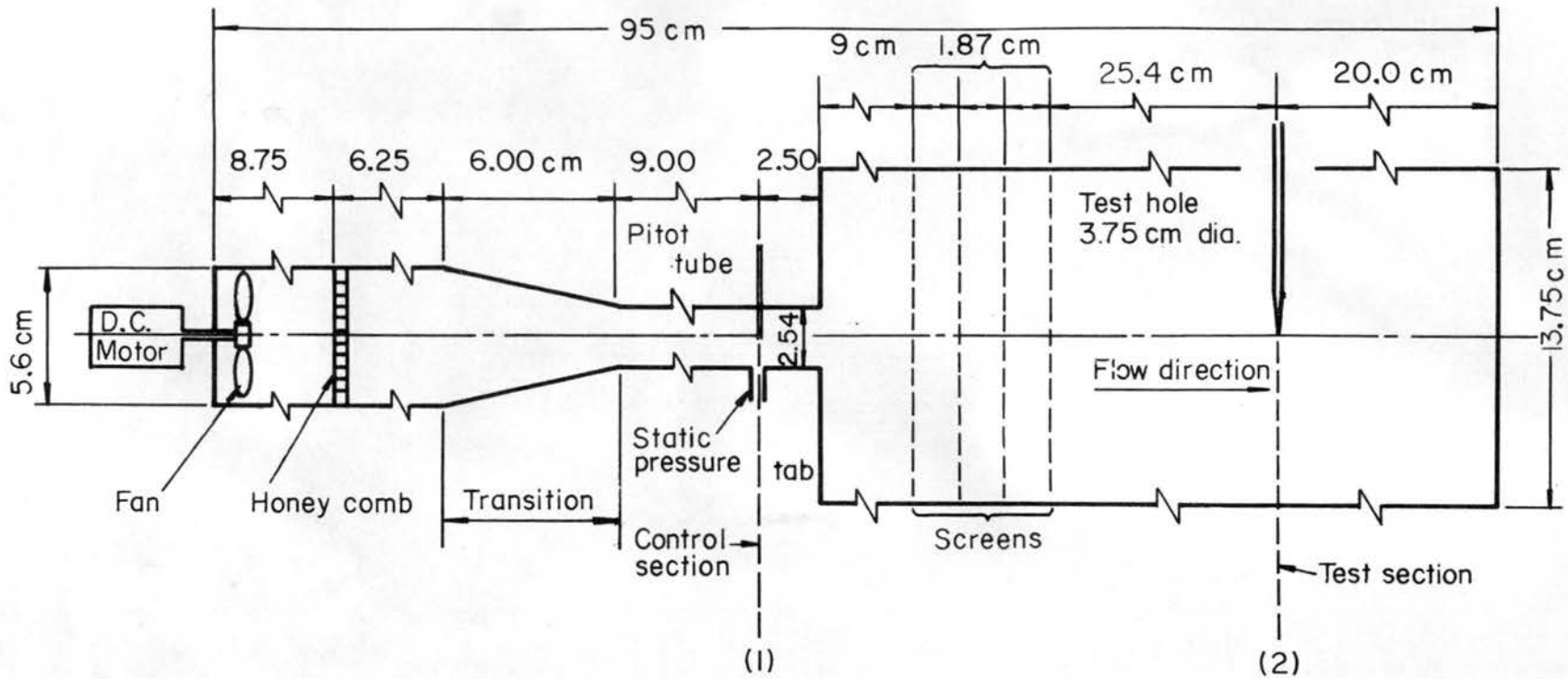

Fig. 29b. (Concluded) Details of the flow facility.

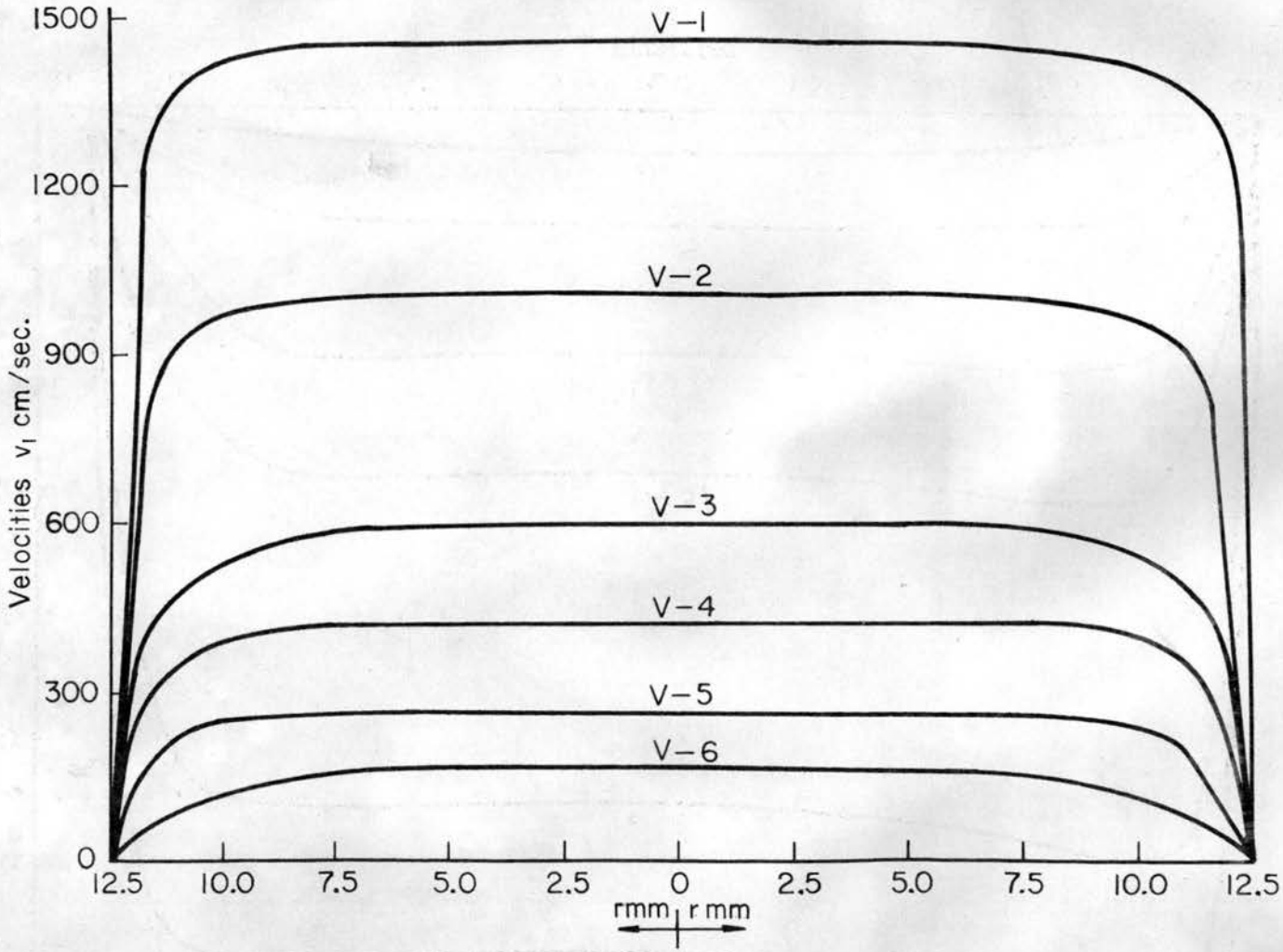

Fig. 30a. Velocity profile in the control section, Ref. 20.

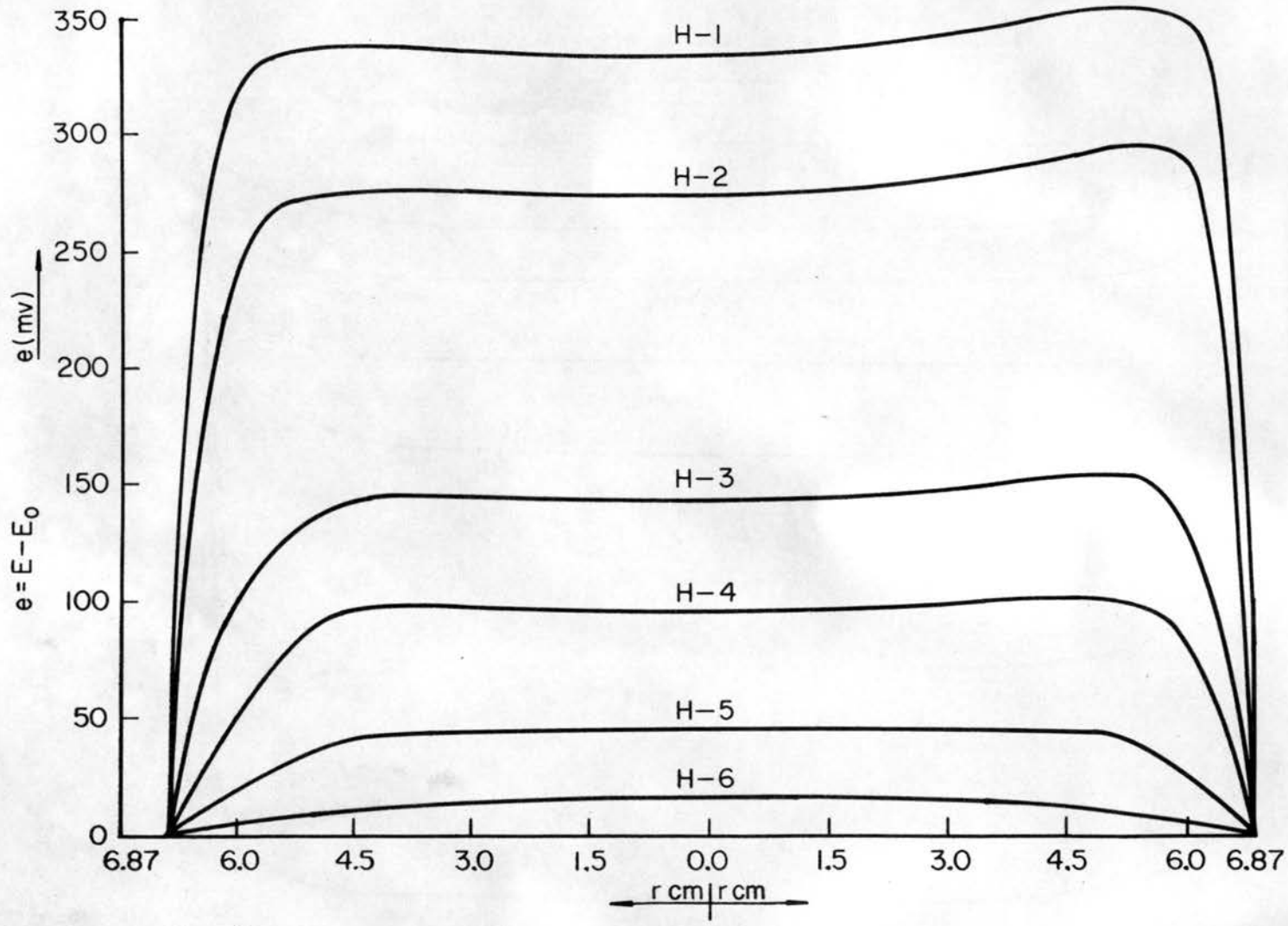

Fig. 30b. (Concluded) Profiles of hot wire output in the test section, Ref. 20.

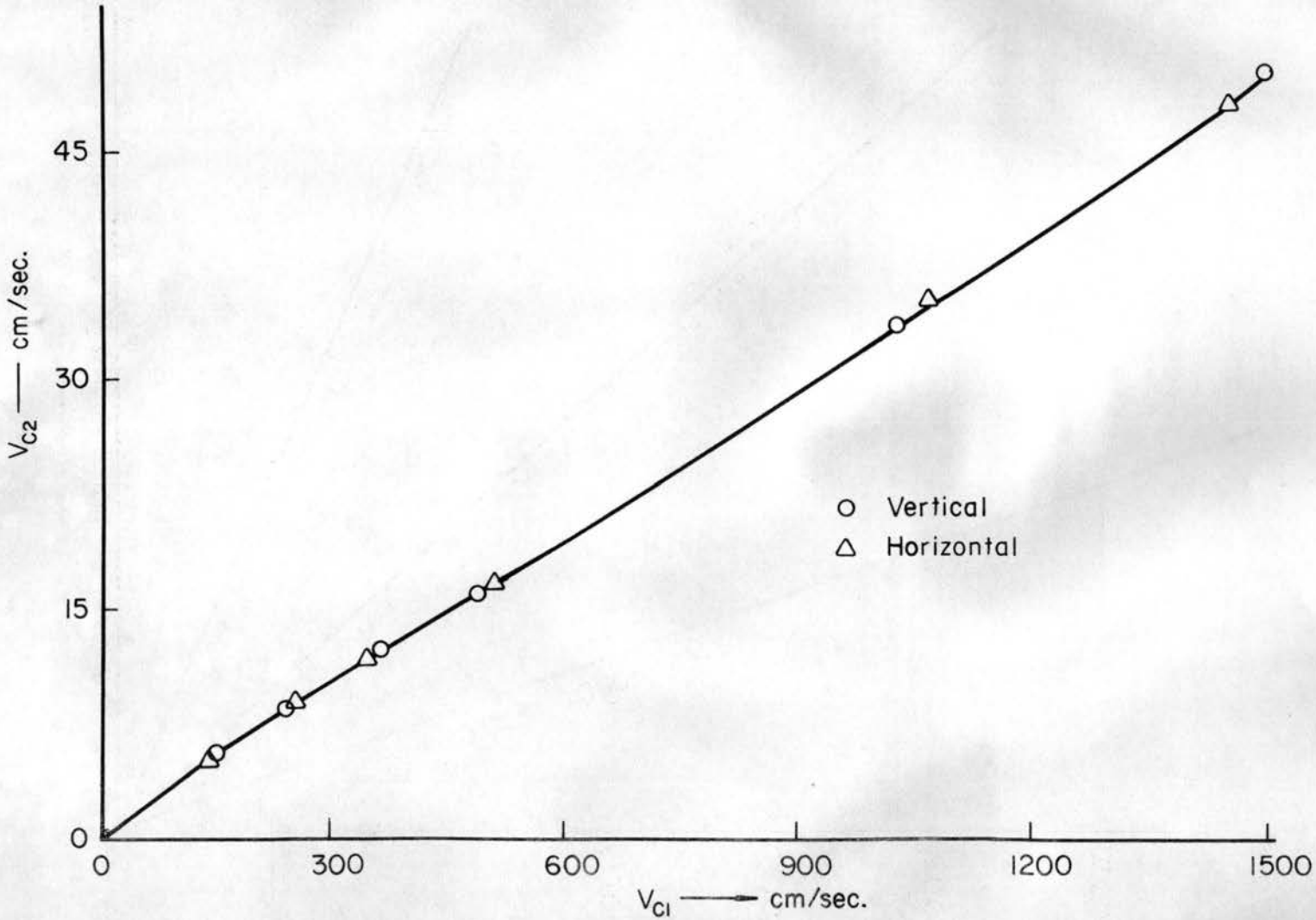

Fig. 31. Calibration curve of the microtunnel.

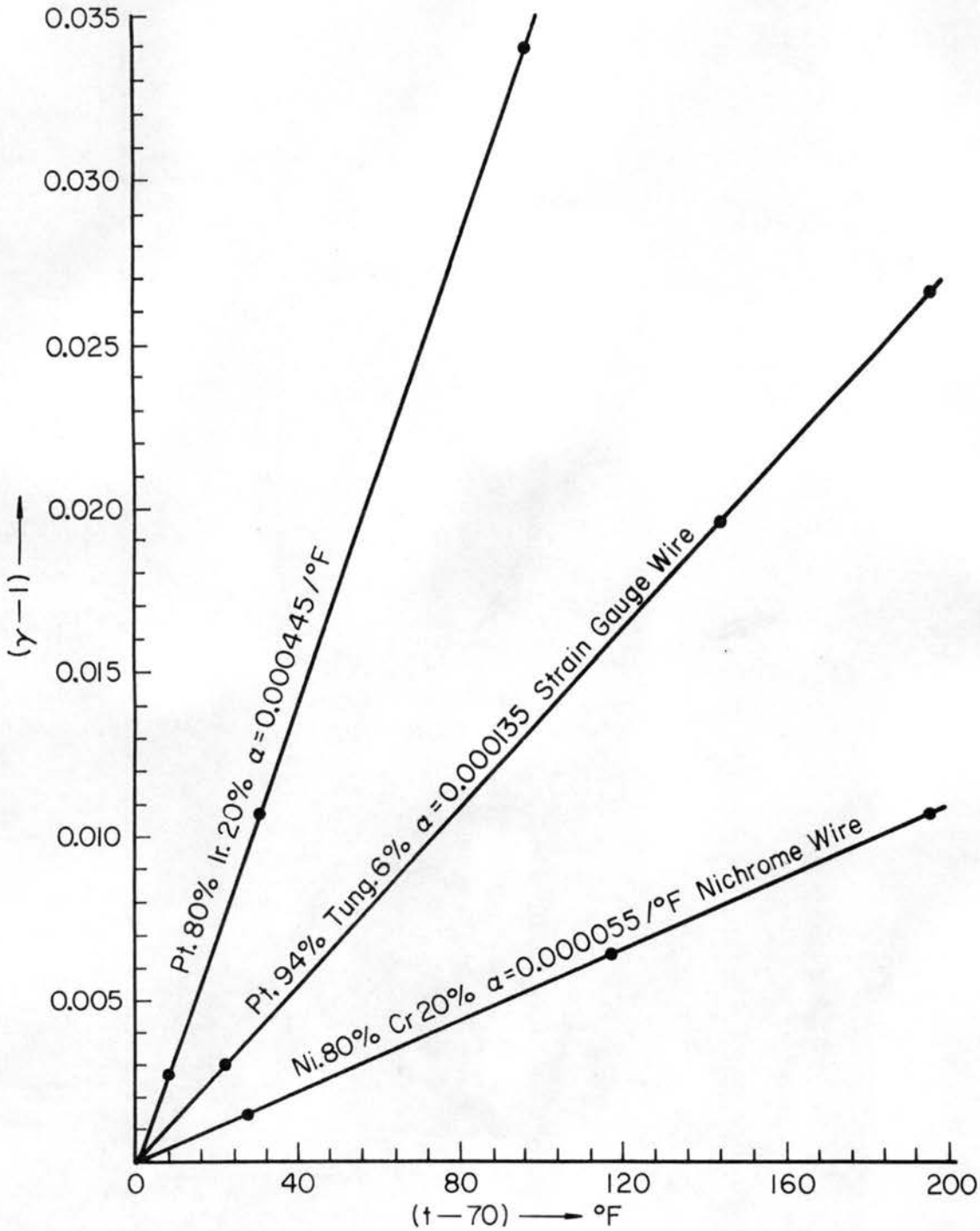

Fig. 32. Variation of resistance with temperature for the cylinder materials used.

unclassified
Security Classification

DOCUMENT CONTROL DATA – R & D

(Security classification of title, body of abstract and indexing annotation must be entered when the overall report is classified)

1. ORIGINATING ACTIVITY *(Corporate author)*
Fluid Dynamics and Diffusion Laboratory
College of Engineering, Colorado State University
Fort Collins, Colorado 80521

2a. REPORT SECURITY CLASSIFICATION
Unclassified

2b. GROUP

3. REPORT TITLE
Periodicity of Combined Heat Transfer from Horizontal Cylinders

4. DESCRIPTIVE NOTES *(Type of report and inclusive dates)*
Themis Technical Report No. 22. March 1973

5. AUTHOR(S) *(First name, middle initial, last name)*
Shrinivas K. Nayak and Virgil A. Sandborn

6. REPORT DATE
March 1973

7a. TOTAL NO. OF PAGES
116

7b. NO. OF REFS
42

8a. CONTRACT OR GRANT NO.
14-01-001

b. PROJECT NO.
N00014-68-A-0493-0001

c.

d.

9a. ORIGINATOR'S REPORT NUMBER(S)
CER72-73SKN-VAS23

9b. OTHER REPORT NO(S) *(Any other numbers that may be assigned this report)*

10. DISTRIBUTION STATEMENT
Distribution of this report is unlimited.

11. SUPPLEMENTARY NOTES

12. SPONSORING MILITARY ACTIVITY
U.S. Department of Defense
Office of Naval Research

13. ABSTRACT

Based on experimental and flow visualization studies, a model for directly opposed free and forced convection flow around a heated cylinder (0.01 mm diameter) was developed. Three modes of flow were identified. For velocities less than 15 cm/sec (cylinder Reynolds number, $Re_{dw} = 0.08$) a free convection or a buoyant force dominated flow was observed. The interacting free convection plume and the ambient flow form a stagnation region well upstream of the heated cylinder. Heat was convected from the cylinder through the plume to the stagnation region. In the stagnation region random vortex pockets of heated mass were formed.

For velocities greater than 15 cm/sec but less than 21.4 cm/sec the magnitudes of the forced and free convection flows were nearly equal. A periodic oscillation of the stagnation region was observed. The flow regime where the periodic oscillations occur was found to be defined by a specific relation between Grashof and Reynolds numbers. The periodic oscillations, which were in the range from 3 to 15 cycles per minute, were correlated in terms of Strouhal number and Reynolds number.

For velocities greater than 21.4 cm/sec the forced convection was found to dominate over the free convection. The stagnation region was fixed for each flow velocity at one position above the cylinder. A potential like flow (laminar sheet) was formed shrouding the thermal layer of the cylinder.

The mean heat transfer from the cylinder decreases with increasing Reynolds number for both the case of dominant free convection and the case of equal free and forced convection. The mean heat transfer abruptly and rapidly increases with increasing Reynolds number in the forced convection dominated region. For all these cases the thermal layer surrounding the hot cylinder was approximately 600 times larger than the diameter of the cylinder.

DD FORM 1 NOV 65 1473

Unclassified
Security Classification